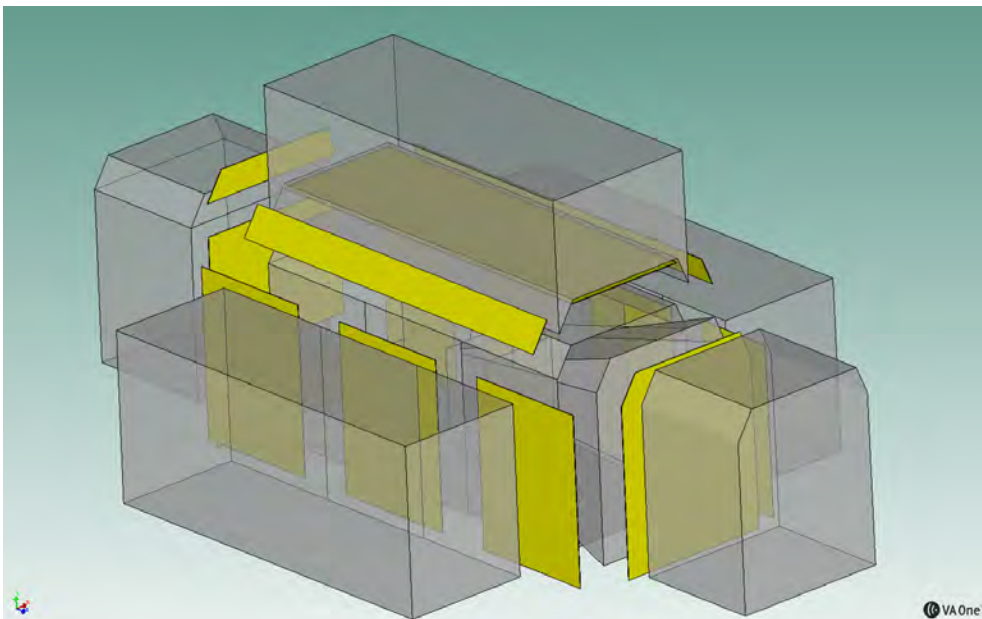


# CHALMERS



## Acoustic simulation of power unit encapsulation for construction and mining applications

*Master's Thesis in the Master's programme in Sound and Vibration*

ANTON GOLOTA

Department of Civil and Environmental Engineering  
*Division of Applied Acoustics*  
*Vibroacoustics Group*  
CHALMERS UNIVERSITY OF TECHNOLOGY  
Gothenburg, Sweden, 2012  
Master's thesis 2012:129



MASTER'S THESIS 2012:129

# Acoustical simulation of power unit encapsulation for construction and mining applications

Anton Golota

Department of Civil and Environmental Engineering  
*Division of Applied Acoustics*  
*Vibroacoustics Group*  
CHALMERS UNIVERSITY OF TECHNOLOGY  
Göteborg, Sweden 2012

Acoustical simulation of power unit encapsulation for construction and mining applications

© Anton Golota, 2012

Master's Thesis 2012:129

Department of Civil and Environmental Engineering  
Division of Applied Acoustics  
Vibroacoustics Group  
Chalmers University of Technology  
SE-41296 Göteborg  
Sweden

Tel. +46-(0)31 772 1000

Reproservice / Department of Civil and Environmental Engineering  
Göteborg, Sweden 2012

# Acoustical simulation of power unit encapsulation for construction and mining applications

Master's Thesis in the Master's programme in Sound and Vibration

Anton Golota

Department of Civil and Environmental Engineering

Division of Applied Acoustics

Vibroacoustics Group

Chalmers University of Technology

## Abstract

Modern drilling equipment is normally driven by a dedicated hydraulic power unit, sometimes mounted on the machine and sometimes a stand alone unit. The power unit is the most important noise source when drilling using rotary methods. The power unit is normally equipped with an encapsulation in order to protect the components within the unit from surrounding environment and to protect operator and close-by workers from hazards like rotating components and noise. Such an enclosure has to be mechanically robust with high noise insulation and sufficient cooling capacity.

The purpose of this study was to examine possible concepts in order to find the optimal solution fulfilling the criteria above, i.e. find a mechanically robust solution for an enclosure with good cooling capability and good noise reduction. The study consists of three parts. The first part has a general description of the noise insulation capability of the power unit. This part explains measurements that were done on complete power pack and on its components. In the second part building of computer models of separate enclosure components using Finite Element Analysis (FEA) and Statistical Energy Analysis (SEA) technique is explained. Also, the validation of the modeling results was done using the results from measurements. The concept presented in the second part of the study also takes effect of airflow into account. Third part: refined modeling on critical parts like air in- and outlets using acoustical FEA was done. Based on the FEA modeling, an improved prototype baffled panel was built. The computer models developed were then validated using results from measurements. Sound reduction properties of the improved enclosure were estimated.

Results described in this thesis show that acoustical computer model of the power

pack encapsulation and its components can be used during design stage of product development, before the prototype unit is built. This approach reduces the cost of product development and allows to investigate acoustically weak parts.

**Keywords:** Encapsulation, Enclosure, Power Pack, SEA, FE, VA-one, Apertures, Transmission Loss.

# Contents

<b>Abstract</b>	<b>iii</b>
<b>Contents</b>	<b>v</b>
<b>Acknowledgements</b>	<b>vii</b>
<b>I. Report Structure</b>	<b>ix</b>
<b>1. Introduction</b>	<b>1</b>
1.1. Project description . . . . .	1
1.2. Literature research . . . . .	3
<b>2. Theoretical background</b>	<b>5</b>
2.1. Decibel scale and A-weighted scale . . . . .	5
2.2. Absorption . . . . .	6
2.3. Transmission loss . . . . .	9
2.4. Statistical Energy Analysis . . . . .	11
2.5. SEA in VA-one . . . . .	13
2.5.1. SEA subsystems . . . . .	14
2.5.2. SEA junctions . . . . .	15
2.5.3. SEA load sources . . . . .	16
2.6. Finite Elements Method (FE) in VA-one . . . . .	17
2.6.1. NCT, Foam and PEM . . . . .	17
2.6.2. Hybrid and custom calculated transmission loss . . . . .	18
<b>3. Thermal and airflow analysis</b>	<b>19</b>
3.1. Airflow rate . . . . .	19
3.2. Airflow impedance . . . . .	20
<b>4. Measurements</b>	<b>25</b>
4.1. Noise sources and total noise . . . . .	25
4.2. Absorption . . . . .	27
4.2.1. Field measurements . . . . .	28
4.2.2. Laboratory measurements . . . . .	30

## Contents

4.3. Transmission loss . . . . .	32
4.3.1. Field measurements . . . . .	32
4.3.2. Laboratory measurements . . . . .	36
4.4. Temperature and airflow . . . . .	39
4.4.1. Estimated noise from the airflow . . . . .	39
4.5. Conclusion . . . . .	40
<b>5. Computer models</b>	<b>41</b>
5.1. Absorption modeling . . . . .	41
5.2. Model of solid panel . . . . .	43
5.2.1. SEA model . . . . .	43
5.2.2. FE model . . . . .	48
5.2.3. SEA model vs FE model . . . . .	50
5.3. Model of baffled panel . . . . .	51
5.3.1. Field setup model . . . . .	51
5.3.2. Laboratory setup model . . . . .	52
5.3.3. Fluid Dynamic Simulation . . . . .	56
5.4. Model of the power pack encapsulation . . . . .	60
5.5. Results . . . . .	65
5.6. Conclusion . . . . .	68
<b>6. Improved front baffled panel</b>	<b>71</b>
6.1. Developing a new baffled panel . . . . .	71
6.1.1. VA-one prediction . . . . .	72
6.1.2. Fluid Dynamic Simulation . . . . .	75
6.1.3. Expectations . . . . .	78
6.2. Laboratory measurements of the prototype panel . . . . .	78
6.3. Estimated emitted sound power . . . . .	83
6.4. Conclusion . . . . .	84
<b>7. Summary</b>	<b>87</b>
7.1. Future work . . . . .	87
<b>References</b>	<b>89</b>

# Acknowledgements

I would like to acknowledge the help of following people:

Renny Rantakokko and Samuel Enblom from Measurement Technique Group of Rocktec Division of Atlas Copco for supervising my work.

Prof. Patrik Andersson from Applied Acoustics department of Chalmers University of Technology for fruitful discussion and supervision of my work.

Anders Wilson and Robert Fiedler from VA-one central support for guiding with VA-one software.

Jari Hyvarinen from Anker-Zemer Engineering AB for fluid dynamic calculation.

*Contents*

# I. Report Structure

This report summarizes work that was done to investigate the power pack encapsulation and to simulate it as a computer model.

The “Introduction” chapter contains information about the power pack encapsulation and explains the main concepts of encapsulation simulation along with reference to articles about sound transmission through apertures.

The “Theoretical background” chapter includes basic theory about statistical energy analysis, transmitted and absorbed sound. Besides, this chapter contains information about VA-one software. This chapter gives the background needed for understanding how measurements were done and computer models were developed.

The “Thermal and airflow analysis” chapter focuses on estimation of airflow impedance curve and shows how to calculate required amount of airflow. This information is needed to select an optimal fan for the cooling system.

The “Measurements” chapter describes the measurements that were done and discusses the obtained results. The “Conclusion” subsection summarizes main aspects discussed in this chapter.

Chapter 5 - “Computer models” explains the models that were built. Comparison of the modeled and measured results is presented in this chapter. The “Conclusion” subsection contains discussion and summary.

The “Improved front baffled panel” chapter describes the work that was done to improve sound reduction performance. The results from simulations and measurements of prototype construction are also discussed here. The “Conclusion” subsection summarizes the main points discussed in this chapter.

The last chapter “Summary” includes project discussion and future work.

## *I. Report Structure*

# 1. Introduction

The current chapter contains a description of the unit under investigation and a literature study. The project description section includes general information about the encapsulation, photos of the encapsulation, its components, and the whole unit. It describes the approach that was chosen to build computer models. The literature study section includes an overview of articles that describe different aspects of simulation and theoretical models of encapsulation. It also includes references on research about methods of reducing noise from a machine by manipulating its cooling system.

## 1.1. Project description

This work was done for Atlas Copco Rock Drills AB which specializes in mining equipment and construction tools. A power pack for surface core drilling rig CT20 was the object of this research and computer simulation. The encapsulated power pack and the platform with power pack and drill rig are shown at Figure 1.1.



Figure 1.1.: Photos of the power pack's encapsulation in front of the power pack unit (left), and the encapsulated power pack with core drilling rig (right).

An acoustic enclosure is a structure that houses noise sources and protects the environment from the noise emitted by sources. The power pack enclosure is machine mounted. The enclosure is close fitting, since it surrounds the power pack equipment very closely and the volume of the machine is comparable to the volume of the enclosure. The enclosure consists of removable steel panels treated with absorption material. The power pack with removed encapsulated panels is shown at Figure 1.2.

## 1. Introduction



Figure 1.2.: Photo of the power pack without encapsulation.

The encapsulation panels are attached to the power unit frame. The noise treatment for the power pack encapsulation was chosen in a manner to provide the best absorption and to withstand the hostile environment. Photos of the solid panel of the encapsulation from inside and outside are shown at Figure 1.3.



Figure 1.3.: Photos of the solid panel of the encapsulation from inside of the power pack (left) and from outside (right).

Some of the panels have openings to provide a required airflow for the cooling system. The panel openings are protected with baffles. The side panels are equipped with chevron-blade baffles (see Figure 1.4). The chevron-blade baffles have better reduction

performance than the front baffles.



Figure 1.4.: Photos of the front baffled panel (left), the chevron-blade baffled side panel (right)

The main aim of this thesis was to simulate and improve the power pack enclosure. This aim was divided into a number of subtasks: simulation of the solid panel, the front baffled panel, and the complete encapsulation; design proposal and simulation of the improved front baffled panel. A number of measurements were done to validate the models during development and to compare the final results obtained by modeling and measuring.

The acoustical models of the power pack and its components were done in VA-one software. VA-one is a commercial software by ESI-group that allows to build and solve complex vibro-acoustic problems. VA-one has a number of modules that allow to extend possibilities of the solver.

The idea of this work was to model the power pack's components as finite elements models and then to substitute them with statistical energy analysis models.

## 1.2. Literature research

The purpose of the literature study is to summarize literature research of the problem of encapsulation and reduction of emitted noise pollution from the power pack. The literature research was mainly focused on information about existing models of estimation sound reduction performance of enclosures and sound transmission through apertures. Partly, the literature research was dedicated to the reduction of emitted noise from the power pack by manipulating the heat exchanger and the fan.

## 1. Introduction

Different theoretical models [Lyon 63], [Jac 66] for sound reduction of enclosures were developed during the past decades. Lyon built models for different frequency ranges. He investigated the following cases: wall and air cavity are both stiffness controlled; cavity is stiffness and wall is resonance controlled; wall and cavity are both resonance controlled. The Jackson model assumes that the enclosure and the source are infinite. In his model he showed that negative transmission loss is possible at low frequency. Also, Jackson mentioned that the Helmholtz resonator effect could occur in the enclosure with opening.

In the article [Old 91-1] published by Oldham and Hillarby, authors developed low and high frequency models of acoustical enclosures. In the second part of the article [Old 91-2] they validated their models by comparison of predicted and experimental results. One of the suggested models was developed with help of statistical energy analysis.

In the article [Per 10] Pereira, Guettler and Merz used hybrid a SEA-FE model developed in VA-one software to model the interior noise in a vehicle. They built FE models of differently shaped leaks and investigated their transmission loss properties, then SEA models were populated with those results.

Different aspects of sound transmission through the aperture, as well as negative transmission phenomenon were explained in articles [Sau 70] , [Old 93] and [Mec 86]. Theoretical estimation of transmission loss of small circular holes and slits was done by Gomperts and Kihlman in their publication [Gom 67]. They compared results obtained from their model with measured transmission loss. The authors claimed that even small slits transmit a considerable amount of sound energy over whole frequency range. In the article [Sga 07] the authors present different theoretical models that allow to predict transmission loss through openings with different size and geometry. They investigated effects of diffuse field and normally incident sound load on transmission loss. An experimental procedure of measuring transmission loss of the apertures is described in [Tro 09].

In the article [Mug 76] Mugridge investigated different types of the fans from acoustic and aerodynamic points of view. He showed that radiator properties are linked to fan performance and that emitted noise from cooling system could be reduced with careful selection of fan and heat exchanger. In his research Mugridge showed that increasing the area or the thickness of radiator's plates could decrease the emitted sound power level from fan up to 13 dB. Tandon [Tan 00] explains ways of noise reduction from machines. He achieved a fan noise reduction of 10 dB only by increasing the mass of the fan base.

## 2. Theoretical background

In this section the theory is presented. The physics of the transmitted and absorbed energy as well as the ways of measuring it in different circumstances is explained. The VA-one theory is based on [VA1g],[VA1f] and [VA1s].

### 2.1. Decibel scale and A-weighted scale

The units of sound pressure levels, sound power levels, sound intensity levels and transmission losses are decibels. Decibel scale is logarithmic scale and it is defined by the specific value as a reference point. The scales and the reference values used in this work are listed below.

Sound power level

$$Lw = 10 \log_{10} \left( \frac{W}{W_{ref}} \right), \quad W_{ref} = 10^{-12} W \quad (2.1)$$

Sound pressure level

$$Lp = 20 \log_{10} \left( \frac{\tilde{p}}{p_{ref}} \right), \quad p_{ref} = 2 * 10^{-5} Pa \quad (2.2)$$

Sound intensity level

$$Li = 10 \log_{10} \left( \frac{I}{I_{ref}} \right), \quad I_{ref} = 10^{-12} W/m^2 \quad (2.3)$$

A sound power level and a sound pressure level are often characterized in a way similar to how they are subjectively perceived. In this work the A-weighted filter was used to match the measured or modeled sound pressure and power levels to how a human perceives it. The spectrum of the A-weighted filter as compared to a linear spectrum is shown at Figure 2.1.

## 2. Theoretical background

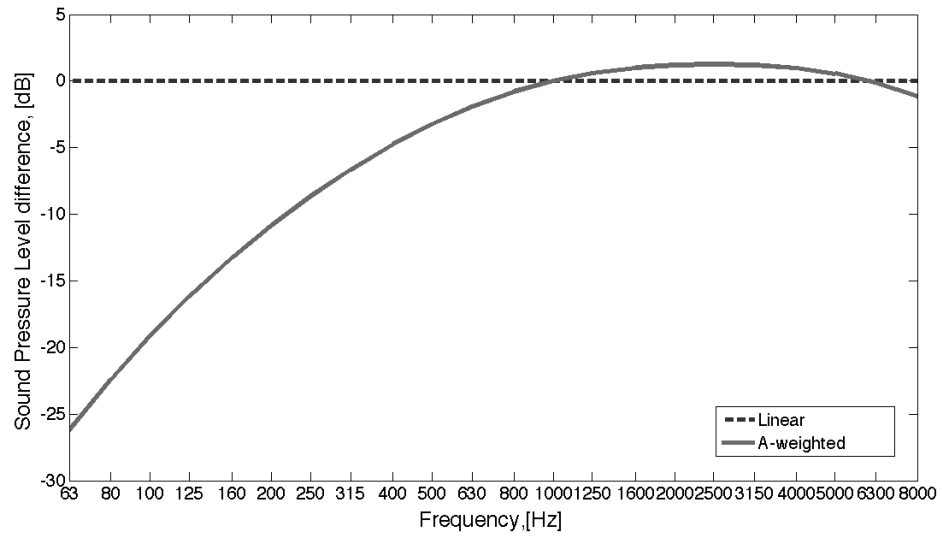


Figure 2.1.: Spectrum of the A-weighted filter.

## 2.2. Absorption

When sound waves interact with materials the energy contained in the incident wave is reflected, transmitted, and absorbed.

Sound absorber materials transform the energy carried by the organized particles' motion into the random motion. Most losses of acoustical energy occur due to drag force caused by friction of the wall or skeleton of the foam and the fluid in the thin acoustical boundary layer [Ver 06].

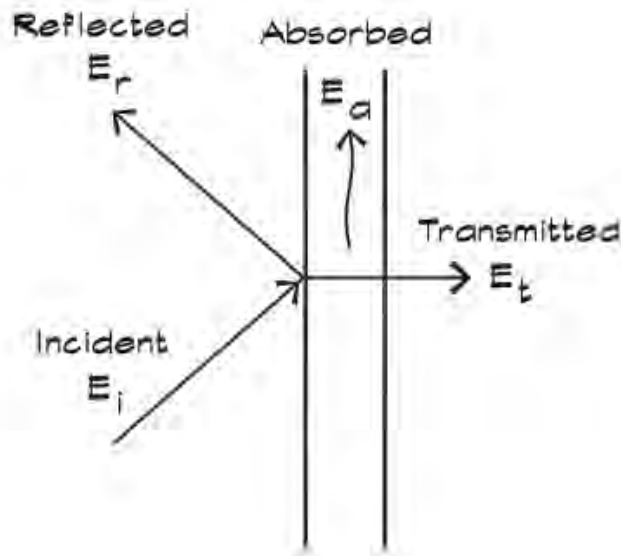


Figure 2.2.: Sketch of interaction of the incident sound wave with the surface. [Lon 06]

The energy balance of interaction of the incident sound wave with the surface is presented at Figure 2.2 and can be written as

$$E_i = E_r + E_t + E_a \quad (2.4)$$

Equation 2.4 can be rewritten to 2.5 to determine the combination of the transmitted and absorbed energy

$$\frac{E_r}{E_i} + \frac{E_{t+a}}{E_i} = 1 \quad (2.5)$$

The acoustic performance of the absorbent is characterized by the sound absorption coefficient  $\alpha$ . And it is defined as a ratio of the sound energy that is not reflected to the incident sound energy (2.6). The energy reflection coefficient is defined as a ratio of the reflected to the incident energy (2.7).

$$\alpha_\theta = \frac{E_{t+a}}{E_i} \quad (2.6)$$

$$\alpha_r = \frac{E_r}{E_i} \quad (2.7)$$

Equation 2.5 can be substituted by equations 2.6 and 2.7:

$$1 = \alpha_\theta + \alpha_r \quad (2.8)$$

## 2. Theoretical background

A plane sound wave that moves in positive  $x$  direction can be expressed as

$$p(x) = Ae^{j(\omega t - kx)} \quad (2.9)$$

where  $\omega$  - wave angular frequency, [rad/s]

$k$  - wave number, [rad/m]

$t$  - given point in time, [s]

If an incident wave arrives at infinite surface at  $x = 0$ , the equation for the combined incident and reflected waves in front of the surface can be written as

$$p(x) = Ae^{j(\omega t - kx)} + Be^{j(\omega t + kx)} \quad (2.10)$$

A particle velocity becomes

$$u(x) = \frac{j}{k\rho_0c_0} [-jkA + jkB]e^{j\omega t} = \frac{1}{\rho_0c_0} [A - B]e^{j\omega t} \quad (2.11)$$

If the surface is perfectly reflecting then the amplitude  $A = B$  and the particle velocity is equal to 0 at the boundary. The ratio of the incident to the reflected pressure amplitudes can be written as a complex amplitude ratio

$$r = \frac{B}{A} \quad (2.12)$$

A reflection coefficient in equation 2.8 can be expressed as a complex reflection amplitude ratio  $r$  for the pressure defined in equation 2.12

$$\alpha_r = |r|^2 \quad (2.13)$$

and the absorption coefficient then can be written as

$$\alpha_\theta = 1 - |r|^2 \quad (2.14)$$

The reflecting factor in equation 2.14 can be extended to a function of an incident angle, frequency, material and geometry of absorption [Lon 06].

The random incident angle sound absorption coefficient can be measured in a reverberation room according to ISO 354 [ISO 354].

The equivalent sound absorption area of the empty reverberation room and the reverberation room containing a test specimen can be calculated using the Sabine absorption equations

$$A_{empty} = \frac{55,3V}{cT_1} - 4Vm \quad (2.15)$$

$$A_{test} = \frac{55,3V}{cT_2} - 4Vm \quad (2.16)$$

where

- V - volume of the room, [m<sup>3</sup>]
- c - speed of sound, [m / s]
- T<sub>1</sub> - reverberation time of the empty room, [s]
- T<sub>2</sub> - reverberation time of the room with a test specimen, [s].
- m - damping coefficient for waves in the air.

A damping coefficient for waves in the air is calculated according to ISO 9613-1 [ISO 9613] using climatic conditions that were measured in the room.

The equivalent sound absorption area of the test specimen in square meters can be found from the following equation

$$A_T = A_{test} - A_{empty} = 55.3V \left( \frac{1}{c_2 T_2} - \frac{1}{c_1 T_1} \right) - 4V (m_2 - m_1) \quad (2.17)$$

The sound absorption coefficient of a specimen or a test object can be calculated using formula 2.18

$$\alpha_s = \frac{A_T}{S} \quad (2.18)$$

where

- A<sub>T</sub> is the equivalent sound absorption area, calculated with equation 2.17
- S is the area covered by a test specimen, [m<sup>2</sup>]

## 2.3. Transmission loss

The transmission factor over surface is defined by a ratio of the transmitted sound power to the incident sound power:

$$\tau = \frac{W_{tr}}{W_{in}} \quad (2.19)$$

The sound reduction index or the transmission loss is a logarithmic quantity defined as:

$$R = 10 \log_{10} \left( \frac{1}{\tau} \right) \quad (2.20)$$

By measuring the intensity it is possible to determine the transmitted sound power [Vig 08]. This method is useful when the classical method with diffuse fields doesn't work due to the flanking transmission. The equation for the reduction index using the intensity method is shown below:

$$R_I = 10 \log_{10} \left( \frac{\tilde{p}_s^2}{4\rho_0 c_0 I_R} \right) + 10 \log_{10} \left( \frac{S}{S_R} \right) \quad (2.21)$$

## 2. Theoretical background

where  $\tilde{p}_S^2$  - sound pressure in the sending room, [Pa]

$c$  - speed of sound in the air, [m/s]

$\rho$  - density of the air, [kg/m<sup>3</sup>]

$I_R$  - mean intensity over the surface  $S_R$ , [W/m<sup>2</sup>]

$S_R$  - area of a grid section, [m<sup>2</sup>]

$S$  - area of a party wall, [m<sup>2</sup>]

Equation 2.21 can be simplified to 2.22 for the measurements in situ.

$$R_I = Lp_S - Li_R + 10 \log_{10} \left( \frac{S}{S_R} \right) - 6dB \quad (2.22)$$

where  $Lp_S$  - mean sound pressure level in the sending room, [dB]

$Li_R$  - mean intensity level, [dB]

If only transmission through the partition with the area  $S$  is interesting then equation 2.22 can be simplified to the following [Nie 07]:

$$R_I = Lp_S - Li_R - 6dB \quad (2.23)$$

Equation 2.23 assumes a diffuse field in the sending room. With known volume and reverberation time it is possible to calculate the lower limit of the diffuse field under the hood using the Schroeder equation [Lon 06].

$$f_s = 2000 \sqrt{\frac{T}{V}} \quad (2.24)$$

where  $T$  - reverberation time, [s]

$V$  - volume of the room, [m<sup>3</sup>]

The procedure of measuring the transmission loss in the laboratory was based on the experiments described in [Tro 09]. The baffled panel should be placed between a diffuse and an anechoic space. In the reverberant room, the sound power incident on the baffle is deduced from the average pressure using the following relation

$$W_{in} = \frac{\langle p^2 \rangle}{4\rho c} S \quad (2.25)$$

where  $\langle p^2 \rangle$  is the mean square pressure averaged for all measured positions, [Pa]

$S$  - cross section area of the baffled panel, [m<sup>2</sup>]

$c$  - speed of sound in the air, [m/s]

$\rho$  - density of the air, [kg/m<sup>3</sup>]

In the anechoic space the sound power transmitted through the baffled panel can be calculated from the sound intensity field using equation 2.26

$$W_{tr} = IS \quad (2.26)$$

where  $I$  is an average intensity over the scanned surface,  $[W/m^2]$

$S$  - cross section area of the baffled panel,  $[m^2]$

The transmission loss can be found from equations 2.19 and 2.20.

The calculated and measured transmission loss can take negative values, which is also found in results of the theoretical models and the experiments in the literature (see [Old 93], [Sga 07], [Tro 09], [Sau 70], [Old 93], [Mec 86], [Gom 67]). Of course, in reality the transmitted power cannot be larger than the actual incident power. There are three assumptions in the formulas for the calculated and the measured transmission loss that may cause the negative values. They all are related to the estimation of the incident power. First, for the larger openings the energy density is considerably larger in the neighborhood of the opening, while the calculations assume a constant energy density in the whole enclosure or the sending room. Second, a significant amount of power can be transported at oblique angle through the large openings. The calculations in the SEA model and in the experimental results assume that only the normal component of the oblique waves transports the power through the aperture face. Third, for the small apertures, the edge effect may be significant, therefore considering only the power incident on the area of the aperture (and not including the edge effect) leads to an underestimation of the incident power. This can give a transmission loss larger than unity. The error in the first and the third assumptions originates from the increased energy density locally around the aperture [And 12].

The apertures in the enclosures can create Helmholtz resonator cavities, which increase the noise emitted from a source housed within them. The transmission loss through the opening could be negative in the vicinity of the aperture's resonant frequencies [Lon 06]. The transmission loss behavior depends on the size and the geometry of the aperture and on characteristics of the incident acoustic field.

## 2.4. Statistical Energy Analysis

The statistical energy analysis (SEA) has been widely used and applied to the different noise and vibration control problems. The SEA allows to calculate the energy flow between the connected resonant systems. Statistical analysis does not give any exact information on the system behavior, instead it presents average values over the frequency band and average value for an ensemble of systems which are nominally identical to the actual one, but with a certain statistical spread. Subsystems with many local modes are typically represented using Statistical Energy Analysis subsystems. In SEA the local modes of subsystems are described statistically and the average response of the subsystems is predicted. It is usually not necessary to provide many details when modeling the subsystems using SEA. Therefore, SEA is suitable for modeling the vibro-acoustic systems at the design stage when detailed information about system properties is not

## 2. Theoretical background

available.

Modal energy or energy per mode in subsystem is a primary variable in SEA. The loss factor is used to characterize the energy loss mechanism in the subsystem and the coupling loss factors are used to characterize the power flow between the subsystems.

Figure 2.3 shows a simple block diagram that illustrates SEA method for two subsystems. The total energy in each system is  $E_1$  and  $E_2$ , the modal density is denoted as  $n_1$  for the first subsystem and  $n_2$  for the second subsystem. The input power is marked as  $W^{in}$ , the transmitted power is marked as  $W'$ , and the dissipated or lost power is marked as  $W^{diss}$ , where the index shows the corresponding subsystem.

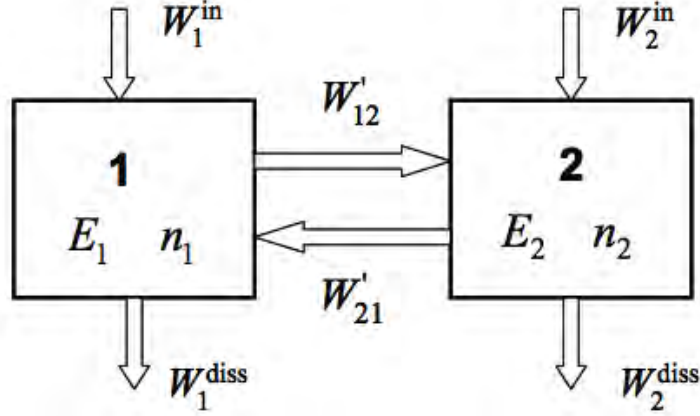


Figure 2.3.: Diagram illustrating power flow between two subsystems.[Fig 08]

The power flow between subsystems can be written as

$$\begin{aligned} W'_{12} &= E_1 \omega \eta_{12} \\ W'_{21} &= E_2 \omega \eta_{21} \end{aligned} \quad (2.27)$$

The equations 2.27 are written for a one-third octave band  $\Delta\omega$ , and  $\omega$  denotes the center frequency of the band.  $\eta_{12}$  and  $\eta_{21}$  are the coupling loss factors from corresponding systems. These equations assume that the waves carrying the energy in one system are uncorrelated with the waves carrying the energy through coupling to the other system.

The net power flow can be written as

$$W_{12} = W'_{12} - W'_{21} = E_1 \omega \eta_{12} - E_2 \omega \eta_{21} \quad (2.28)$$

Equation 2.29 shows the expression for the modal energy

$$E_m = \frac{E}{n \Delta\omega} \quad (2.29)$$

where  $E$  - total energy in the system in the frequency band  
 $n$  - modal density  
 $\Delta\omega$  - bandwidth

With assumption that each resonant mode in the system has the same energy and that the coupling of the individual resonant mode of the first system with each resonant mode of the second system is approximately the same, following equation can be written

$$\frac{\eta_{21}}{\eta_{12}} = \frac{n_1}{n_2} \quad (2.30)$$

Equation 2.30 indicates that when  $E_1 = E_2$  (equal total energies in two systems) then more energy is transferred from the system with smaller modal density to the system with bigger modal density than in another direction.

Combination of equations 2.28, 2.29 and equation 2.30 gives the following formula

$$W_{12} = \omega n_1 \eta_{12} (E_{m1} - E_{m2}) \Delta\omega \quad (2.31)$$

where  $W_{12}$  - net power flow between the system 1 and the system 2 in the band  $\Delta\omega$  centered at  $\omega$

$E_{m1}, E_{m2}$  - modal energies for the system 1 and the system 2.

The principle of the SEA method is given by equation 2.31, which is a simple algebraic equation with an energy as an independent dynamic variable. It states that the net power flow between two coupled systems in a narrow frequency band, centered at a frequency  $\omega$ , is proportional to the difference in the modal energies of two systems at the same frequency. The flow is from the system with the higher modal energy to the one with the lower modal energy.

Equal energy of the modes usually exists if the wave field is diffuse, therefore, SEA works better in the middle and high frequency range. At low frequency the finite element analysis describes each mode explicitly [Ver 06].

## 2.5. SEA in VA-one

The VA-one software is a vibro-acoustic tool based on the methods of the statistical energy analysis. It allows to construct the mathematical models of the energy flow for the complex structures. The implementation of statistical energy analysis in VA-one is based on a wave approach. In the wave approach, which was used here, a system is discretized into a series of the substructures (beams, plates, shells, acoustic ducts, acoustic cavities) that support the wave propagation. Each substructure contains a number of wave types such as bending, extensional, shear waves, etc. Each of this wave type is represented by a separate SEA subsystem. The subsystem can be viewed from the

## 2. Theoretical background

modal and the wave view points. From the modal point of view the system is a collection of the resonant modes, and from the wave point of view it is a collection of the propagating waves.

The SEA model consists of three main modal objects: subsystems, junctions and load sources.

### 2.5.1. SEA subsystems

The SEA subsystem objects are used to create various structural and acoustic components that transmit energy through a vibro-acoustic system.

The SEA module of VA-one software specifies three main types of subsystems:

- SEA structure
- SEA cavity
- SEA semi infinite fluid

The dimensions of the structure and cavity subsystems are assumed to be large or uncertain as compared with the wavelength. The subsystems contain both direct and reverberant fields. The semi infinite fluid describes only the direct field propagation.

The SEA plates and shells are used to describe two-dimensional wave propagation in the structural systems. The plate consists of a surface with three or more boundary edges defined by the nodes.

There are four main types of plate subsystems: flat, single-curved, cylinder and double-curved shells. The differences between the subsystems is related to whether the stiffening effects are accounted for when calculating the properties of the wave fields of the subsystem. Only flat plates were used in the models described in this work. The curvature is negligible in the flat plate.

Each plate subsystem can refer to physical properties of five different types of plates: uniform, sandwich, composite, laminate and ribbed. Uniform and ribbed plates were widely used in the SEA models described in this work. Wave field properties for the uniform plate were calculated using the thin plate theory. Presence of ribs influences the wave field properties of the ribbed plate. Ribs are defined by physical properties of a beam and position on the plate. The beam property calculator script computes a beam physical properties for typical beam sections.

The SEA acoustic cavity subsystems are used to represent wave propagation in the three dimensional space. All cross-sectional dimensions of the cavity are assumed to be large as compared with a wavelength. The acoustic cavity consists of set of faces that enclose the volume of acoustic fluid. The properties of the wave field are based on the speed of sound within the cavity. The overall damping of the cavity can be specified either as a damping loss factor or an absorption calculated from the noise control

treatments or an overall average absorption for the cavity. The absorption computed from the noise control treatment was assigned to the cavities used in the models here. The absorption of a cavity relates the damping of the cavity to the surface area of the cavity. The dissipated power is mainly scaled with changes of the surface area of the cavity but not with the volume of the cavity. The rigid boundary condition is assumed for the SEA acoustic cavity. To model certain cavity face with transparent boundary condition, one should connect it to an adjacent acoustic cavity with special properties or to a Semi-Infinite Fluid object.

The SEA Semi-Infinite Fluid (SIF) object is a sink, and not exactly the SEA subsystem, since it does not contain a reverberant field. In the SEA equations it appears as a damping and it can be used to predict the sound pressure that radiates from the subsystem into an unbounded exterior acoustic fluid. VA-one calculates the power radiating into the semi-infinite fluid with the following assumptions: first, that radiation from the subsystem occurs into the baffled acoustic half space, and second that the vibration fields of the subsystems that are connected to the SIF object do not correlate.

### 2.5.2. SEA junctions

The junctions are used as connections between the various subsystems in the model. They describe the way in which energy is transmitted between the different subsystems. There are three types of junctions in VA-one:

- Point
- Line
- Area

The point junction assumes that the connection is small compared with a wavelength. Line junction assumes that the connection is large compared with a wavelength. The area junction assumes that the connection is finite and baffled. All individual junctions are assumed to be incoherent. The junction can be a hybrid junction that couples the FE and the SEA subsystems together. All types of junctions were used in the models described in this work.

The point junction describes the transmission of the vibration energy between the coupled SEA subsystems. It can be used to describe connection between the subsystems that are small compared with a wavelength.

The line junction describes the energy flow between the SEA subsystems coupled along a line. The line junction describes connection between the subsystems that are continuous and large compared with a wavelength.

The area junction represents energy transmission between the SEA plate or shell and the acoustic cavity or between two acoustic cavities. An FE area junction is used to

## 2. Theoretical background

couple a face of the FE structural subsystem to the nearby FE acoustic subsystem. The hybrid area junction is used to couple the FE structural or acoustic subsystem with the SEA fluid subsystem. The hybrid area junction assumes a rigid baffle boundary condition. The impedance of each SEA subsystem is projected onto the FE mode shapes in the model.

Leaks and apertures of different shapes could be added to the SEA area junction. VA-one supports rectangular, circular, and slit types of apertures. The user-defined leak with user-defined transmission loss spectrum could also be assigned on the junction area.

### 2.5.3. SEA load sources

The sources are used to model energy injection into the subsystems in the vibro-acoustic system. Implemented models were excited with either user-defined power or diffuse acoustic field excitation or constraint excitation.

- User-defined power. This type of source is used as a direct user-defined model of the power that is applied to the subsystem.
- Diffuse acoustic field (DAF). This type of source is used to model a diffuse acoustic pressure load. It can be applied to the face of the SEA subsystem or the FE face. The diffuse acoustic field is characterized by a band-limited RMS pressure spectrum that defines surface pressure across the subsystem face. The surface pressure is an average of the surface pressure at a number of positions across the subsystem. In the reverberation chamber the blocked surface sound pressure level is 3 dB higher than the interior sound pressure level. Diffuse field excitation should be used in conjunction with the semi-infinite fluid when describing the excitation of a subsystem.

This type of the source is used to model the diffuse acoustic pressure load applied to the FE face. The DAF excitation is represented by a “blocked cross-spectral force matrix” for the FE model. Due to the diffuse field load on the given FE face, the blocked force is computed using a special diffuse field reciprocity relationship. The reciprocity relationship relates the blocked force to the radiation impedance for a given face. For the FE subsystem, the radiation impedance is computed using the hybrid area junction formulation assuming that the face is baffled and radiates into a semi-infinite half space.

- Constraint excitation. This type of excitation fixes a response of the subsystem at a known level. An input power that must be supplied to the subsystem in order to satisfy this constraint becomes unknown in the SEA equations.

## 2.6. Finite Elements Method (FE) in VA-one

The subsystems with a very few local modes are often best represented with the Finite Element (FE) subsystems. In the FE, the local modes of the subsystems are described deterministically based on detailed information about the local properties and boundary conditions of the subsystem. Accuracy of the results obtained by the FE model depends on how explicitly properties and boundary conditions of the subsystem are described. The FE subsystems are suitable for describing the response of the first modes and for giving detailed answers on design questions regarding local response of the subsystem. VA-one can model both the FE structural and the FE acoustic subsystems.

The FE acoustic cavity subsystem is used to represent enclosed acoustic fluids in the vibro-acoustic model. Such subsystem can be used to extend SEA model using the hybrid junctions. The FE acoustic cavity subsystem could be created by meshing the existing SEA acoustic cavity subsystem.

The FE faces can be created from elements on the skin of the acoustic cavity. The faces are the interfaces between the SEA and the FE subsystems. They are also used for applying the Noise Control Treatments (NCT) or excitation to the FE acoustic cavity.

The FE structural subsystem is used to represent structural components in the vibro-acoustic model that are stiff or that have relatively few modes.

In VA-one, modes' shapes of the FE subsystems are obtained and used as basis functions to describe response of the FE subsystems in the model. At each frequency of interest a modal dynamic stiffness matrix is assembled. This matrix accounts for the dynamic stiffness of modes, mass, stiffness and damping of any NCTs applied to the FE subsystems.

The excitation applied to the system is represented by an assembled modal cross-spectral force matrix. This is a complex full matrix that defines the auto-spectrums and the cross-spectrums of the forces applied to the modes. Then full random vibration analysis is performed and the modal displacement response is computed at each frequency of interest. The response across the various FE subsystems is then obtained by 'recovering' the nodal response data from the modal responses.

### 2.6.1. NCT, Foam and PEM

The Foam module was used to create advanced models of the noise treatment. With this module it is possible to predict the structural-acoustic effects of complex noise treatment that consists of several layers. The treatment layers can be applied to either FE structural or acoustic subsystems or to SEA subsystems. The Foam module provides six different layer models to recreate foam and fibrous materials. Seventh layer is a fluid and it could be used to insert gaps between the layers to model unbounded conditions between layers.

## 2. Theoretical background

The Noise Control Treatments (NCT) are multi-layered poro-elastic materials designed to isolate structural and acoustic cavities and to provide damping and absorption to the individual subsystem. The Treatment Lay-up is one of the ways to model the noise control treatment and it was used in the models described in this work. The Treatment Lay-up calculates the mathematical model of the lay-up based on behavior of the individual layers and it can be applied to the faces of the FE or the SEA subsystems. It is assumed that the NCT is modeled as an infinite layer, which interacts with a finite region.

The PEM is based on a finite element implementation of poro-elastic, elastic and acoustic equations of motion. For each frequency and each group of contiguous PEM subsystems, the PEM solver computes the finite element dynamic stiffness matrices of a group of elements. Then it computes the coupling matrices of PEM elements with degrees of freedom of the FE structural and acoustic subsystems coupled to the PEM group. After that it projects the coupling matrices onto the structural and acoustic modes and condenses out PEM degrees of freedom from the matrix equation of a coupled system to obtain the modal impedance matrix of the PEM group.

### 2.6.2. Hybrid and custom calculated transmission loss

The hybrid transmission loss calculates the transmission loss between the SEA Diffuse Acoustic Field and the SEA Semi-Infinite Fluid separated by the FE subsystem. The hybrid transmission loss is computed by finding the net power radiated into the Semi-Infinite Fluid and then normalizing it by the incident power. The incident power is calculated based on the sound pressure over the area of the face.

It is possible for the TL to be negative. The TL indicates the power transmitted into the receiving fluid normalized by the net power that is incident on a specified area in a diffuse acoustic field. A negative TL indicates that more power is transmitted into the receiving fluid than is incident on a blocked panel of the same area. The edge effects mean that the actual power that is removed from the source fluid is greater than the power that is incident on the panel if it was blocked.

The custom calculated transmission loss could be obtained in acoustic cavity - panel under test - SIF scenario. The volume of the acoustic cavity should be virtually increased (e.g. 1000 m<sup>3</sup>). If the acoustic cavity is excited with constraint pressure then the incident sound power can be calculated with equation 2.25 and the transmitted power can be collected from the SIF object. The transmission loss can be obtained from the incident and the transmitted sound power ratio (see equations 2.19 and 2.20).

### 3. Thermal and airflow analysis

The encapsulation of the power pack should provide a sufficient noise reduction but should not affect thermal and airflow performances. It is possible to achieve good noise reduction by tuning the cooling system properties. Well designed cooling system should deliver enough volume of air through the system to remove heat.

Thermal characteristics of the enclosure were investigated in two phases.

The first phase was dedicated to estimation of a sufficient airflow rate. The second phase was to find out an enclosure airflow impedance curve. To find the impedance curve a simple model based on a ventilation duct was built. The airflow conditions were estimated at the points where maximum static pressure loss was expected. This model and described procedures were based on the example described in [Ste 91]. The application manual for Cummins power generator shows the same approach on calculation of required cooling air flow rate [Cum 04].

The enclosure impedance curve was plotted together with system curves of different fans. Such data representation is useful and helps to choose suitable fan.

#### 3.1. Airflow rate

Airflow through the enclosure is a result of pressure difference, which creates air flow from the high pressure region to the the low pressure region. The amount of cooling air that flows through the enclosure is usually determined by the amount of heat removed from the enclosure.

The simple thermodynamic model was used to define the sufficient airflow volume. The power pack requirements limit the ambient temperature up to 50°C. And the components inside the enclosure can be heated up to 75°C. It gives the minimum temperature difference  $\Delta T = 25^\circ\text{C}$ .

The required cooling air weighted flow through the power pack can be calculated from the general weighted flow equation.

$$W = \frac{Q}{C_p \Delta T} \quad (3.1)$$

where Q - total heat dissipation, [W]

W - air flow, [kg/s]

$C_p$ - specific heat capacity, [J/kg\*K]

### 3. Thermal and airflow analysis

T - difference between outside and inside temperature, [K].

The total heat dissipation was assumed to be 150 kilowatt. This value is based on the engine specification and it contains heat that is emitted into ambient and heat that goes to a coolant.

The specific heat capacity is a table value and it is temperature dependent.  $C_p = 1009 \frac{J}{kg \cdot K}$  for 20°C.

Equation 3.1 is a mass flow rate. Usually a fan's performance is measured in cubic meter per minute. To get the volumetric flow rate the following equation should be used:

$$G = \frac{W}{\rho} * 60 [sec/min] \quad (3.2)$$

where G - volume flow, [m<sup>3</sup>/ min]

$\rho$  - density of the air, [kg/m<sup>3</sup>].

The density is a table value and it is temperature depended.  $\rho = 1.205 \frac{kg}{m^3}$  for 20°C.

Cubic foot per minute (CFM) is an volume flow unit in the imperial system and it is widely used in fan specifications. To get CFM, the volume flow obtained in equation 3.2 should be converted to cubic foot per minute.

$$F = G * 35.3 \quad (3.3)$$

With given initial data and with help of the equations 3.1, 3.2, and 3.3 the required volume flow can be calculated.

$$\begin{aligned} G &= 296 [m^3/min] \\ F &= 10452 [ft^3/min] \end{aligned} \quad (3.4)$$

The fan that delivers required volume flow could be selected based on calculations described in this part.

## 3.2. Airflow impedance

The airflow through the enclosure creates a static and a velocity pressure. The static pressure is the pressure that is applied on the wall of the enclosure even when there is no air flow. Therefore it is independent of the air velocity. The velocity pressure is the pressure that makes air move at certain velocity through the enclosure. The velocity pressure depends on the air velocity and acts in the direction of the airflow. The static and the velocity pressure is usually expressed in terms of height of a column of water. The water column height is called the head of water and it is denoted as  $H_s$  for the static head and as  $H_v$  for the velocity head.

### 3.2. Airflow impedance

As the air flows through the enclosure it will experience losses due to different obstacles. The convenient way of expressing static pressure loss is in terms of the velocity head at the specific point. For example, there are friction losses at the inlet (see point 1 at Figure 3.1 ). These losses can be expressed as the ratio of the velocity head to the static pressure loss at the inlet. The losses were judged to be equal to one velocity head [Ste 91]. Then the equation 3.5 can be used to find the actual pressure loss in terms of centimeters of water, based on the velocity of the air flow at that point.

$$H_v = \left( \frac{V}{1277} \right)^2 \quad (3.5)$$

where  $H_v$ - velocity head, [cm H<sub>2</sub>O]

V - air velocity, [cm/s]

and constant 1277 is a simplified value that contains acceleration of gravity and air density at 20°C.

If more energy is lost in the enclosure, a larger fan is required to supply that energy. Air velocity must be low to avoid large losses. The system with high losses will require a fan that can supply the needed cooling of air at high pressure.

Since detailed airflow analysis of the encapsulated power pack is out of scope of this work, a simple model was built to analyze the pressure drops. Model was based on the airflow inside the duct with the inlets, the outlets, and geometry inconstancy (see Figure 3.1). At the points marked with numbers, maximum static pressure loss is expected.

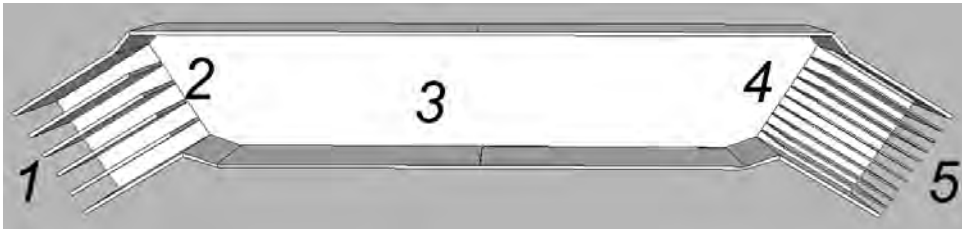


Figure 3.1.: Sketch of the simplified model used to describe the airflow impedance.

The losses in terms of velocity heads for the points marked at Figure 3.1 are described below.

1) Air inlet.

The number of velocity heads losses depends on type of a duct opening. In our model the plain duct ends were used. The duct end of this type can be expected to show a static pressure loss of 0.93 velocity heads and could be rounded to 1.0 velocity head [Ste 91]. The static pressure loss in terms of velocity heads losses can be found from the following equation:

### 3. Thermal and airflow analysis

$$H_1 = 1.0H_{v1} \quad (3.6)$$

There are five inlets in the model used. The length of the single inlet is 0.87 m and the height is 0.12 m.

#### 2) Turn and expansion.

The turn used in the model was assumed to be sharp. Such turn creates the pressure loss, which in this work was assumed to be 0.5 velocity heads [Ste 91].

Usually, a loss of one velocity head is the result of expansion [Ste 91]. Therefore, total losses at the point 2 can be found from equation 3.7.

$$H_2 = 1.5H_{v2} \quad (3.7)$$

Assumed area of this section is equal to  $0.6 \text{ m}^2$ .

#### 3) Losses due to the friction.

Here losses occur due to the friction of the heat exchanger and the rough components inside the enclosure. The estimated pressure loss was equal to 2.0 velocity heads [Ste 91].

The losses can be found from equation below:

$$H_3 = 2.0H_{v3} \quad (3.8)$$

The area of this section is equal to  $1.2 \text{ m}^2$ .

#### 4) Contraction and turn.

The contraction leads to the pressure loss of 0.5 velocity heads. The turn is similar to the turn in second point and the pressure loss here is estimated to be 1.0 velocity head [Ste 91]. Therefore, the losses in this point are:

$$H_4 = 1.5H_{v4} \quad (3.9)$$

The area of this section is equal to  $0.6 \text{ m}^2$ .

#### 5) Exhaust.

This gives information about how much energy is thrown away at the exit. Since the cool air exhausts from the enclosure, it will expand suddenly, so it will lose its velocity completely [Ste 91].

$$H_5 = 1.0H_{v5} \quad (3.10)$$

There were 16 outlets considered for the air outlet. The area of the single outlet is  $0.06 \text{ m}^2$ .

The method, which was used, assumes several different CFM flow rates through the box. It is possible to determine the static pressure drops for different points for each flow rate. The range of airflow rates is from 100 CFM to 20000 CFM.

### 3.2. Airflow impedance

Using equation 3.11 it is possible to calculate the air velocity with given CFM rate and known area of the cross section. In the model used, the air is delivered through five inlets and exhausted through 16 outlets. The number of ducts that are formed from the inlets and the outlets should be included into equation. The area parameter in such case should be the area of one duct.

$$V \left[ \frac{cm}{sec} \right] = \left( \frac{1 \left[ \frac{feet^3}{min} \right] * 0.02831 \left[ \frac{m^3}{feet^3} \right] * \frac{1}{60} \left[ \frac{min}{sec} \right]}{Area [m^2] * Number\ of\ Ducts} \right) * 100 \left[ \frac{cm}{m} \right] \quad (3.11)$$

Since losses were estimated in terms of velocity heads, equation 3.5 should be used to convert the air velocity into velocity heads.

The static pressure loss for the specific point can be determined from the corresponding equation 3.6 - 3.10.

Then, to get the pressure loss for selected flow rate, a sum of pressure loss for each point was calculated. The airflow impedance curve was plotted from the total static pressure loss. See Figure 3.2 for the airflow impedance curve of the model used.

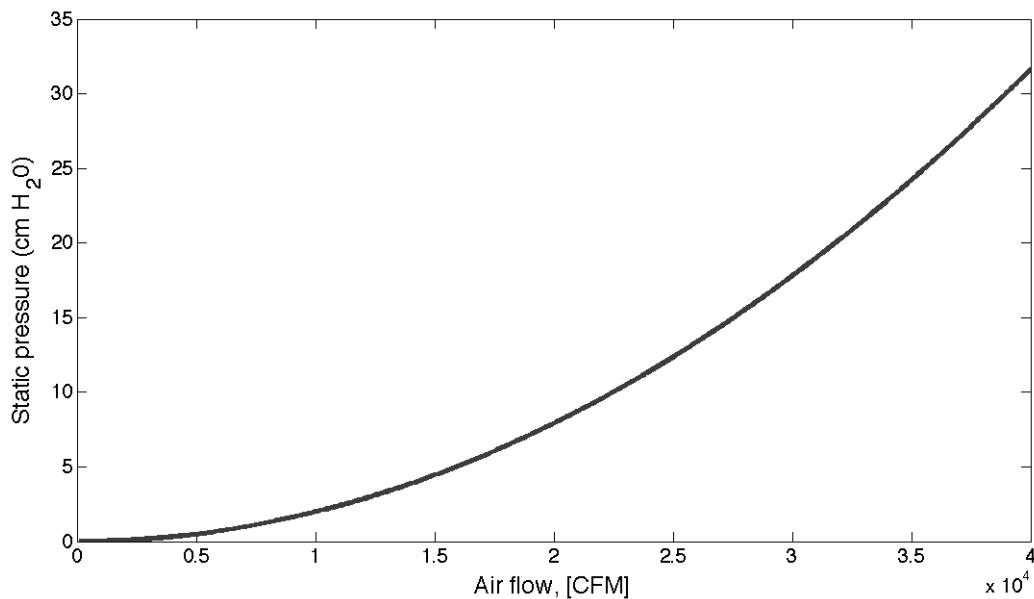


Figure 3.2.: The airflow impedance curve.

Several system curves of different fans were used and are plotted in Figure 3.3 together with the airflow impedance. Different fans' specification is presented in Table 3.1. The fans' diameter is 32 inch (80 cm).

### 3. Thermal and airflow analysis

Table 3.1.: Fan specifications

Fan	No of blades	Blade angle, [°]	Speed, [RPM]	Optimal Airflow, [cfm]	Lw, [dB]
1	8	45	1750	15700	107
2	16	45	1750	15800	101
3	8	41	2600	23300	110
4	8	50	1750	15300	111
5	5	16.5	1750	13700	106
6	12	41	1750	14400	107
7	8	21.5	2600	15500	112

The optimal airflow can be determined from Figure 3.3. It is the projection of intersection of the enclosure impedance curve with the system curve of a fan on airflow axis. The sound power level is specified for the optimal airflow rate and it can vary due to different flow rates.

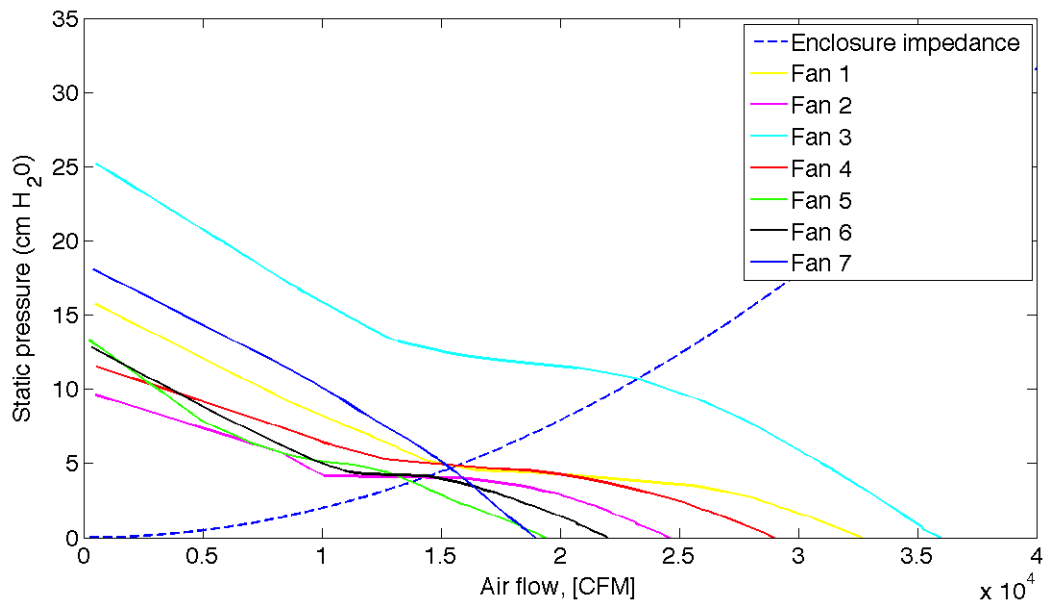


Figure 3.3.: The system curves of the fans and the enclosure impedance

Estimated amount of the airflow is 10452 CFM ( $296 \text{ m}^3 / \text{min}$ ). Any of listed fans (see Table 3.1) can deliver the required airflow, therefore any of them can be used.

## 4. Measurements

The current chapter contains information about the measurements that were done and the results of these measurements. The values which were obtained during the measurements were used to validate and to populate the computer models.

### 4.1. Noise sources and total noise

Four main noise sources were defined: the engine with the cooling system, the external fan, the exhaust, and the intake filter. The intensity method based on ISO 9614-2 [ISO 9614] was used to measure emitted noise spectrums from the power pack's main noise contributors and from the working encapsulated power pack. See Figure 4.1 for sources' spectrums. The total sound power of each contributor is presented in Table 4.1.

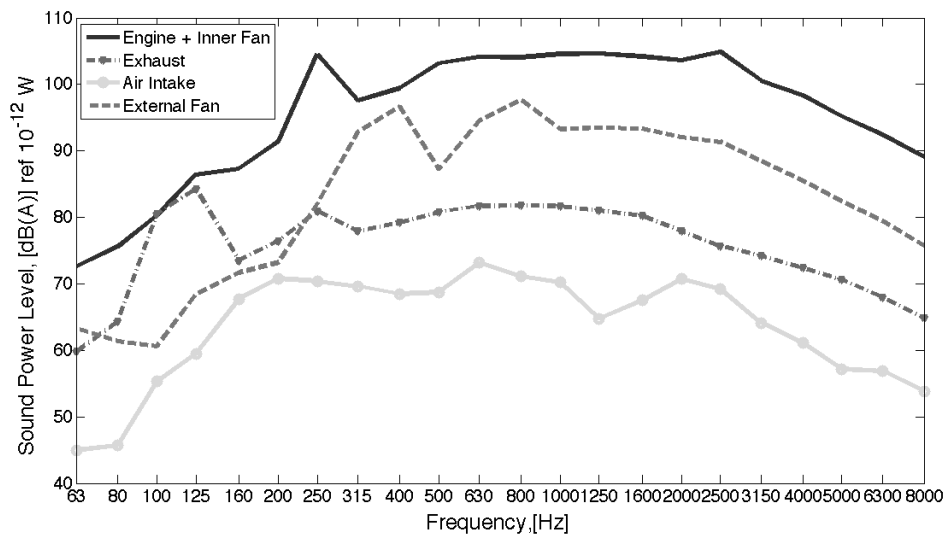


Figure 4.1.: The sound power spectrums of the main noise sources.

#### 4. Measurements

Table 4.1.: Total sound power levels of the main noise sources.

Source	Description	Sound power, [dB(A)]
Engine and inner fan	ISO 9614-2	114
External fan	ISO 9614-2	104
Exhaust	ISO 9614-2	92
Air intake	ISO 9614-2	81

The total emitted sound power level of the power pack without encapsulation, the encapsulated power pack, and the encapsulated power pack with the working external fan is presented in Table 4.2. The sound power spectrums for the mentioned cases are presented at Figure 4.2.

The sound power level for the encapsulated power pack with the external fan as well as the sound power level for the power pack without encapsulation plus the external noise sources (the external fan, the exhaust, the air intake) were calculated from the separate measurements using equation

$$Lw = 10 \log_{10} \left( 10^{\left(\frac{Lw1}{10}\right)} + \dots + 10^{\left(\frac{Lwn}{10}\right)} \right) \quad (4.1)$$

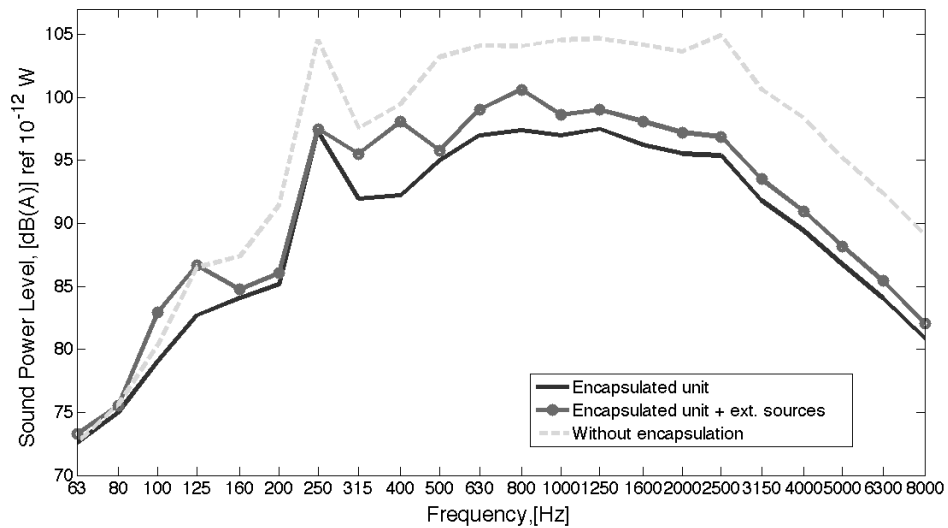


Figure 4.2.: The sound power spectrums of the working unit.

Table 4.2.: Total sound power levels of the investigated cases

Cases	Description	Sound power Level, [dB(A)]
Encapsulated power unit	ISO 9614-2	106.8
Encapsulated power unit with external noise sources	Calculated	108.9
Power unit without encapsulation with external noise sources	Calculated	114.5

The sound pressure level was measured from each side at the distance of 1 meter from the enclosure. The reference source with known sound power was placed under the hood. This measurement was done to validate the developed VA-one model. The spectrum of the mean sound pressure level at 1 m distance and the spectrum of the background noise are presented at Figure 4.3.

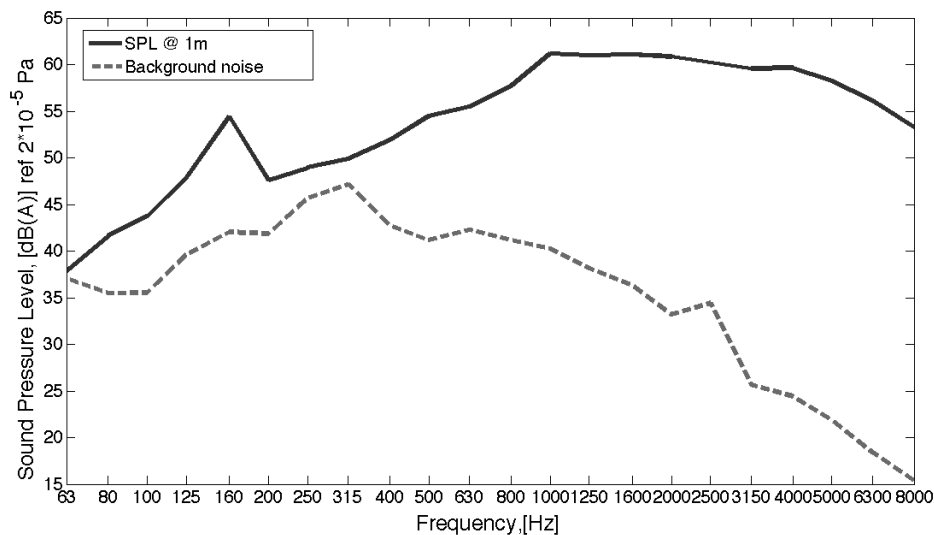


Figure 4.3.: The mean sound pressure level at the distance of 1 meter from the enclosure.

## 4.2. Absorption

The noise treatment inside the enclosure consists of 50 mm foam covered with thin viscous-elastic material (Figure 4.4). The viscous-elastic layer protects foam from hostile environment, but it decreases absorption properties of the foam in high frequency region.

#### 4. Measurements

The absorption coefficient of the noise treatment was measured with the impulse technique inside the encapsulation during the field measurements and in the laboratory. Impulses were created by popping balloons. The reverberation time (T20) was measured by the B&K inspector. The absorption was calculated using the Sabine equation (see equations 2.16 and 2.18).



Figure 4.4.: The absorption material installed on the power pack encapsulation

##### 4.2.1. Field measurements

The reverberation time inside the enclosure was measured using the impulse technique. The impulse response was measured at four microphone positions. The volume under the hood is equal to 5.29 cubic meters. The mean reverberation time equals to 0.18 seconds. The frequency representation of the reverberation time is shown at Figure 4.5. The lower limit of the diffuse field was calculated with the Schroeder equation and was equal to  $f_s = 370\text{Hz}$ . Therefore, the results from the measurements are not reliable below this frequency.

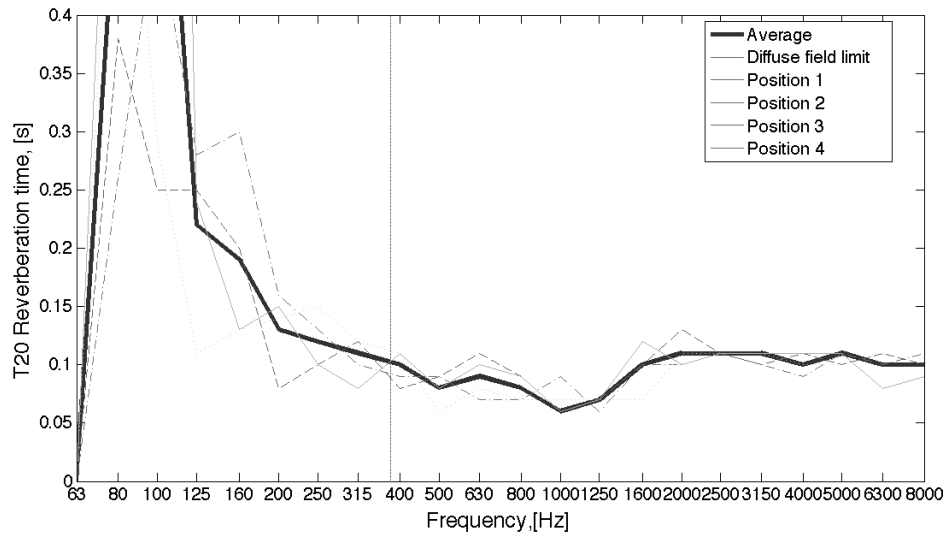


Figure 4.5.: The mean reverberation time and the reverberation time measured at four positions.

The absorption coefficient of the noise treatment was calculated as described in Section 2.2. The calculated absorption coefficient and the coefficient provided in a data sheet from a sub supplier are presented at Figure 4.6.

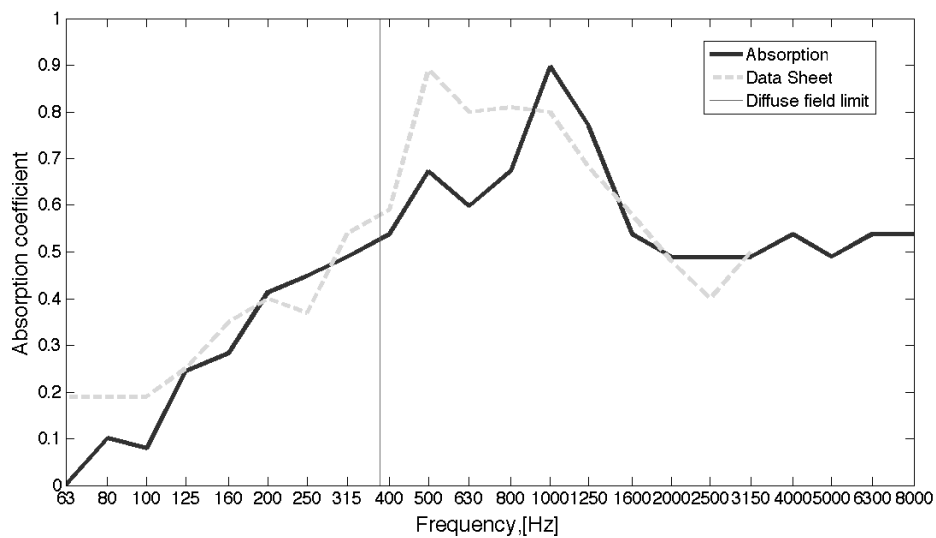


Figure 4.6.: The measured and the provided absorption coefficients of the treatment used in the enclosure.

#### 4. Measurements

##### 4.2.2. Laboratory measurements

The absorption coefficient of the power pack's noise control treatment was measured in the laboratory. Volume of the reverberation room equals to  $73.5 \text{ m}^3$  and the mean reverberation time is 1.55 seconds. The Schroeder frequency of the chamber is around 300 Hz. The spectrum of the background noise is presented at Figure 4.7.

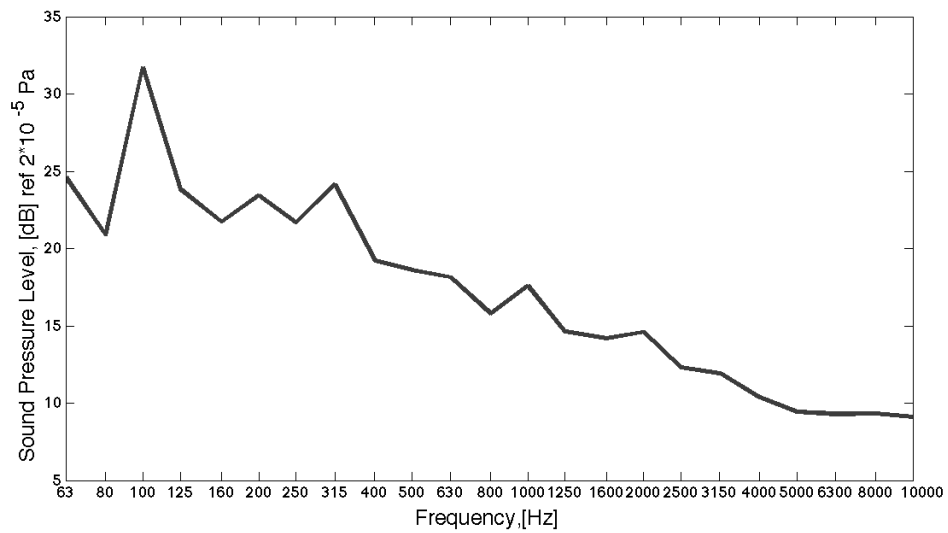


Figure 4.7.: The spectrum of the background noise in the laboratory.

The impulse responses were measured at three microphone positions in the reverberation room. See Figure 4.8 for the reverberation time - frequency representation of the measurements done in the empty room.

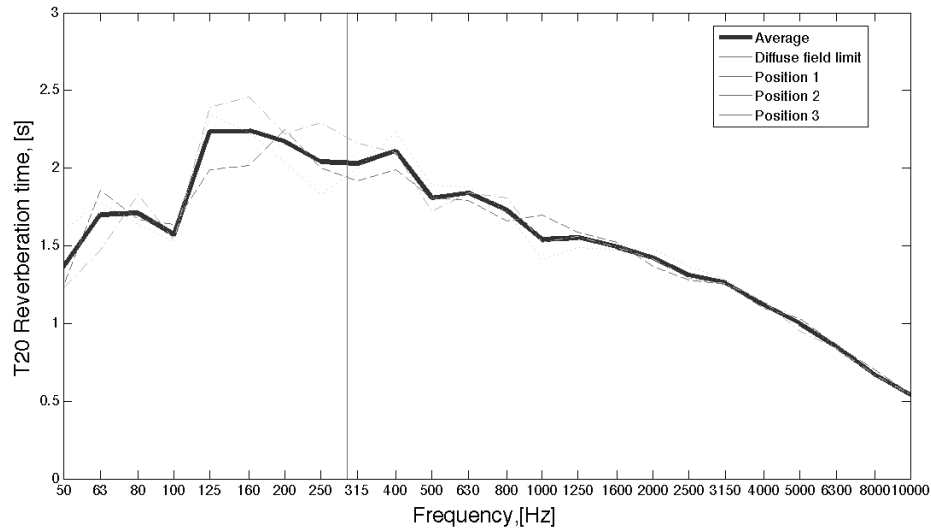


Figure 4.8.: The mean reverberation time and the reverberation time measured at three positions in the empty room.

The floor of the chamber was covered with the same absorption material as installed in the enclosure. The absorption panels covered an area of  $6 \text{ m}^2$ . The edges of the panels were covered with a tape to decrease the edge effect for the high frequency. The reverberation time - frequency representation of the measurements done in the room with the samples is presented at Figure 4.9.

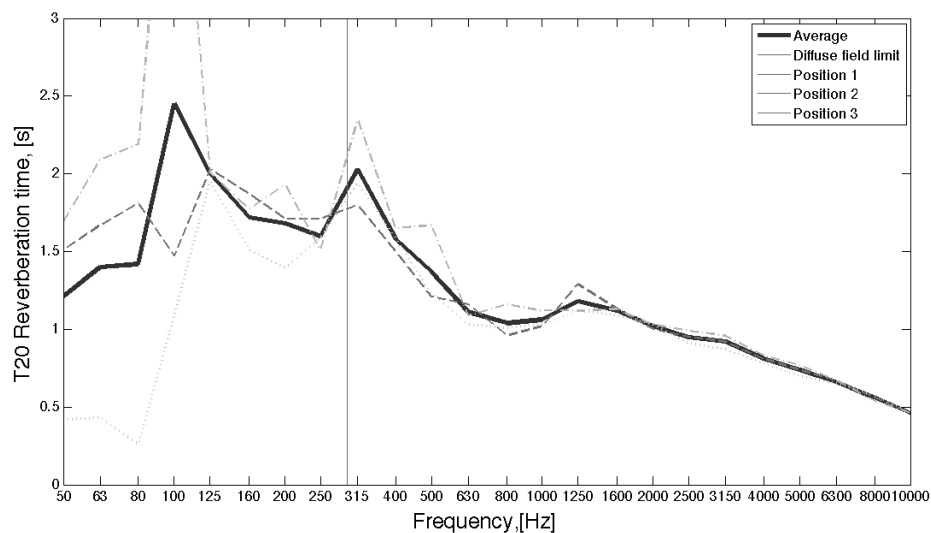


Figure 4.9.: The mean reverberation time and the reverberation time measured at three positions in the room with the absorption material samples.

#### 4. Measurements

The absorption coefficient was calculated according to ISO 354 as described in Section 2.2.

The foam absorption coefficient measured in the laboratory and inside the power pack enclosure, as well as the data from a sub supplier are presented at Figure 4.10 .

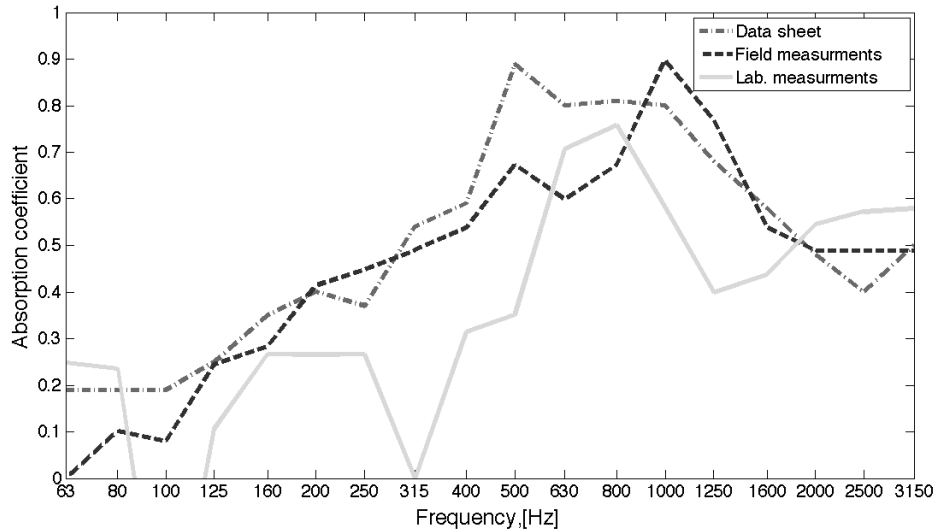


Figure 4.10.: Comparison of the absorption coefficients obtained during laboratory and the field measurements with the data from a sub supplier.

### 4.3. Transmission loss

The transmission loss of each baffled panel, solid panel, and leakage through the apertures on the enclosure's roof was measured in the field. The transmission loss of the front baffled panel was measured in the laboratory. The transmission loss was measured as described in Section 2.3. The reference sound power source was used to excite the sending volume.

#### 4.3.1. Field measurements

The reference sound power source was placed under the empty frame (see Figure 4.11). The sound pressure level at four positions was measured under the hood. The intensity scans were performed outside of the enclosure over the areas of interest. The transmission losses were calculated with equation 2.23.



Figure 4.11.: The reference source under the hood.

The transmission loss of the front and the rear baffled panels and the transmission loss of the leakage at the roof are presented at Figure 4.12.

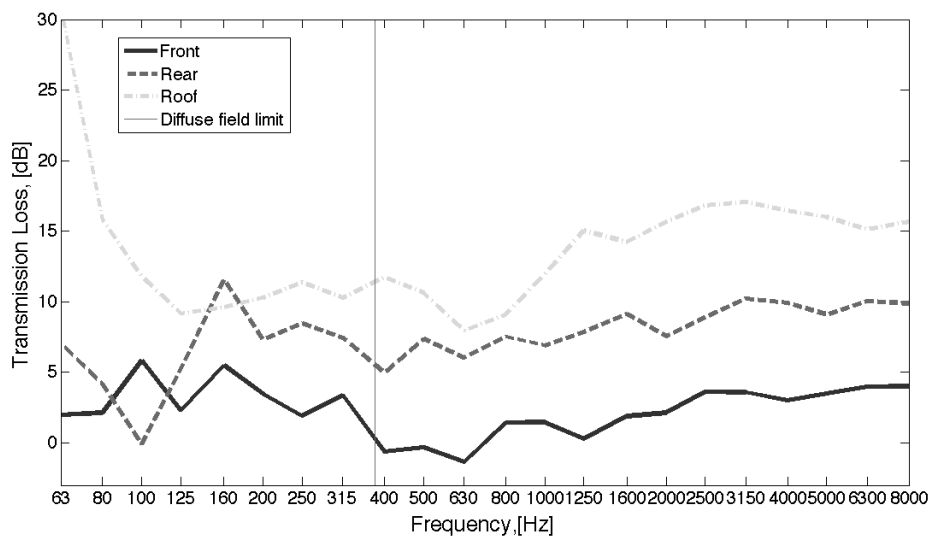


Figure 4.12.: Comparison of the transmission losses of the front and the rear baffled panel together with the transmission loss measured through the leaks at the roof.

The transmission loss of the baffled panels at the left side of the encapsulation is presented at Figure 4.13. The transmission loss of the baffled panels at the right side of the encapsulation is presented at Figure 4.14.

#### 4. Measurements

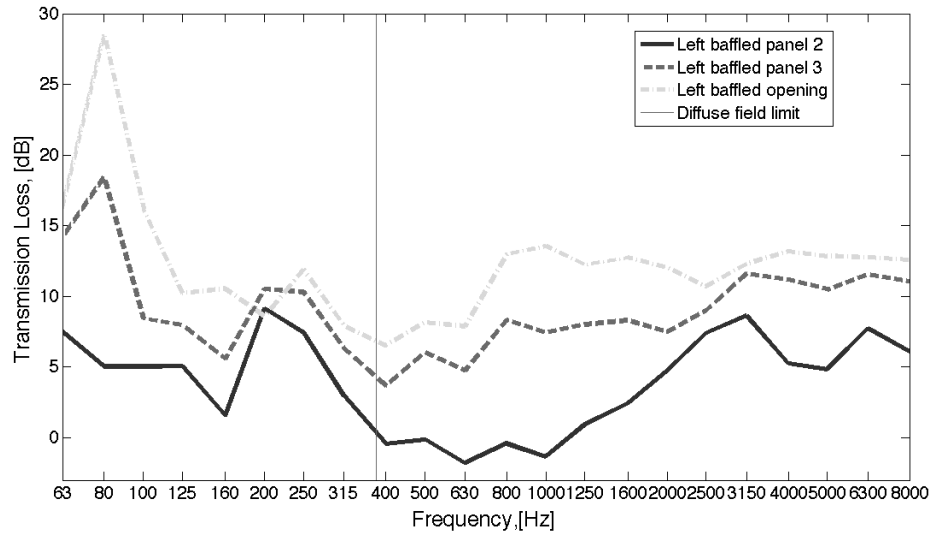


Figure 4.13.: The transmission losses of the baffled panels at the left side of the encapsulation.

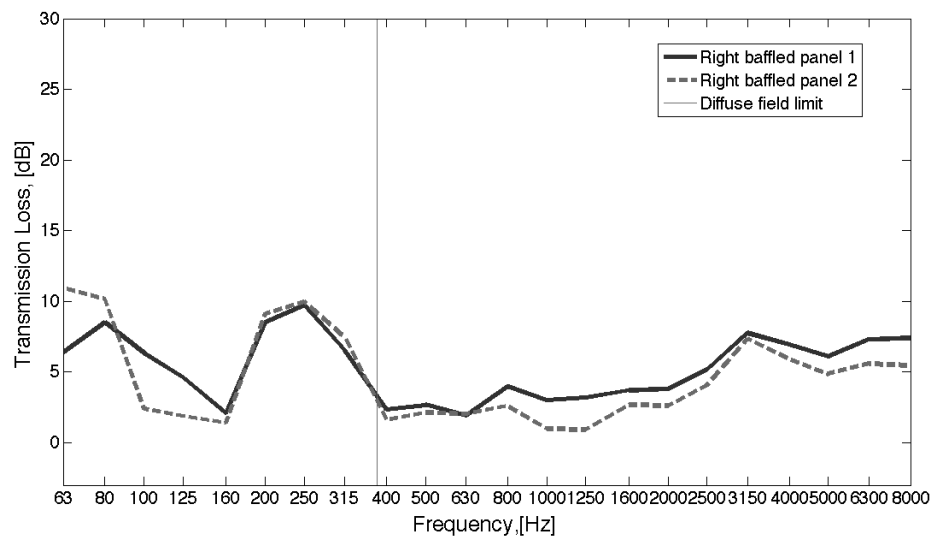


Figure 4.14.: The transmission losses of the baffled panels at the right side of the encapsulation.

The transmission loss of the solid panel without openings is presented at Figure 4.15.

### 4.3. Transmission loss

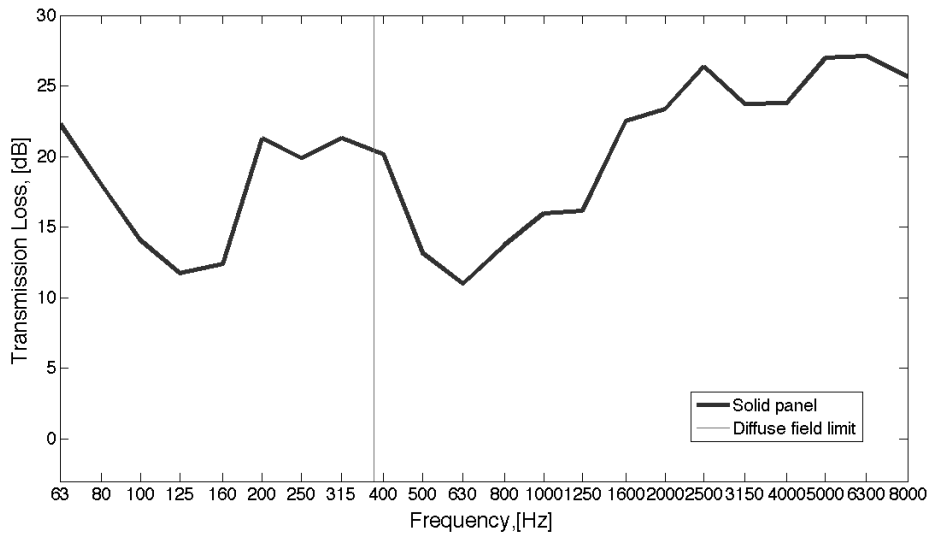


Figure 4.15.: The transmission loss of the solid panel.

The transmission loss of all baffled panels and the leakage through the aperture at the roof are presented at Figure 4.16. The transmission loss of the front baffled panel is highlighted since this panel was ranked as a panel with the weakest reduction performance.

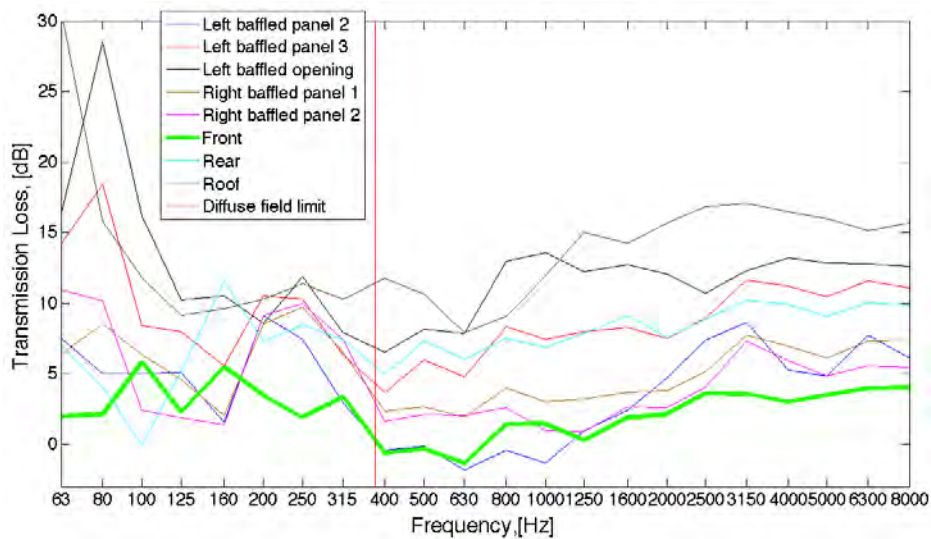


Figure 4.16.: The transmission losses of all baffled panels.

## 4. Measurements

### 4.3.2. Laboratory measurements

The transmission loss measurements of the front baffled panel were done in the laboratory. The baffled panel was mounted in the wall between the reverberation and the treated semi-diffuse rooms (see Figure 4.17)



Figure 4.17.: Photos of the setup for the laboratory measurements of the transmission loss of the front baffled panel.

The measurements procedure was based on the experiments described in [Tro 09].

The volume of the emission chamber is 72 cubic meters. The mean reverberation time is 1.55 seconds (see Figure 4.8 for the reverberation time - frequency representation). The sending room was excited with the reference sound power source. Two positions were used for the reference source. One position was in the middle of the room. Another position was one meter away from the baffled panel. This setup should give better agreement with the field measurements, since mainly direct field load incidents the panel face.

The sound pressure level was measured at six positions in the sending room. See Figure 4.18 for the spectrums of the measured sound pressure levels.

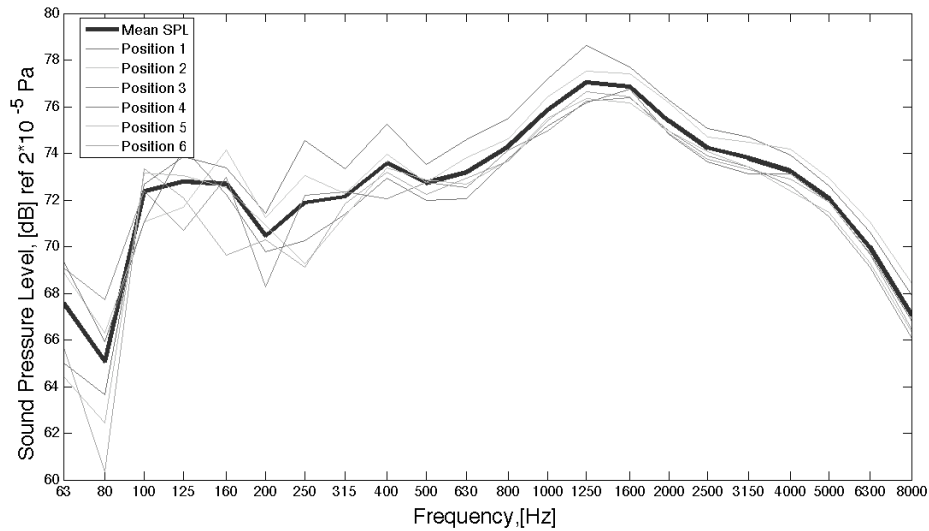


Figure 4.18.: The mean sound pressure spectrum and the sound pressure spectrums measured at six positions.

The receiving room was treated with different types of absorption material and acoustic carpets in order to damp diffuse sound field. The intensity scans were performed over the baffled surface in the receiving room. In the free field the pressure and the intensity levels in a direction of propagation are numerically the same. Since the measurements were done not in the free-field condition, the reflected sound waves could influence the results. The difference between the pressure and the intensity could be used as a quality measure, for example in the diffuse field the intensity could be low even when the pressure is high [BaK 93]. This difference is called the pressure-intensity (P-I) index. The P-I indexes - frequency representation for three intensity scans are shown at Figure 4.19.

#### 4. Measurements

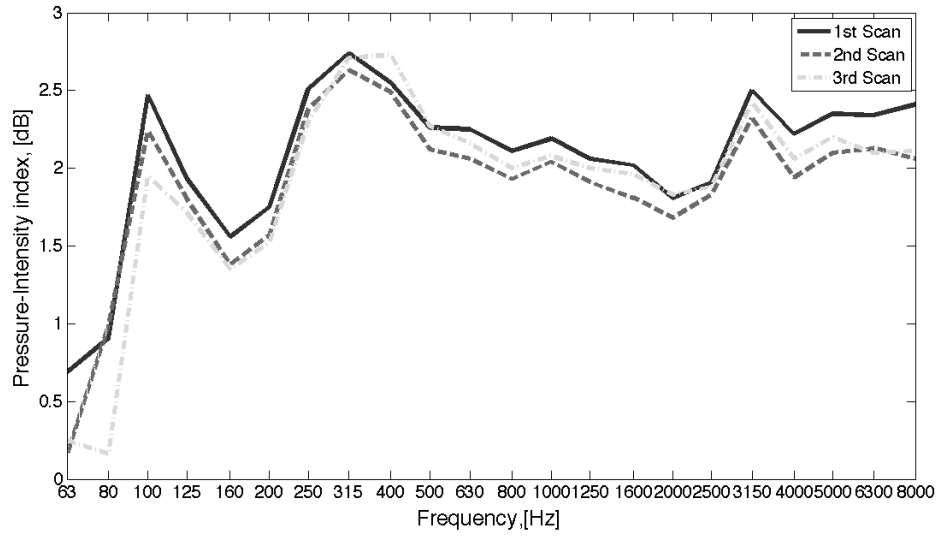


Figure 4.19.: The Pressure-Intensity index for the intensity scans.

The transmission loss for the cases when the reference source was in the center of the room and one meter away from the baffled panel, as well as the result from the field measurements are shown at Figure 4.20.

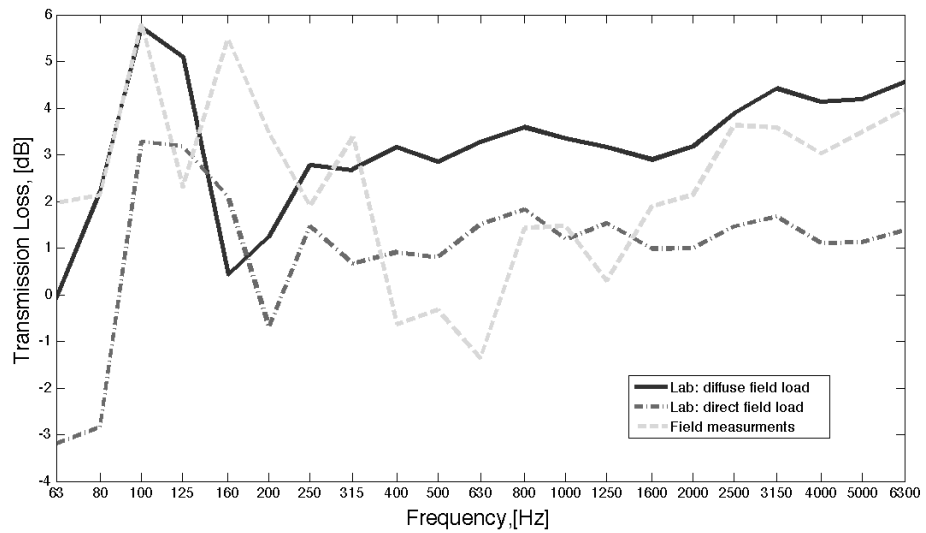


Figure 4.20.: The transmission losses during the laboratory and the field measurements of the front baffled panel.

## 4.4. Temperature and airflow

The airflow and the temperature measurements were done on the working power pack unit. The area facing the front baffle was scanned with the airflow probe. The air velocity and the air temperature are presented in Table 4.3. The ambient temperature during measurements was 6°C.

Table 4.3.: The temperature and the airflow measured at the panel inlets.

	Airflow, [m/s]	Temperature, [°C]
Slot 1 (upper)	6.7	8.7
Slot 2	8.9	7.4
Slot 3	10	8.1
Slot 4	12	8.7
Slot 5 (lower)	13.7	8.5

The temperature under the hood and the surface temperature were also measured and are presented in Table 4.4.

Table 4.4.: The temperature under the hood and on the component's surfaces.

	Temperature, [°C]
Air cavity under the hood	22.9
Radiator (top)	24.5
Radiator (bottom)	3
Average at the surface	73
Maximum at the surface	135

### 4.4.1. Estimated noise from the airflow

For small Mach numbers, the Lighthill scaling law (see equation 4.2) for quadruple noise source can be used to estimate the contribution of the noise from the airflow [Abo 06].

$$\overline{W}_q = \frac{\rho_0 U^8 D^2}{c_0^5} \quad (4.2)$$

where  $U$  - flow speed, [m/s]

$D$  - distance between two baffles, [m]

$\rho$  and  $c$  - air properties.

The estimated noise sound power from the turbulent air flow was computed and it equals to 63 dB. The sound power levels of the main noise contributors are much higher

#### 4. Measurements

than the noise from the air flow (see Table 4.1 for major noise sources). Thus, the noise from the air flow can be neglected in the model.

### 4.5. Conclusion

The measurements, which are described in this chapter, were made in the field and in the laboratory. Obtained sound power levels of the main noise contributors will be used to load the VA-one model of the complete power pack unit. The sound power spectrums of three cases will be used to validate the results of computer simulation of the same cases. The mean sound pressure level measured one meter away from the power pack will be used to validate the power pack model loaded with the sound power spectrum of the reference source. The airflow measurements are required for the fluid dynamic simulation.

The absorption measurements are needed to compare the results with the treatment designed in VA-one. Although, the absorption was measured in the real encapsulation in the field and in the laboratory under the controlled conditions, the agreement between the absorption coefficients obtained and provided by a sub supplier is not very good (see Figure 4.10). The absorption coefficients provided by a sub supplier were measured in the impedance tube, which assumes one dimensional normal incident waves. On the other hand, the impulse technique that was used in the laboratory and during the field measurements assumes random incident angle. Moreover, the diffuse field limitations affect the results in low frequency range. Therefore, the manner of how the samples were installed in the reverberation room as well as the edge effect and the area covered could have a significant impact on the absorption coefficients obtained.

The transmission loss of all panels was measured and ranked. Both field and laboratory measurements depend on the diffuse acoustic field assumption, hence results in low frequency are not reliable. The field and laboratory results could not be comparable since the direct field was dominant during the field measurements while the diffuse field was supreme in the laboratory. The measurements in the laboratory were more controlled as compared to the field measurement. Therefore, it was decided to validate the transmission loss obtained from the VA-one models of the front baffled panel with the results from both laboratory and field measurements.

## 5. Computer models

The purpose of this study was to build the acoustical model of the power pack encapsulation and its components and to investigate the possibilities of increasing sound reduction properties of the encapsulation. The results obtained during the measurements were used to validate the model. The acoustic simulations were done in VA-one software. The fluid dynamic simulations here and in Subsection 6.1.2 were done by Jari Hyvarinen (see Acknowledgements) in ANSYS software.

### 5.1. Absorption modeling

The absorption used in the FE models was designed as a noise control treatment layout. The noise control treatment, which was built, was based on factory presets and consisted of a foam and rubber panel. A typical car foam with thickness 0.05 m was used to represent the foam installed in the power pack enclosure. The absorption coefficient of the typical car foam is presented at Figure 5.1.

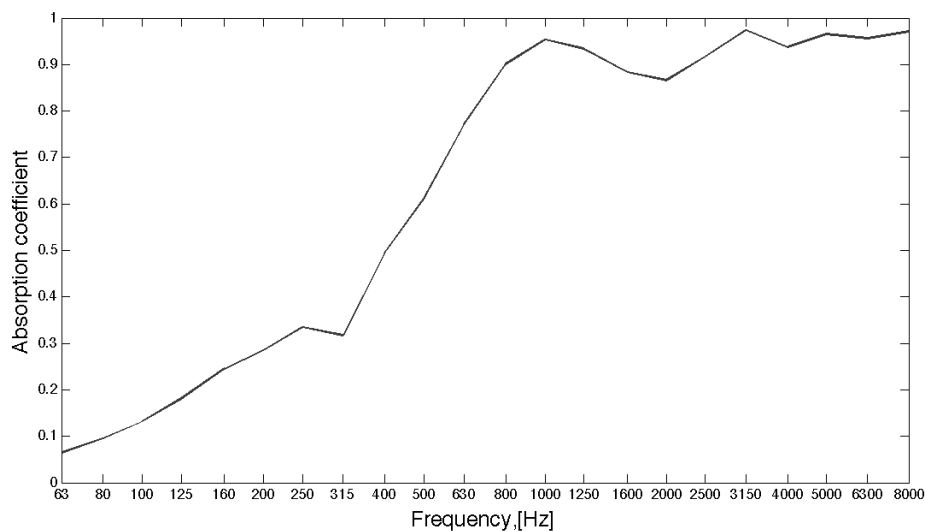


Figure 5.1.: The absorption coefficient of the typical car foam.

The absorption material used in the power pack enclosure is protected with a visco-elastic layer that decreases absorption properties at high frequency region (see Figure

## 5. Computer models

4.10). A hard rubber panel with thickness 0.0001 m was used as a visco-elastic layer. The absorption coefficient of the modeled noise control treatment is presented at Figure 5.2.

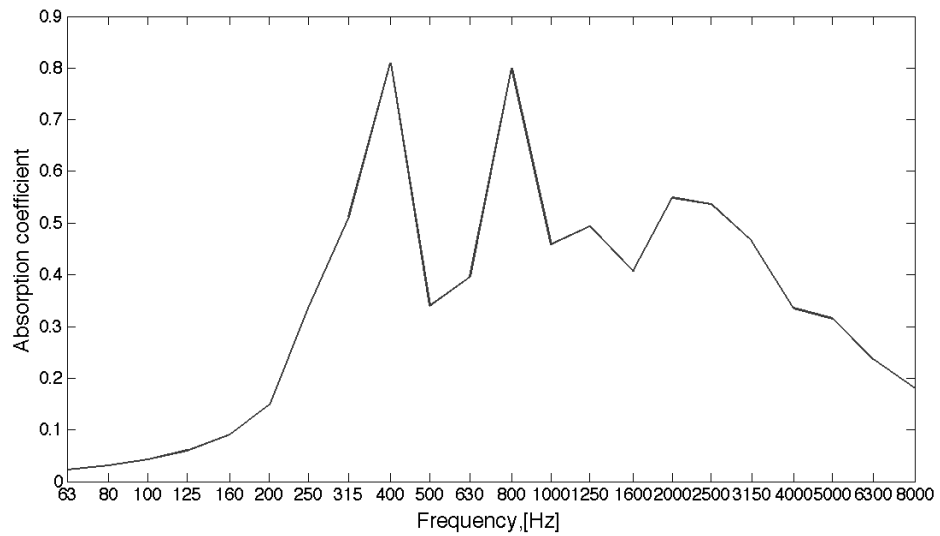


Figure 5.2.: The modeled absorption coefficient for the VA-one models.

The absorption coefficient of the modeled noise control treatment, the measured absorption coefficient in the field and in the lab, and the absorption coefficient provided in a data sheet of the absorption material from a sub supplier are presented at Figure 5.3.

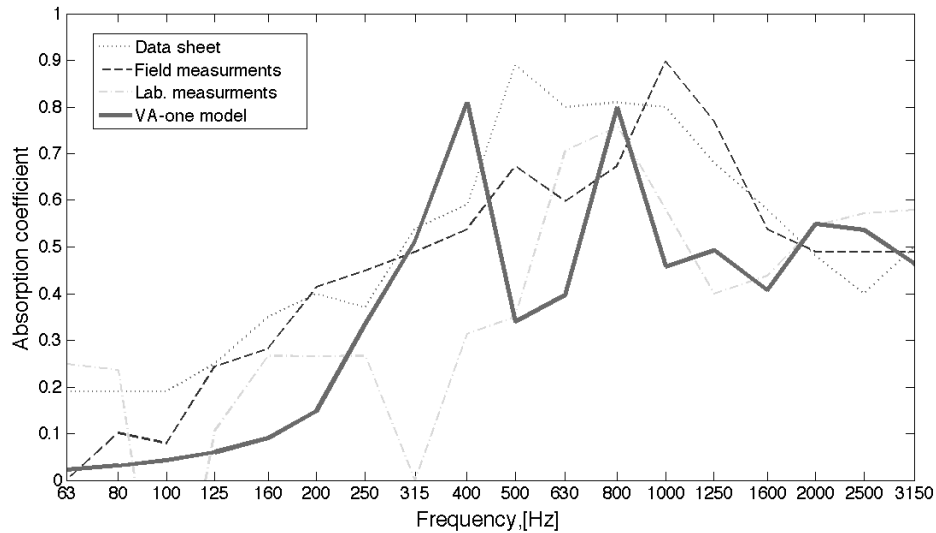


Figure 5.3.: Comparison of the absorption coefficients modeled in VA-one, measured in the laboratory, measured in the field, and provided in a data sheet.

The noise control treatment layer could be extruded as a poro-elastic material subsystem. VA-one version<sup>1</sup>, which was used, did not allow solving the model with merged foam and panel configuration, therefore only a typical car foam layer was used in the PEM model of the absorption.

## 5.2. Model of solid panel

The SEA and FE models of the solid panel were built in VA-one to investigate the panel noise reduction properties. The CAD model of the solid panel was imported in VA-one and recreated as a FE model. The SEA models were built directly in VA-one. The SEA and FE models of the panel have the same dimensions as the physical panel from the enclosure. The height of selected panel is 1.12 m and the width is 0.93 m.

### 5.2.1. SEA model

The simple SEA plate was built to find the coincident frequency of the panel. The plate material was set to steel and the thickness was set to 3 mm. The SEA acoustic cavity was built on one side of the panel. The wave numbers in the plate and in the air were compared and are presented at Figure 5.4.

<sup>1</sup>VA-one 2011

## 5. Computer models

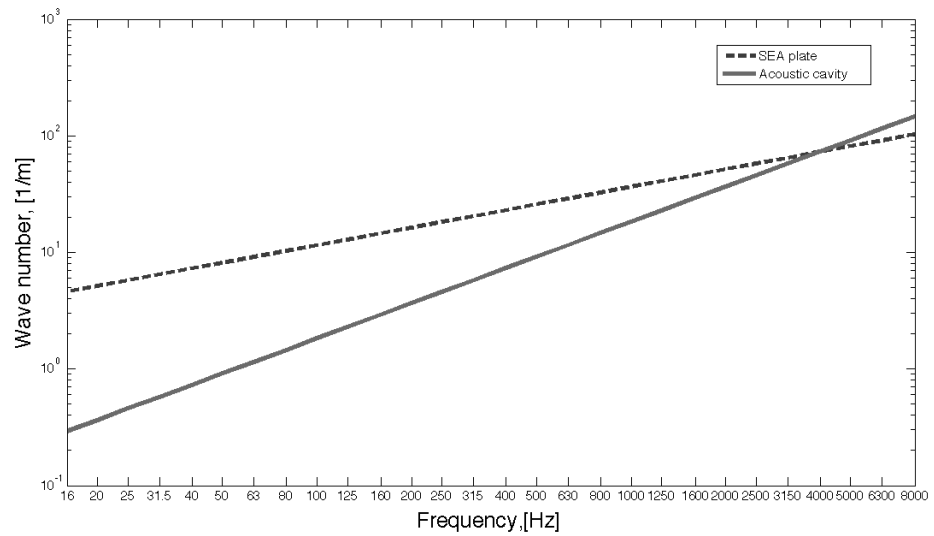


Figure 5.4.: The wave numbers in the simple steel plate and in the air.

The coincidence frequency of the simple 3 mm steel plate is around 4000 Hz. The SEA plate was coupled to the anechoic space on one side and the reverberation space on the other side. This configuration represents the lab condition, in which the transmission loss can be measured [Klo 02]. The semi-infinite fluid object represents the anechoic space. The reverberation space was recreated with the acoustic cavity. Its volume was virtually increased to 1000 m<sup>3</sup> and it was excited with a constraint pressure equal to 1 Pa for all frequencies. See Figure 5.5 for the SEA model of the plate.

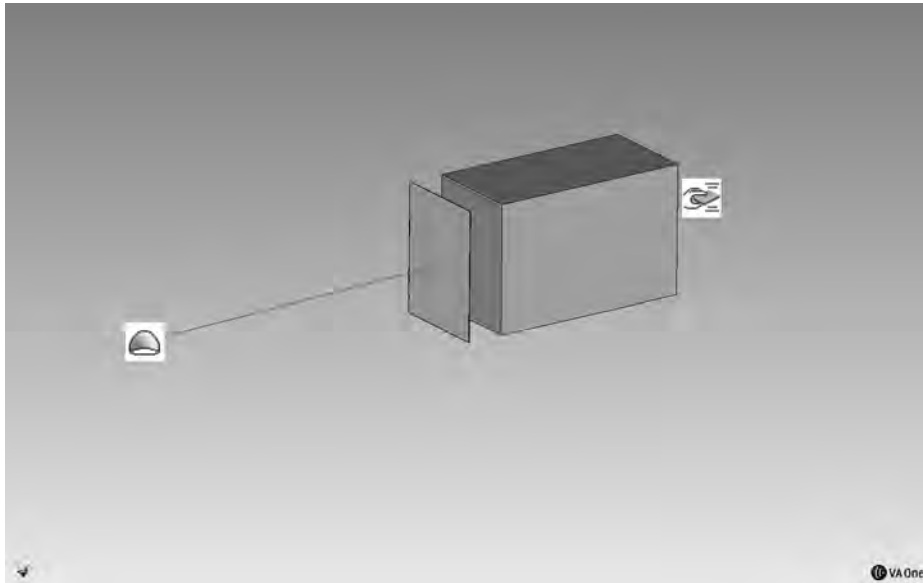


Figure 5.5.: The VA-one model for the transmission loss measurements of the simple SEA plate.

The transmission loss of the simple SEA plate was calculated using the procedure explained in Subsection 2.6.2 and is presented at Figure 5.6.

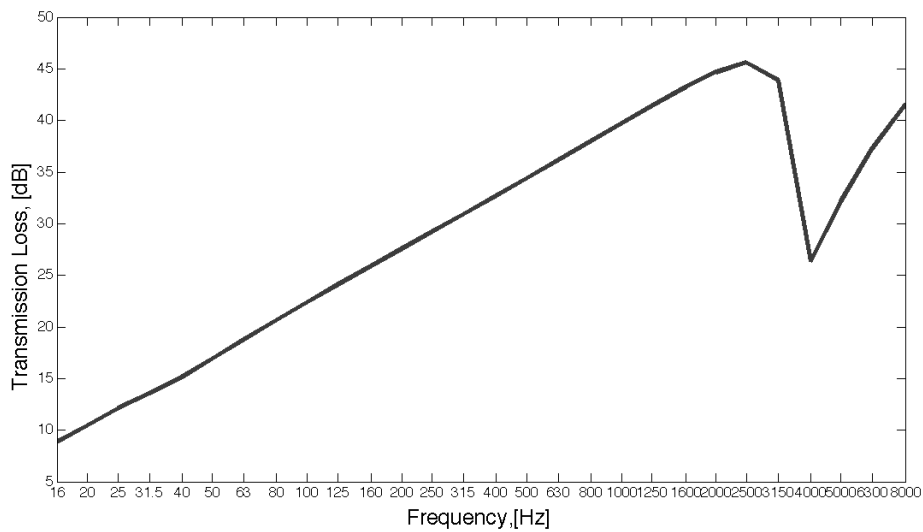


Figure 5.6.: The transmission loss of the simple steel SEA plate.

The model of the SEA plate was changed from the simple plate to the ribbed plate. The ribbed plate was represented by two horizontal ribs and bended edges on the panel.

## 5. Computer models

The Beam Property Calculator script was used to design the ribs that correspond to the ribs on the plate and the ribs for the bended edges. Two ribs were designed as a thin rectangular steel beam with the thickness 0.003 m, the height 0.05 m, and the width 0.1 m. The distance between the ribs was set to 0.3 m. The edges of the plate were designed as a L-shaped steel beam with the sides 0.02 m and 0.05 m, the thickness was set to 0.003 m. The space between the edges was set to 0.9 m, which is the same as the width of the plate. The wave number of the ribbed plate was compared to the wave number in the air and is presented at Figure 5.7.

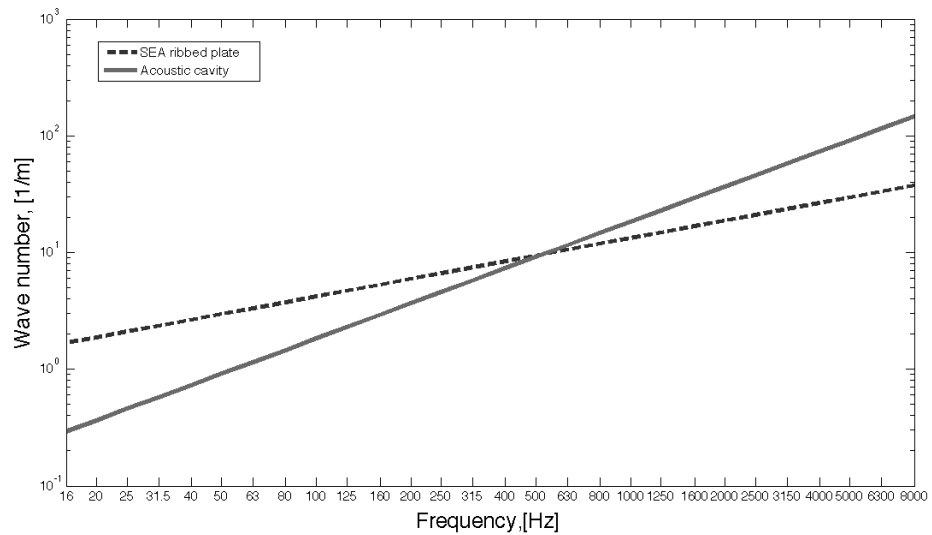


Figure 5.7.: The wave numbers in the ribbed SEA plate and in the air.

The ribs increased the stiffness of the plate. Therefore, the wave number decreased and the coincident frequency shifted to 500 Hz. The transmission loss of the ribbed plate is presented at Figure 5.8.

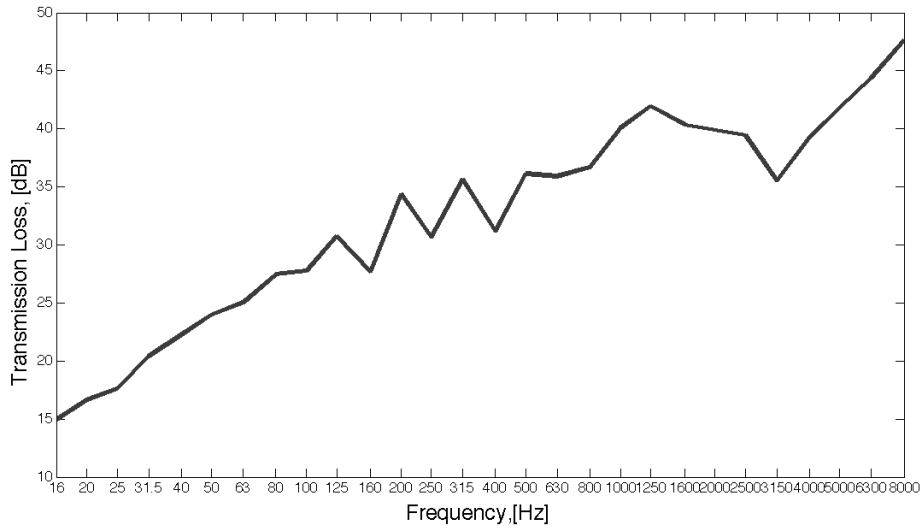


Figure 5.8.: The transmission loss of the ribbed SEA plate.

The SEA subsystem should have at least one mode per band to transmit energy. Modes per band of the ribbed SEA plate were checked in VA-one and are presented below at Figure 5.9. Below 125 Hz the ribbed plate has less than one mode per band, thus it is not reliable to use the results of the SEA modeling of the ribbed plate below 125 Hz. A dip around 200 Hz indicates that there is no mode in that band.

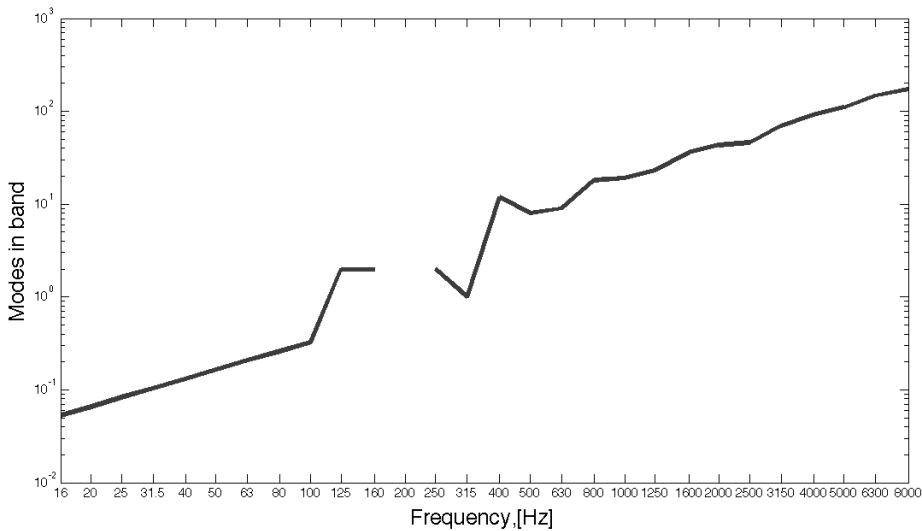


Figure 5.9.: Modes in bands for the ribbed SEA plate.

## 5. Computer models

### 5.2.2. FE model

The CAD model of the solid panel was imported into VA-one and recreated as a FE model. The FE panel was meshed into 7103 nodes and 7078 elements. The frequency range of the solver was set from 16 Hz to 3150 Hz. The distance between neighboring nodes was equal to 0.016 m. The trustful solution can be achieved with information about six nodes per wavelength. The wavelength for the bending waves for the 3 mm steel plate was calculated and is present at Figure 5.10. The mark shows the frequency limit for the current model. Above this frequency less than six nodes fit into the wave length.

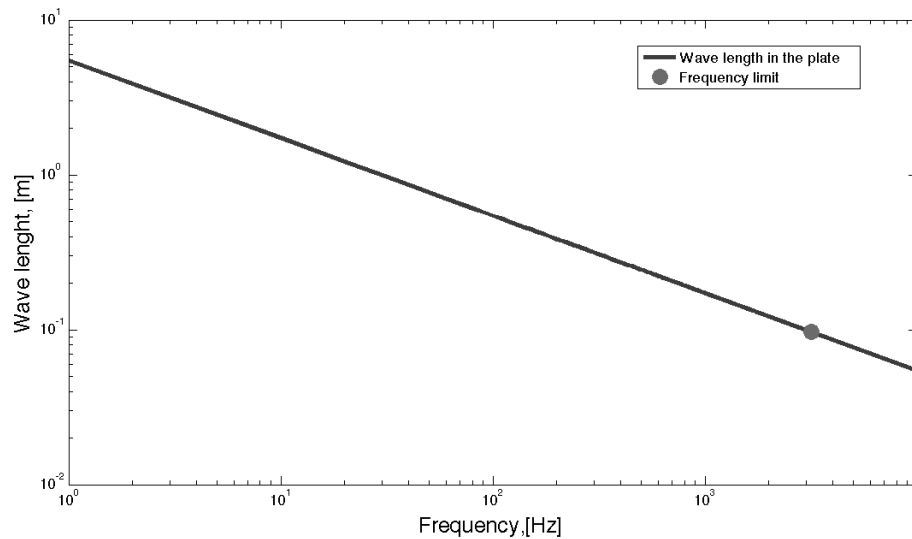


Figure 5.10.: The wavelength-frequency representation for the FE plate.

The FE faces were created on the plate surfaces to represent coupling between the FE subsystem and the load. The diffuse acoustical field was assigned to one side of the FE panel. Both sides of the panel were connected to the semi-infinite fluid elements. The developed FE model of the solid panel is presented at Figure 5.11.

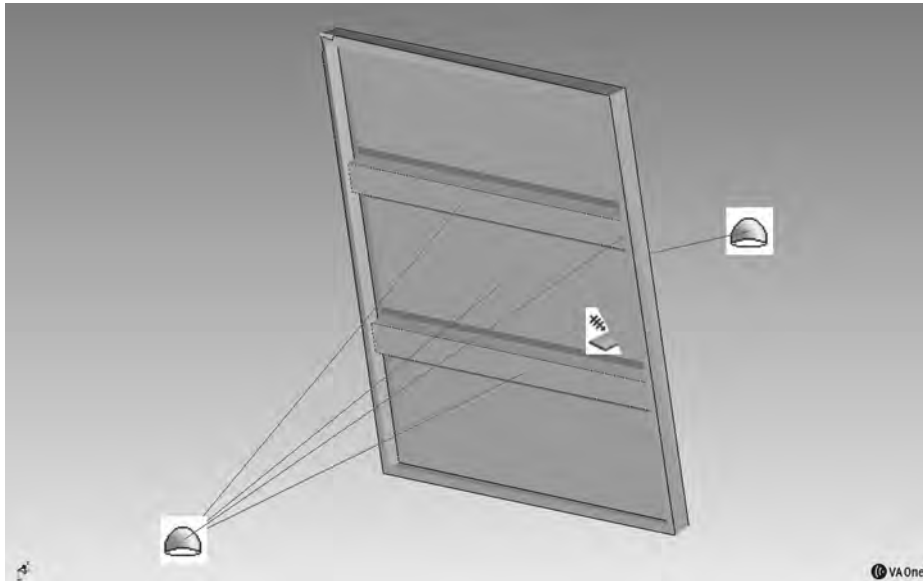


Figure 5.11.: The VA-one model of the FE plate.

The hybrid transmission loss of the FE plate was measured in VA-one and is presented at Figure 5.12.

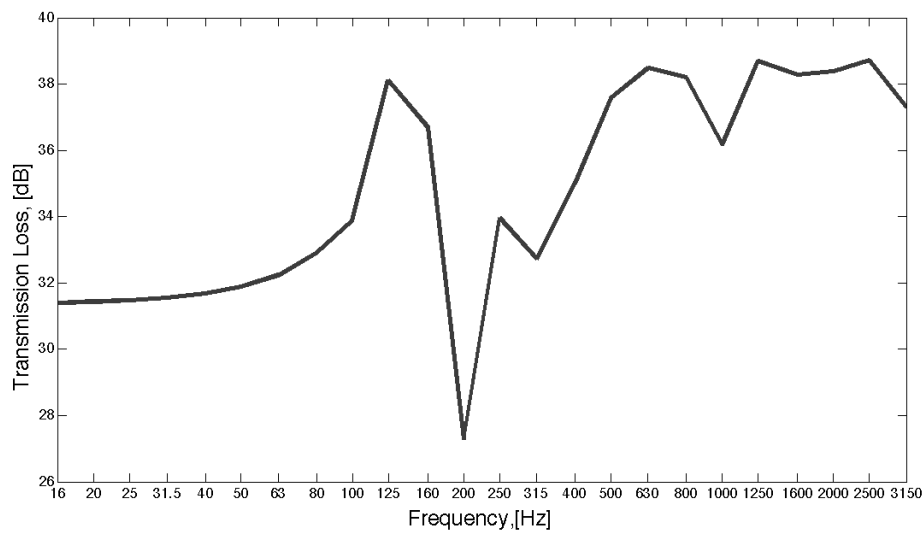


Figure 5.12.: The transmission loss of the FE plate.

## 5. Computer models

### 5.2.3. SEA model vs FE model

The comparison of the transmission loss of the ribbed SEA panel modeled using the ribbed plate's properties, as well as the FE panel is presented at Figure 5.13.

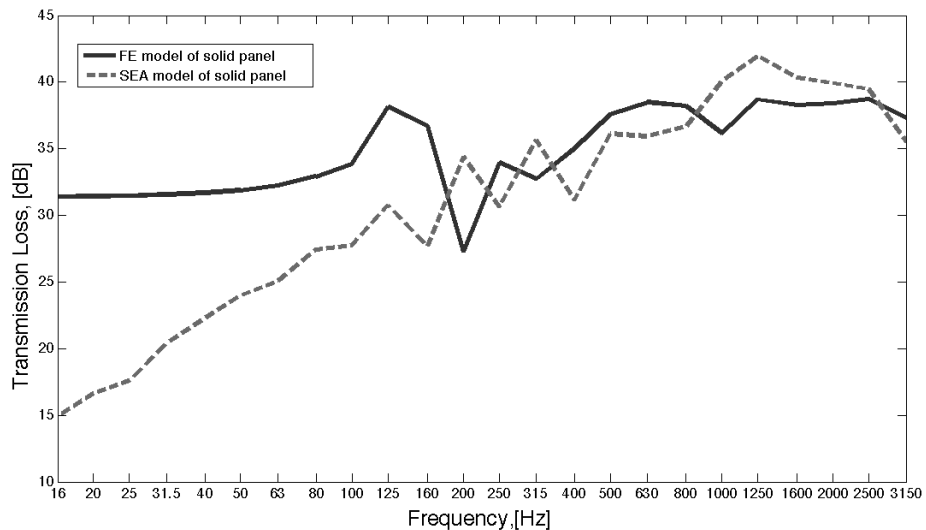


Figure 5.13.: The transmission loss of the FE model and the SEA model of the solid panel.

From Figure 5.13 it can be seen that the transmission losses show good agreement for the frequency range from 160 Hz to 3150 Hz and, therefore, it is possible to substitute the FE model with the SEA model.

The leaks in the enclosure construction is the reason for worsening of the noise reduction properties of the single panels and the overall enclosure. Four slits along the plate perimeter were added to the SEA area junction of the ribbed plate. The width of the slits was set to 0.0005 m and the depth was set to 0.003 m. The transmission loss of the modeled ribbed SEA plate and the transmission loss of the measured solid panel are presented at Figure 5.14.

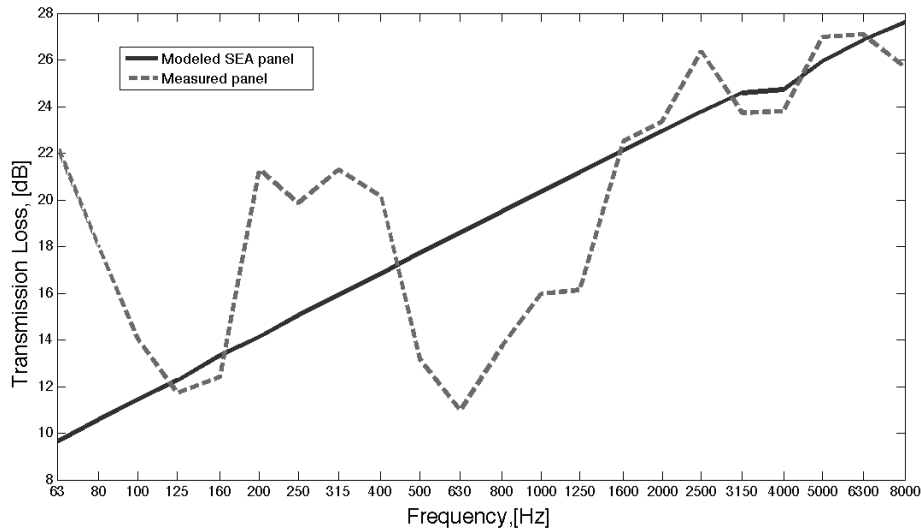


Figure 5.14.: The transmission loss of the measured and modeled solid plate.

### 5.3. Model of baffled panel

In the SEA model the transmission loss of the leaks or the apertures can be described using the analytical models. However, more detailed simulation of given apertures is needed. In situation when the foam treatment covers the leaks the FE and Hybrid FE-SEA approaches can be used [Per 10].

#### 5.3.1. Field setup model

The FE acoustics module of VA-one software was used to model one slot of the front baffle and to measure its sound reduction properties. The FE model was based on the front baffled panel, because this panel was ranked as the one with the lowest noise reduction index (see Figure 4.16). The FE acoustic cavity was created in the space between baffle's boundaries. The dimensions of the cavity correspond to the dimensions of the real baffle. The FE cavity was meshed to 142041 elements and consisted of 27298 nodes. The volume of this cavity was  $0.021 \text{ m}^3$ . The frequency range for this model was set from 62 Hz to 5040 Hz. Three FE faces were created on the front, back and top sides of the baffle. The front and back faces were connected to different semi-infinite fluid objects. The diffuse acoustic field was assigned on the back side of the baffle. The top face of the baffle was modeled as an area with the absorption material. The lay-up noise control treatment was assigned to the top face. The FE model of the slot is presented at Figure 5.15.

## 5. Computer models

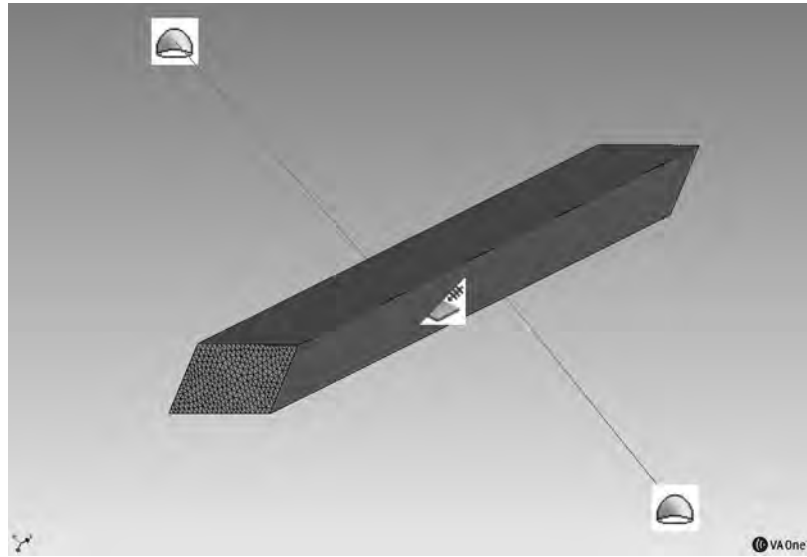


Figure 5.15.: The FE model of the air cavity between the baffles.

The hybrid transmission loss was calculated in VA-one and was compared to the field measurements. See Figure 5.16 for comparison.

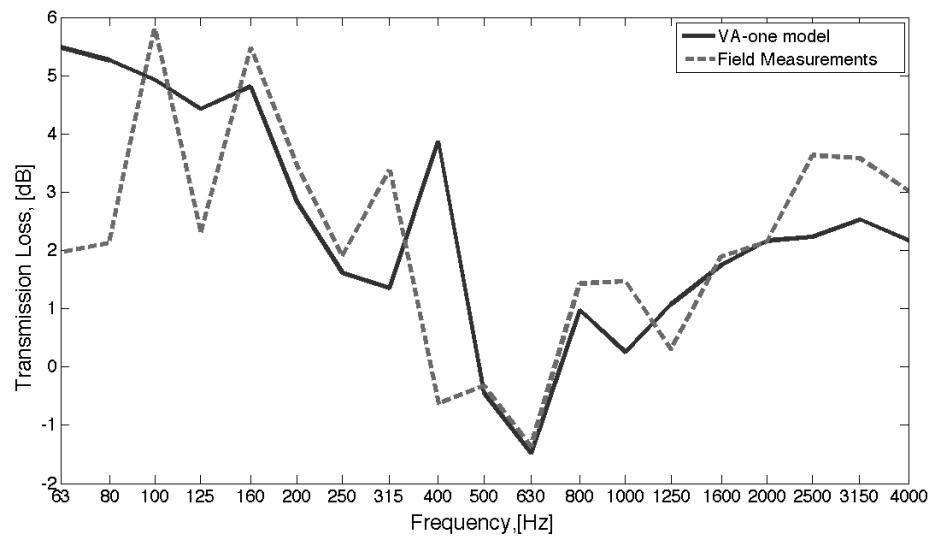


Figure 5.16.: The transmission losses of the measured and modeled baffled front panel.

### 5.3.2. Laboratory setup model

Created computer model of the slot was used to model all cavities in the front baffled panel. The model of the front baffled panel was copied into the SEA model of the

laboratory environment. See Figure 5.17 for the hybrid SEA-FE model.

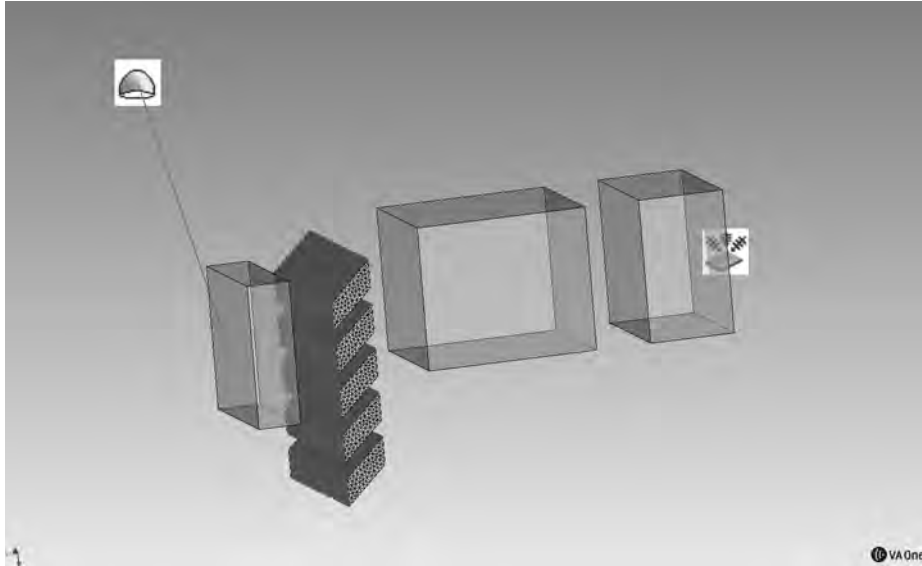


Figure 5.17.: The hybrid FE-SEA model that represents the setup in the laboratory.

The volumes of the reference sound power source and the sending room were connected to one side of the baffled panel. The volume with attached semi-infinite fluid object represented the receiving room. It was connected to another side of the baffled panel. This models the test setup described in Section 4.3.2. The volume on the receiving side of the baffled panel allows some energy return to the receiving room. The sound power was measured in the acoustic cavity in both sending and receiving rooms. The transmission loss was calculated with help of equations 2.19 and 2.20. See Figure 5.18 for comparison of the transmission loss calculated using the VA-one model and measured in the laboratory.

## 5. Computer models

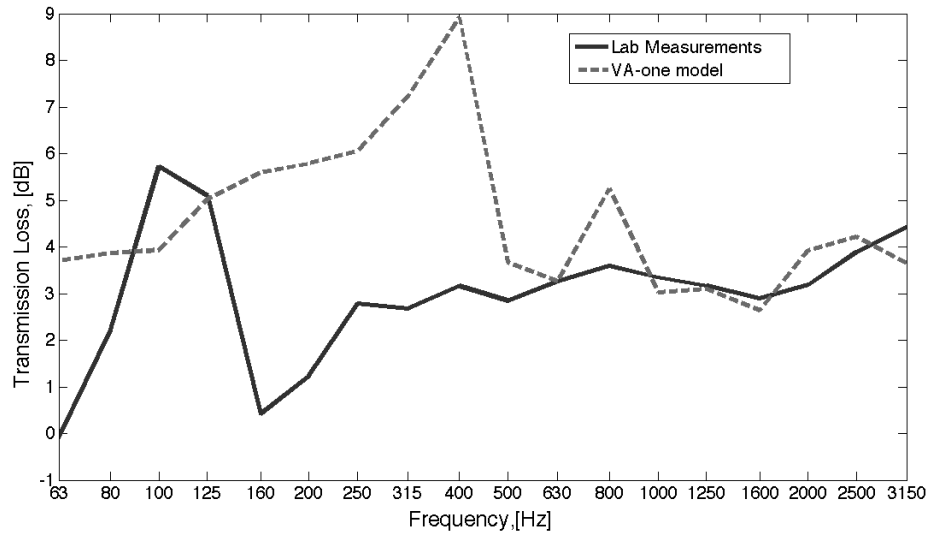


Figure 5.18.: The transmission loss of the VA-one model that simulates experiment in the laboratory and the transmission loss measured during the experiment.

The results have a good agreement above 500 Hz. The peaks around 400 Hz and 800 Hz in the transmission loss of the modeled baffled panel are controlled by the absorption (see Figure 5.2). To improve model in the low frequency range the foam layer of the noise control treatment was extruded as the PEM subsystem. Each PEM subsystem was meshed into 3980 nodes and consisted of 5880 elements. See Figure 5.19 for the FE-PEM model of the baffled panel in the lab environment.

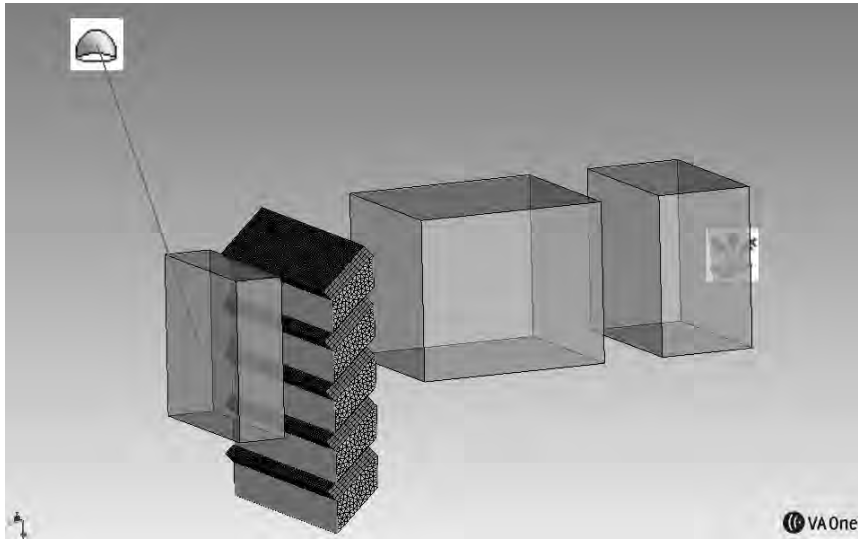


Figure 5.19.: The Hybrid SEA-FE-PEM model that represents the setup in the laboratory.

Comparison of the transmission loss calculated using the FE model with the noise control treatment and using the FE-PEM model is presented at Figure 5.20

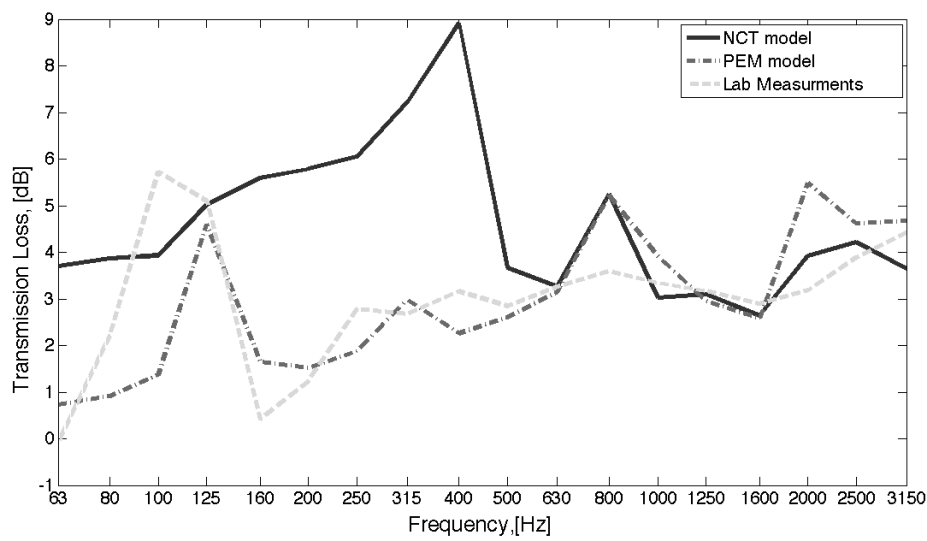


Figure 5.20.: The transmission losses calculated using the FE models with the NCT, the PEM representation of the foam, and the transmission loss obtained during the lab measurements.

As expected, the transmission loss of the FE-PEM model has a good agreement with

## 5. Computer models

the measured results for the low frequency. The transmission loss of the FE-PEM model is overestimated for the high frequency since the PEM foam was modeled without a layer of visco-elastic polymer.

The results of the transmission losses of the PEM and NCT models were merged. Below 630 Hz data from the PEM model were used, above 630 Hz data from the NCT model were used. The noise reduction properties of combined results from the PEM and NCT models were compared with the transmission loss measured in the laboratory (see Figure 5.21).

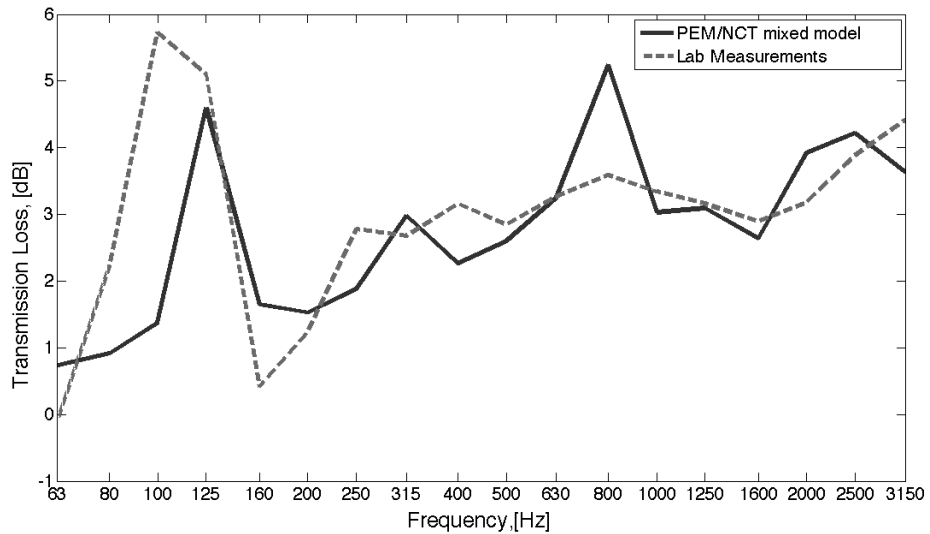


Figure 5.21.: The transmission loss of the measured front baffled panel and the transmission loss of combined results from the PEM and NCT models.

### 5.3.3. Fluid Dynamic Simulation

The computational fluid dynamic (CFD) software was used to estimate the airflow and the pressure drop in the slot of the front baffled panel. Simulations that show the velocity contours and the pressure drops in the slot of the baffled panel for the air flow with velocities 5, 10, and 15 m/s were done in ANSYS. The ANSYS model was created from the imported CAD model of the front baffled panel. The mean air flow velocity was measured with an air flow probe and was equal to 10 m/s (see Section 4.4 for details).

The ANSYS model calculates the velocity contours and the pressure drops in a cross section of the slots. Therefore, it shows the results for two dimensions only. See Figure 5.22 for the ANSYS model. Round arrows indicate periodical boundary conditions. Straight arrows show the direction of the air flow and the air inlet and outlet.

### 5.3. Model of baffled panel

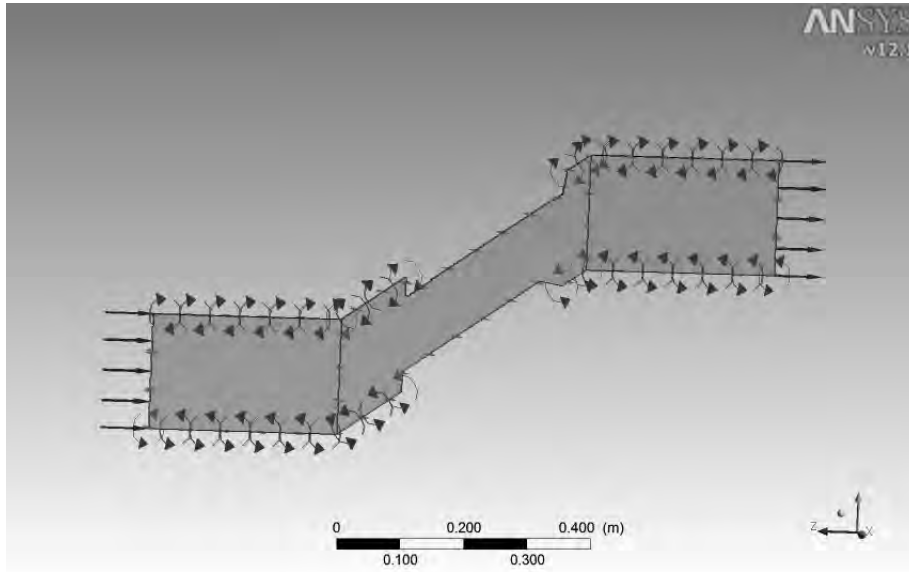


Figure 5.22.: The ANSYS model of the cavity between the baffles.

Figure 5.23 shows the velocity contour for the airflow at 10 m/s. The pressure drops for the same airflow are shown at Figure 5.24.

5. Computer models

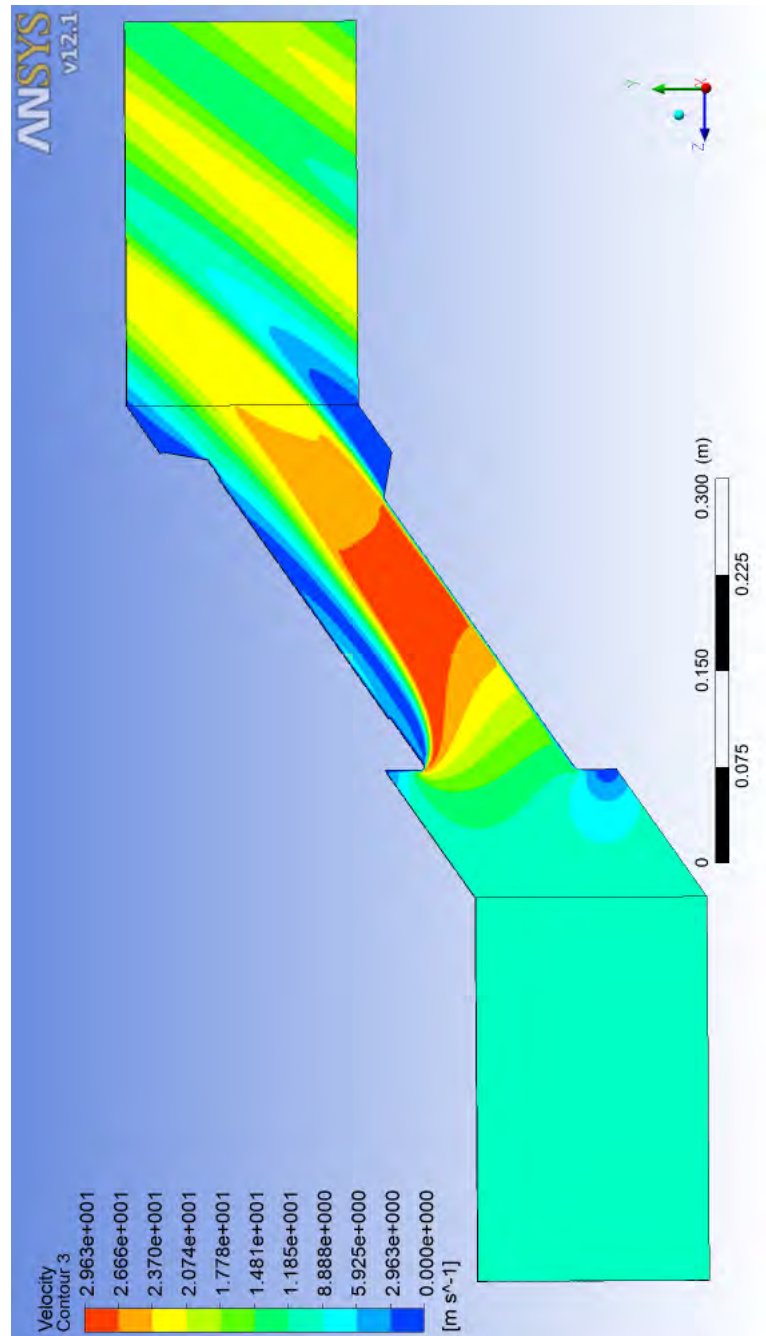


Figure 5.23.: The velocity contour of the cavity between the baffled panel.

### 5.3. Model of baffled panel

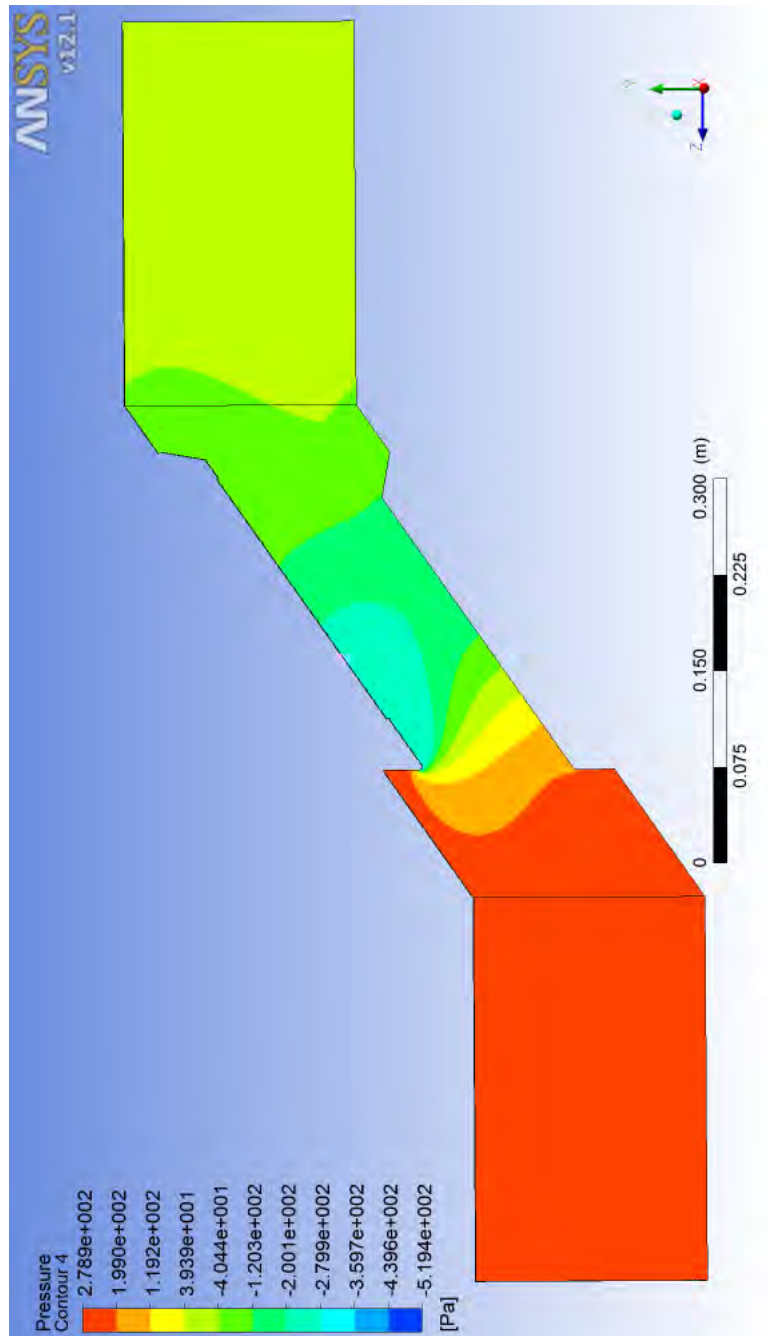


Figure 5.24.: The pressure contour of the cavity between the baffled panel.

## 5. Computer models

### 5.4. Model of the power pack encapsulation

The SEA model of the power pack enclosure was built based on the CAD model. The inner components of the power pack were not included in the model and this model represents the enclosure only. But at the same time, this model is valid for comparison with the encapsulated working power pack. The SEA model of the enclosure was built from fourteen plates. Each plate is a part of the enclosure. See Figure 5.25 for the SEA model of the power pack enclosure. The side panels of the enclosure were modeled as described in Section 5.2.

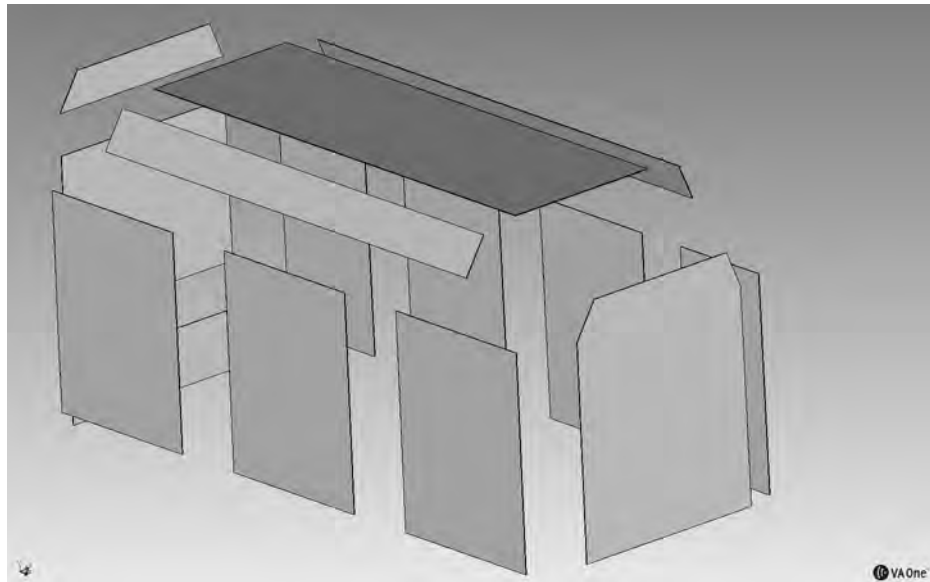


Figure 5.25.: The SEA model of the power pack enclosure.

User defined noise control treatment was modeled on the plates' faces inside the enclosure. The area, which is covered with absorption material varies for each plate, see Table 5.1 for the model details.

#### 5.4. Model of the power pack encapsulation

Table 5.1.: Properties of the panels used for the SEA model of the enclosure.

Panel description	Size, [m]	Area, [m <sup>2</sup> ]	Area of NCT, %
Front baffled panel	1.2 x 1.52	1.8	80
Left solid panel 1	0.65 x 1.3	0.845	90
Left baffled panel 2	0.84 x 1.3	1.105	90
Left baffled panel 3	0.79 x 1.3	1.027	90
Left solid panel 4	0.71 x 1.3	0.923	90
Roof at the left side	0.23 x 3	0.699	100
Rear baffled panel	0.95 x 1.21	1.145	80
Rear interface panel	1.21 x 0.35	0.42	none
Roof at the rear side	1.2 x 0.25	0.23	100
Right baffled panel 1	1 x 1.3	1.3	90
Right baffled panel 2	1 x 1.3	1.3	90
Right solid panel 3	1 x 1.3	1.3	90
Roof at the right side	0.25 x 3	0.76	100
Roof	0.97 x 3	2.91	80

The acoustical space inside the enclosure was modeled as two acoustical cavities. One cavity was used for the volume of the engine with the cooling system and another cavity represented the rest of the volume inside the enclosure. The absorption from the noise control treatment was used as a damping for the cavities under the hood.

It was assumed that the enclosure is situated on the infinite plate and is surrounded with air. Therefore, five acoustic cavities were used to model the air around the enclosure (see Figure 5.26)

## 5. Computer models

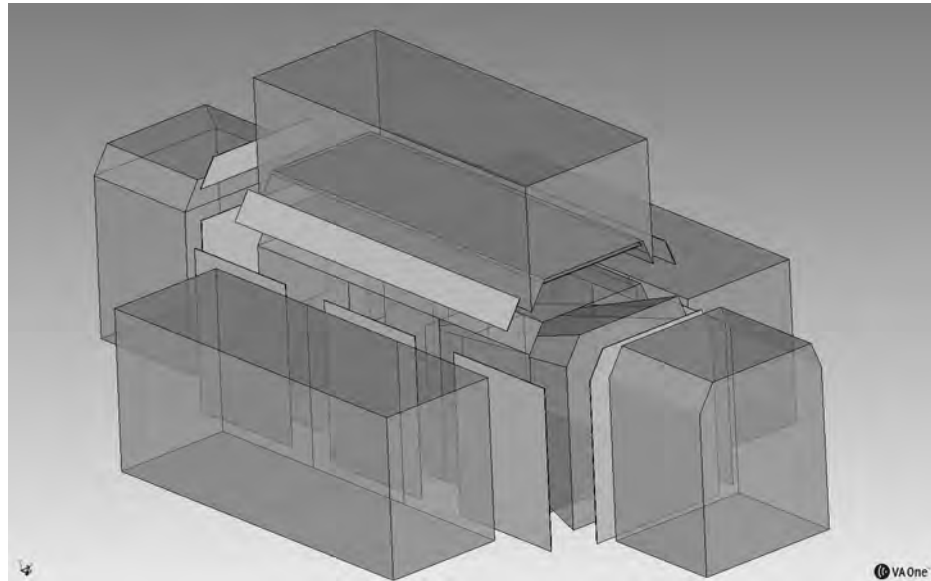


Figure 5.26.: The SEA model of the enclosure with acoustic cavities under the hood and around the enclosure.

The average absorption for the cavities around the enclosure was set to 0.1%. Five cavities were connected to the semi-infinite fluid object that represented the unbounded exterior acoustic space.

The leaks were defined in the area junctions between the cavity inside the encapsulation, the panel, and the cavity outside of the encapsulation. The baffled panels were represented by user defined leaks with user defined spectrums of the transmission loss. The spectrums of the transmission loss for the panels were inserted into the model from the measurements. See Figures 4.16 for the measured transmission losses. As it was discussed in Section 5.2, user defined slits were added to the area junctions of the solid panels.

The results from the measurements described in Section 4.1 were used to characterize the loads on the model. The power source with the spectrums of the engine and the inner fan was assigned to the cavity that represents the volume of the engine and the cooling system. The power sources with the spectrums of the external fan, the exhaust, and the air intake were assigned to the cavities around the enclosure (see Figure 5.27).

#### 5.4. Model of the power pack encapsulation

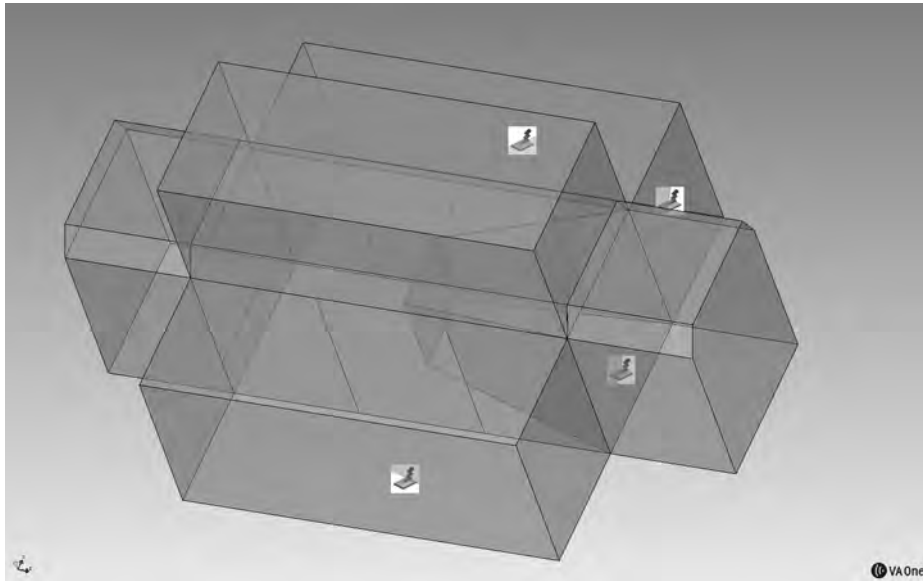


Figure 5.27.: The SEA cavities with assigned loads

A separate model without encapsulation was built in order to validate the loads that were assigned to the cavities. This model consists of two cavities that represent the volume inside the encapsulation. The size of the cavities is the same as the size of the encapsulated unit. The power input from the engine and the cooling system was assigned to the cavity that represented the volume of the engine. Other power inputs, such as the external fan, the exhaust, and the air intake were assigned to the cavity that represented the rest of the volume of the power pack (see Figure 5.28)

## 5. Computer models

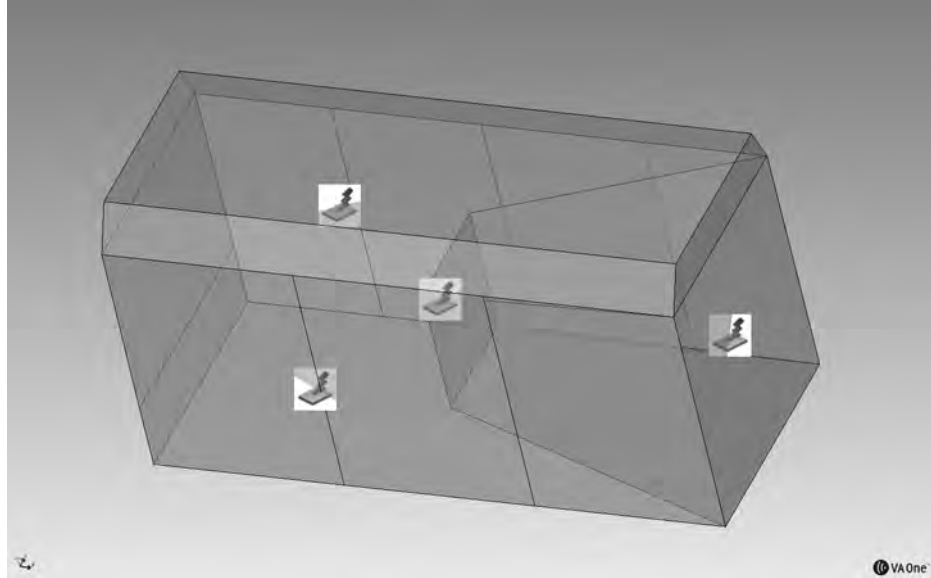


Figure 5.28.: The SEA cavity that was used to validate the assigned load.

A separate model of enclosure was created and was loaded with user defined power spectrum of the reference source. All panels were connected to the semi-infinite fluid object. The distances to all connected subsystems were overwritten to one meter. This model corresponds to the setup described in Section 4.1. Figure 5.29 shows the SEA model.

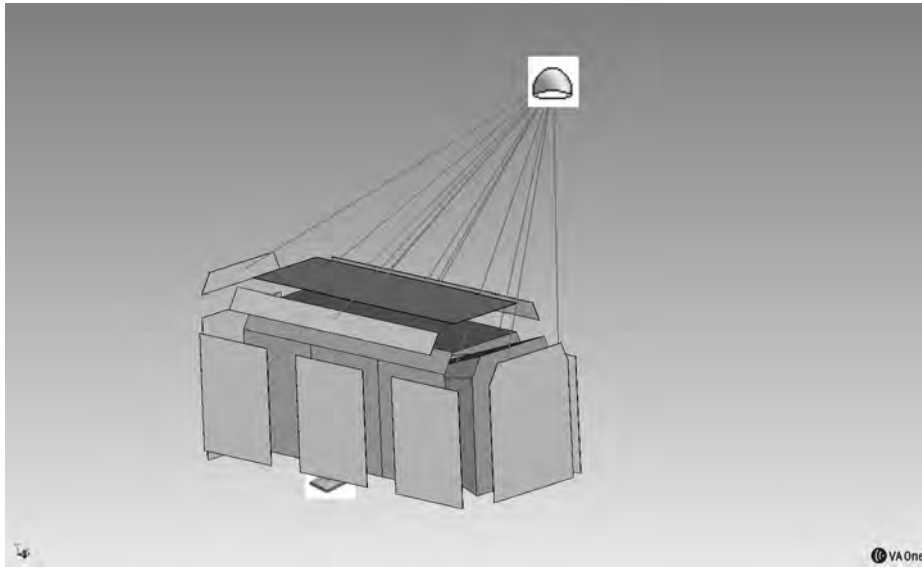


Figure 5.29.: The SEA model that was used to validate the results from the sound pressure level measurement around the enclosure.

## 5.5. Results

The models of power pack were compared to three cases of interest. The power pack without encapsulation should emit similar amount of energy as the corresponding VA-one model. Comparison of the emitted sound power level of the model without encapsulation and the measured sound power level of the power pack without encapsulation was done to validate the power sources assigned to the model. See Figure 5.30 for the spectrums comparison.

## 5. Computer models

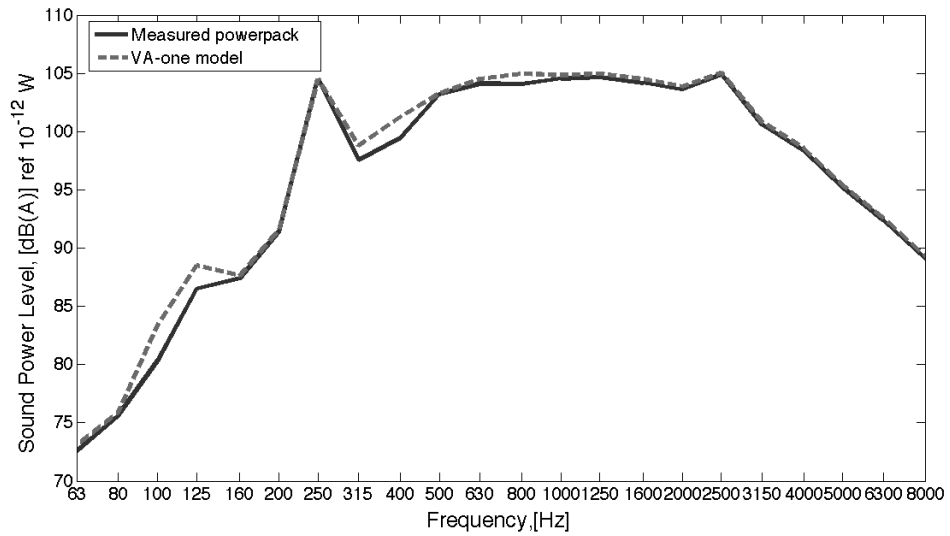


Figure 5.30.: The sound power spectrums of the power pack without encapsulation and the corresponding model.

The total sound power level emitted by the power pack is 114.5 dB(A) and the total sound power level emitted by the VA-one model is 114.8 dB(A).

The spectrums of the mean sound pressure level measured one meter away from the enclosure driven by the reference sound power source, as well as model that simulates the same case (see Subsection 4.1) are shown at Figure 5.31. The total measured sound pressure level is 70.5 dB(A), the total modeled sound pressure level is 70.1 dB(A).

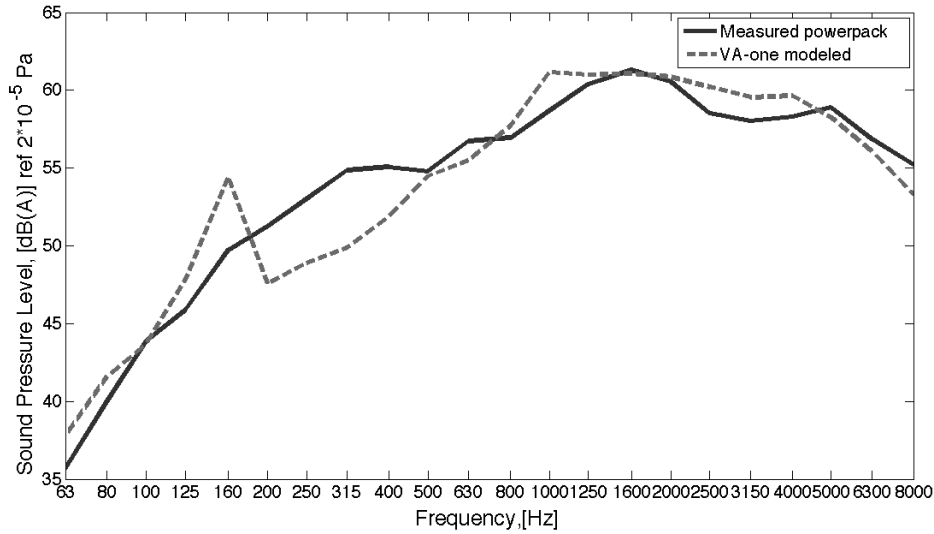


Figure 5.31.: The spectrums of the sound pressure level modeled and measured one meter away from the power pack.

Comparison of the emitted sound power levels of the encapsulated power pack without the external sources and the corresponding VA-one model are shown at Figure 5.32.

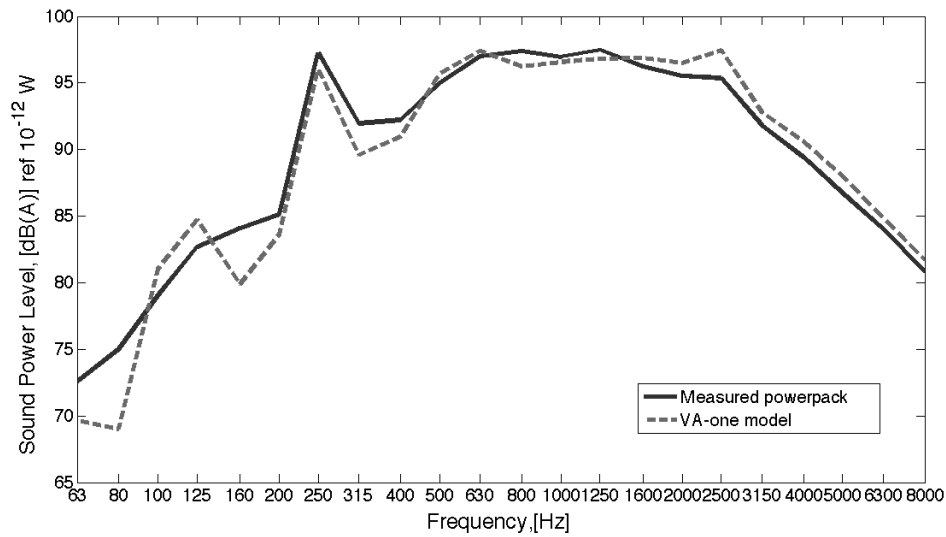


Figure 5.32.: The sound power spectrums of the encapsulated power pack without the external sources and the corresponding model.

The total measured sound power level is 106.8 dB(A) and the total sound power level emitted by the model is 106.9 dB(A).

## 5. Computer models

Comparison of the emitted sound power level spectrum of the power pack with the working external sources and the sound power level spectrum of the VA-one model that represents the same case is presented at Figure 5.33. The total measured sound power level is 108.9 dB(A), the total modeled sound power level is 108.6 dB(A).

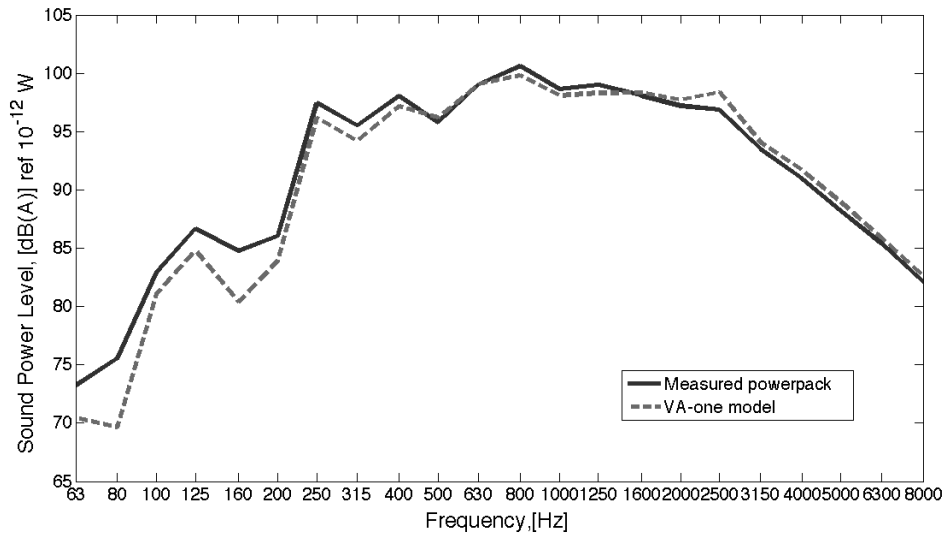


Figure 5.33.: The sound power spectrums of the encapsulated power pack with the external fan and the corresponding VA-one model.

## 5.6. Conclusion

The computer models of the baseline power pack and its components were described in this chapter. The absorption model has a poor agreement in the frequency ranges from 500 Hz to 630 Hz and from 1000 Hz to 1600 Hz (see Figure 5.3). The absorption model was developed using factory preset materials by “try and error” method. Better absorption model requires impedance tube measurements and processing of obtained results in commercial software to obtain resistivity, porosity, tortuosity, Young’s modulus, and more for a foam model.

The transmission losses of the FE and ribbed SEA plate models of the solid panel have a good agreement (see Figure 5.13). Since the reduction properties of the encapsulation are mainly controlled by the leaks, the slits were added to the area junction of the ribbed SEA plate. The transmission loss of such panel was compared with the measurements (see Figure 5.14). The transmission losses of the modeled and measured panels have a good agreement for the frequencies above 1600 Hz. Below 1600 Hz the offset is around 4 - 8 dB.

The model of the cavity slot in the baffled panel was made and its transmission loss

properties were compared with the data obtained during the field measurements. The transmission losses of the modeled and measured panels have a very good agreement (see Figure 5.16). Both modeled and measured transmission loss spectrums have a dip around 600 Hz. This negative transmission occurs because of the opening.

The models that correspond to the laboratory setup were made with the NCT and PEM representations of the absorption. The mixed results of the transmission loss has a good accord with the measurements (see Figure 5.21). The peak around 800 Hz is absorption controlled and correspondence could be better with the better absorption layer model.

The results of the fluid dynamic simulation show that there is a significant pressure drop due to obtuse angle of the air inlet. From Figure 5.23 it is possible to see the velocity contour. Blue regions show slow air velocity. Slow air velocity leads to the pressure drop (see Figure 5.24) that affects a fan performance. In such conditions a fan should overwork to deliver the same amount of the airflow into the system. Better designed baffles should decrease the pressure drop and consequently improve the cooling system performance.

The complete model of the power pack was built based on the data obtained from the simulations and the measurements. Three models were built to validate assigned load on the system, to measure the sound pressure level at one meter distance, and to measure the emitted noise pollution from the working unit. The results of the simulation were compared with the results obtained during the measurements and are presented at Figures 5.30 - 5.33. The comparison of the spectrums let us see a very good agreement between the modeled and real power pack. The junction areas that correspond to the baffled panels were populated with the transmission loss spectrums obtained during the measurements. The junction area that corresponds to the front baffled panel was populated with the measured and modeled transmission loss spectrums. The overall difference between the measured and modeled cases is insignificant and the total difference is around 0.5 dB(A).

## 5. *Computer models*

## 6. Improved front baffled panel

The market requires power packs with greater output. The increase of engine's power leads to the increase of noise from the engine and the cooling system. Therefore, an improved encapsulation design was proposed. The weakest part of current encapsulation is the front baffled panel (see Figure 4.16 for the transmission loss of the baffled panels). The front baffled panel of the current encapsulation should be improved in order to achieve better overall sound reduction properties of the encapsulation.

The model of the improved baffled panel was built in VA-one software. Its transmission loss properties were investigated in the model that simulates the laboratory environment. The fluid dynamic simulation was done in ANSYS software. The prototype of the improved baffled panel was built and its transmission loss was measured in the laboratory. The SEA model of the power pack was updated with the transmission loss of the prototype baffle and overall decrease of the emitted noise was estimated.

### 6.1. Developing a new baffled panel

Improved front baffled panel must have better sound reduction properties. The dimensions of the improved panel must be the same as the dimensions of the baseline one, specifically, the depth must be 30 cm or less. The baffle slot is designed to be L shaped instead of straight and to repeat smooth wing profile. All slots in the baffled panel are subdivided into two or three parts. The air inlet's shape is changed from rectangular into round (see Figure 6.1). The sides of all slots are treated with the absorption material, which should compensate for a decrease of the area of the air inlet.

## 6. Improved front baffled panel

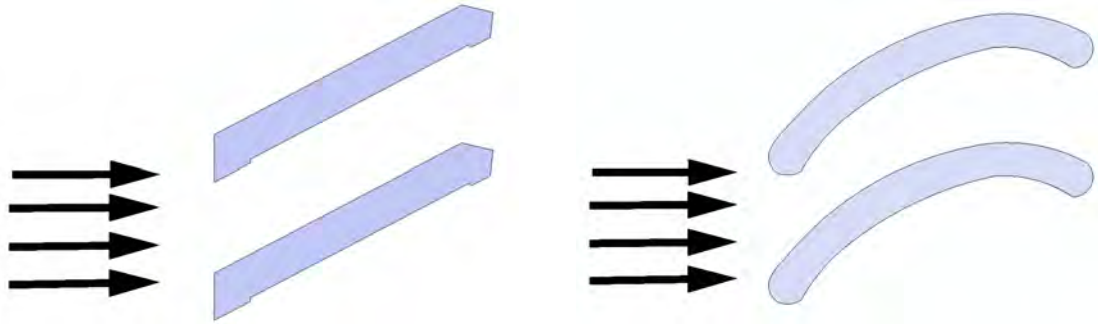


Figure 6.1.: The cross section of the original (left) and proposed (right) air inlet.

### 6.1.1. VA-one prediction

The procedure of the improved baffled panel modeling was the same as described in section 5.3.

The VA-one model of the baseline baffle slot was re-designed in order to have properties of proposed improved baffled panel. See Figure 6.2 for proposed baffled panel model.

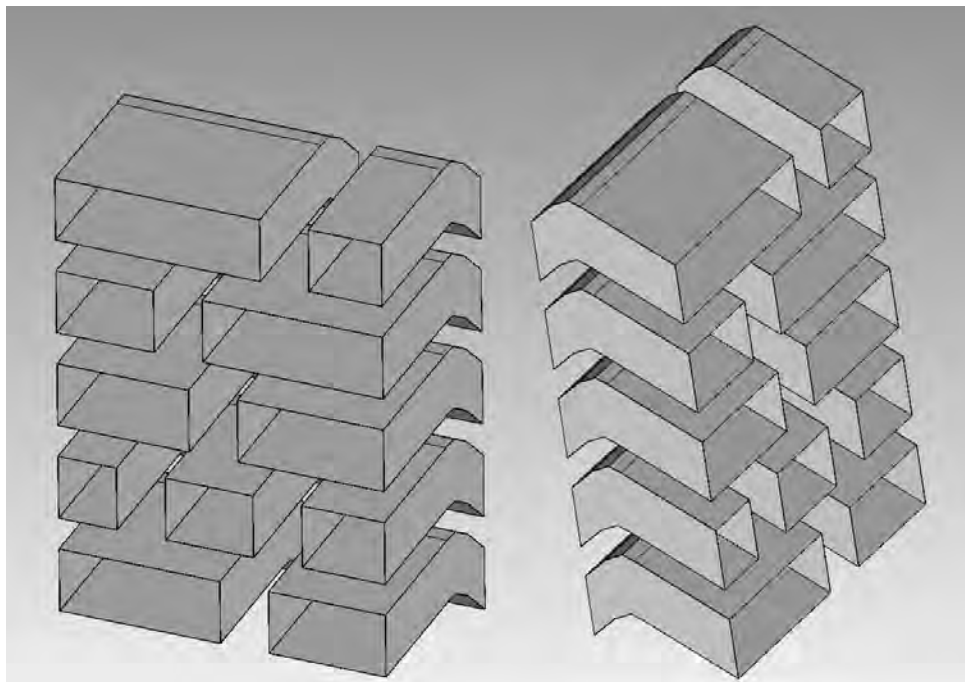


Figure 6.2.: The shell of the improved front baffled panel.

The cavities inside the slots were recreated as the FE acoustic cavities. Desired mesh

### 6.1. Developing a new baffled panel

element's length was selected to be 0.016 m. With assumption that information about six nodes per wavelength is sufficient for accurate results, the upper frequency limit for the selected mesh density was 3572 Hz. The modeled absorption was assigned on the side and top FE faces of the cavities. The noise control treatment layers were extruded as a poro-elastic materials' model, and this model was separately saved. As it was discussed before, the NCT model has a good agreement in the high frequency range and the PEM model - in the low frequency range. See Figure 6.3 for the models of the improved baffled panel that use NCT as the absorption layer and the PEM subsystems as the absorption model.

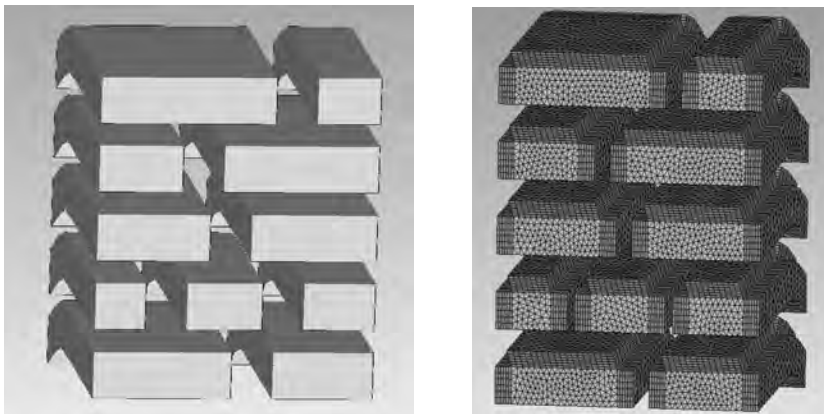


Figure 6.3.: The FE model of the improved baffled panel. The absorption layer is represented as the NCT layer (left) and the PEM subsystem (right).

The models of the improved baffled panel were copied into simulated laboratory environment. The Hybrid FE-SEA model of the laboratory was used to calculate the transmission loss of the baseline baffle and it showed a good agreement with the measured results (see Figure 5.21). The FE-PEM model of the improved baffled panel in the laboratory simulation is shown at Figure 6.4.

## 6. Improved front baffled panel

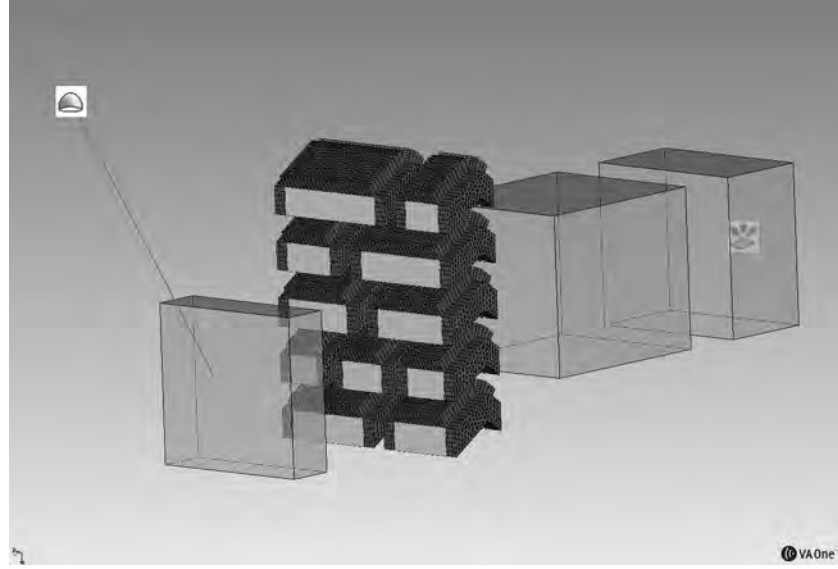


Figure 6.4.: The FE-PEM model of the improved baffled panel in the laboratory simulation.

The transmission losses in both models were calculated with help of equations 2.19 and 2.20 . The transmission losses of the models are presented at Figure 6.5.

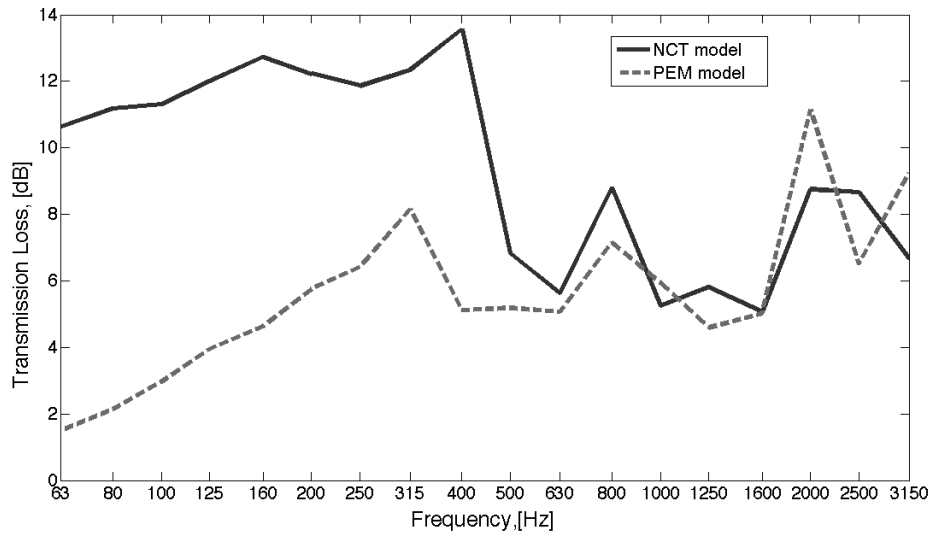


Figure 6.5.: The transmission losses of the VA-one models of the improved baffled panel.

The results of the transmission losses obtained from the NCT and PEM models were combined, since the PEM model has a better agreement in the low frequency range

### 6.1. Developing a new baffled panel

and the NCT model - in the high frequency range. The cross frequency is 630 Hz. The combined transmission loss results of the improved baffled panel and of the baseline baffled panel are plotted together (see Figure 6.6).

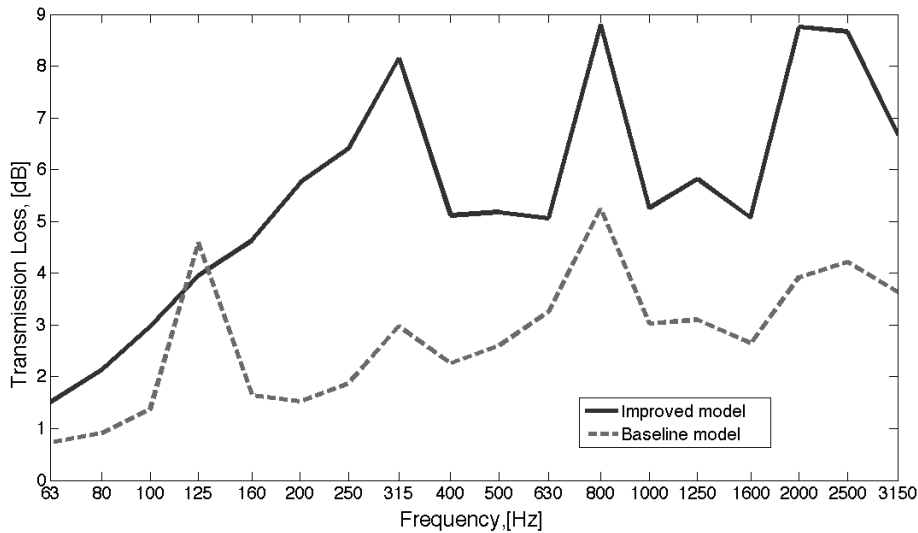


Figure 6.6.: Comparison of the transmission loss of the models of the improved and baseline front baffled panels.

The VA-one simulation, the computation and the comparison of the transmission losses showed that the improved baffled panel has a better noise reduction performance than the baseline baffled panel.

#### 6.1.2. Fluid Dynamic Simulation

The fluid dynamic simulation was done with the improved baffled slot. Calculations of the velocity contours and the pressure drops in the slot of the improved baffled panel for the air flow with velocities 5, 10, and 15 m/s were done. The velocity contour for the air flow at 10 m/s is shown at Figure 6.7. The pressure contour for the same air flow is shown at Figure 6.8.

## 6. Improved front baffled panel

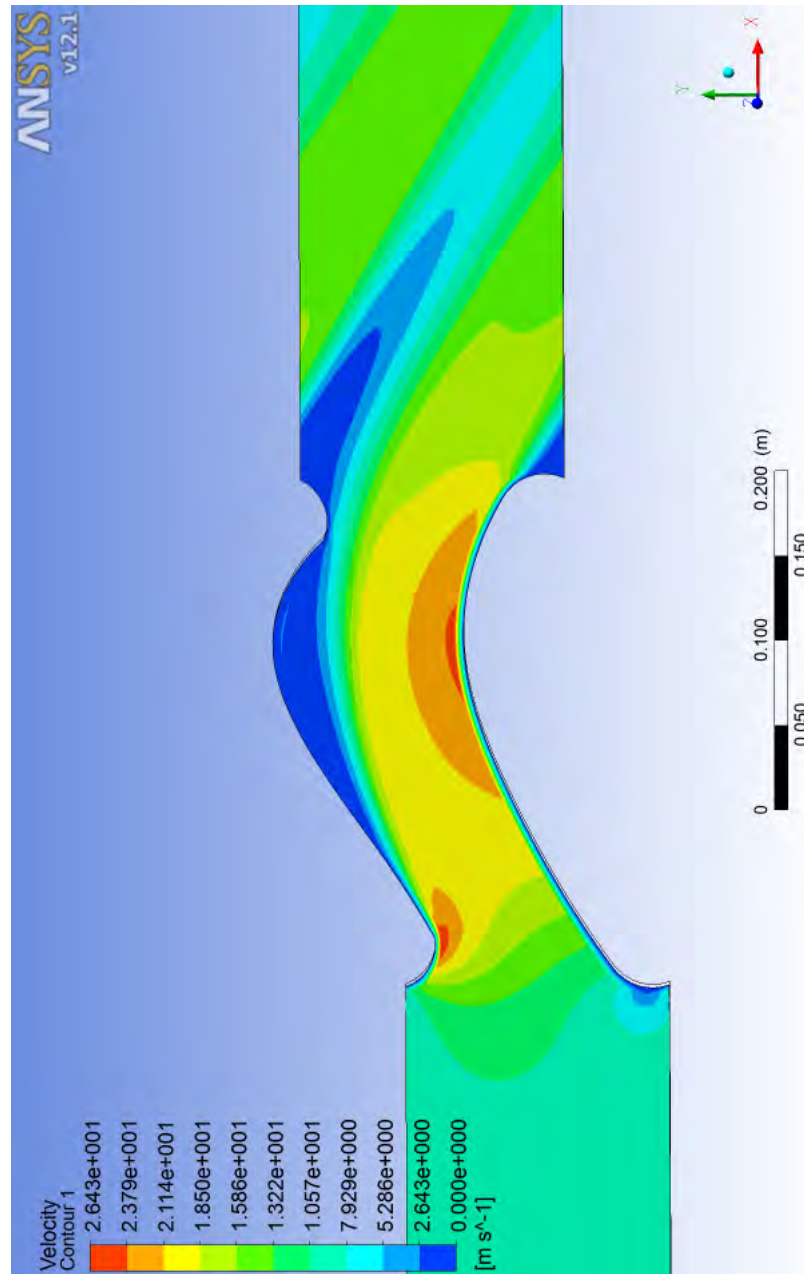


Figure 6.7.: The velocity contour for the cavity between the baffles of the improved panel.

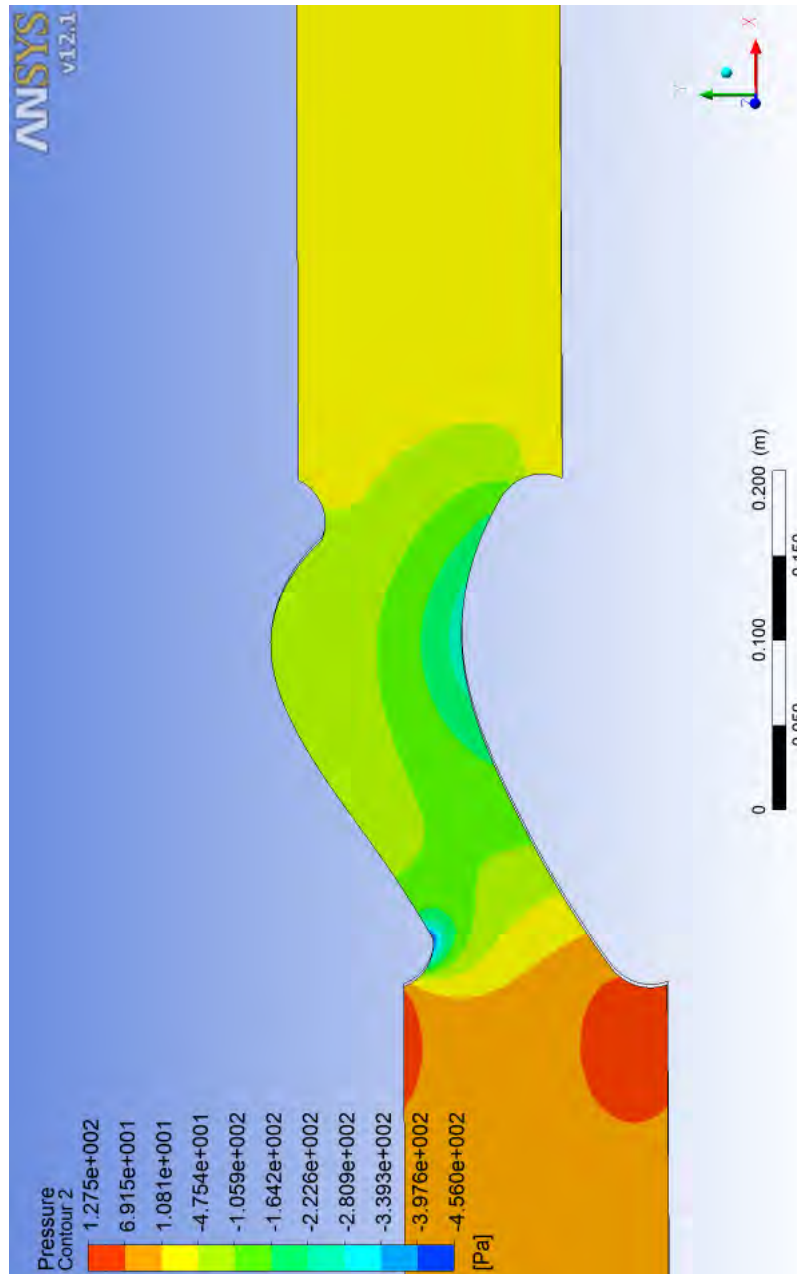


Figure 6.8.: The pressure contour for the cavity between the baffles of the improved panel.

Comparison of the the pressure drop of the original and improved baffled panels for the air flow at 5 m/s, 10 m/s, and 15 m/s is presented at Figure 6.9.

## 6. Improved front baffled panel

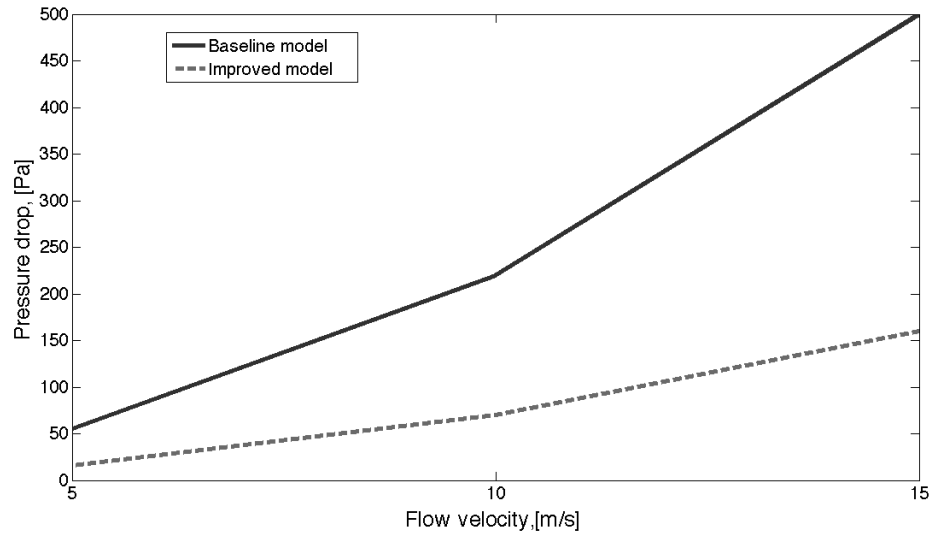


Figure 6.9.: Comparison of the pressure drop in the cavities separating the baffles between the baseline and improved baffled panels.

### 6.1.3. Expectations

The improved baffled panel was designed with an idea to enhance the acoustic performance and at the same time to improve the aerodynamic properties. The computer model of the improved baffled panel was built and its transmission loss properties were compared to the baseline baffled panel model (see Figure 6.6). It is possible to see that noise reduction effect of the improved baffled panel is better, but it is overestimated for frequencies around 315 Hz and 800 Hz due to the absorption model.

The fluid dynamic simulation shows that the wing profile improved the aerodynamic properties of the baffled panel and decreased the pressure drop (see Figure 6.9). The velocity contour shown at Figure 6.7 illustrates the areas with low velocity. For improvement of the aerodynamic properties, the shape of the baffle slot needs to be changed in such way as to replicate the area with the high velocity contour.

The results of the simulation show that the redesigned baffled panel improves noise reduction performance of the encapsulation. It is possible to build a prototype baffled panel based on the computer model's design.

## 6.2. Laboratory measurements of the prototype panel

The prototype of the improved baffled panel was built. The supporting structure was built from wooden panels. The supporting structure is shown at Figure 6.10.

## 6.2. Laboratory measurements of the prototype panel



Figure 6.10.: Photos of the supporting structure of the prototype baffled panel.

The absorption material was attached to the supporting structure the same way it was discussed in “Developing a new baffled panel” subsection (see Subsection 6.1). Complete prototype of the improved baffled panel is shown at Figure 6.11.



Figure 6.11.: Photos of complete prototype baffled panel from front and back.

The prototype baffled panel was mounted into the wall between the diffuse and semi-diffuse environments. The measurement setup was the same as during the baseline baffled panel measurements. For one set of the measurements the reference sound

## 6. Improved front baffled panel

power source was placed at the center of the reverberation room. For another set of the measurements the reference sound power source was placed one meter away from the baffled panel. This setup corresponds to the case when the panel is installed in the enclosure and the direct field incidents the face of the baffled panel. The setup is shown at Figure 6.12.



Figure 6.12.: Measurements of the improved baffled panel in the laboratory.

Average sound pressure level was measured in the sending room. The incident sound power was calculated with equation 2.25. The intensity scans were performed three times in the receiving room and mean transmitted sound power was calculated with equation 2.26. The transmission losses were calculated with equations 2.19 and 2.20. Measured transmission losses for the diffuse field load case and the direct field load case are presented at Figure 6.13.

## 6.2. Laboratory measurements of the prototype panel

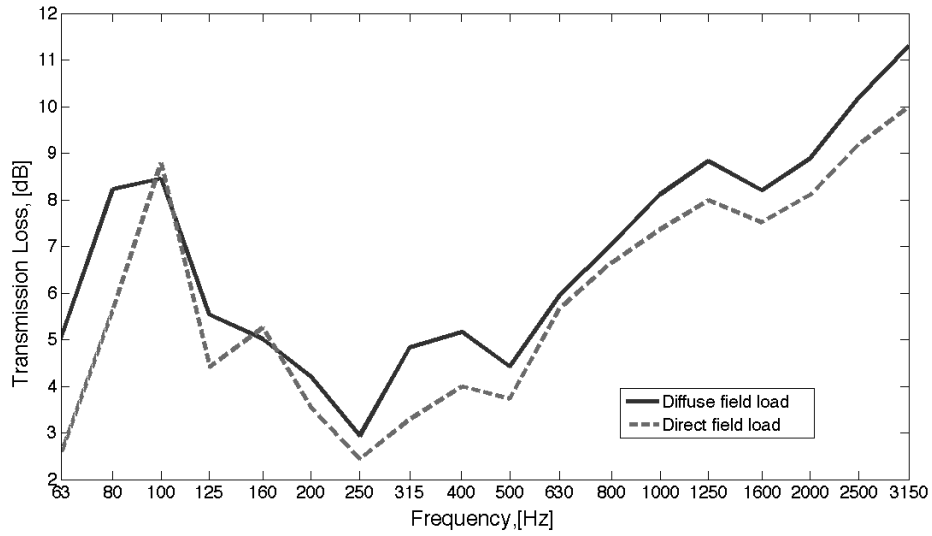


Figure 6.13.: Comparison of the measured transmission loss for the cases of direct and diffuse field load.

Comparison of the noise reduction performance of the improved and baseline baffled panels for the case of the diffuse field load is presented at Figure 6.14 and for the case of the direct field load is presented at Figure 6.15.

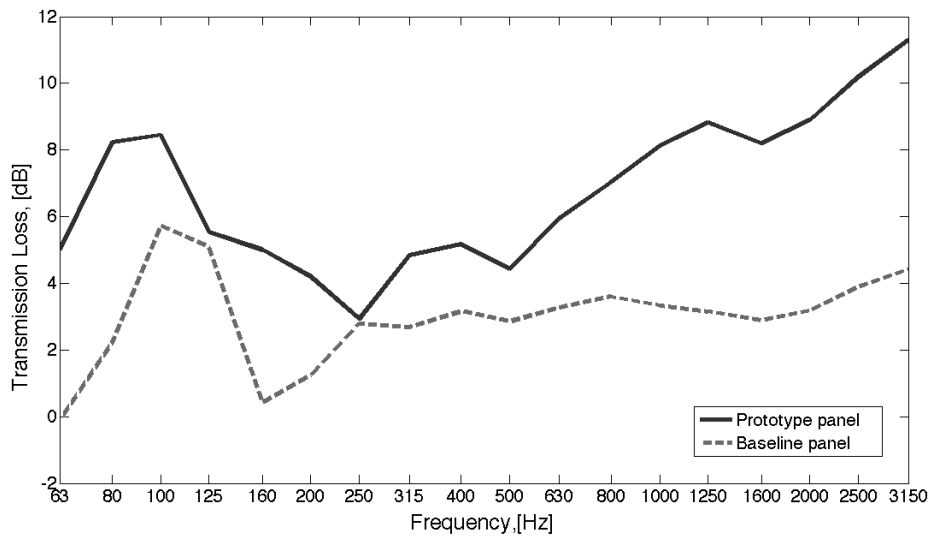


Figure 6.14.: The transmission loss comparison for the prototype and baseline baffled panels for the diffuse field load case.

## 6. Improved front baffled panel

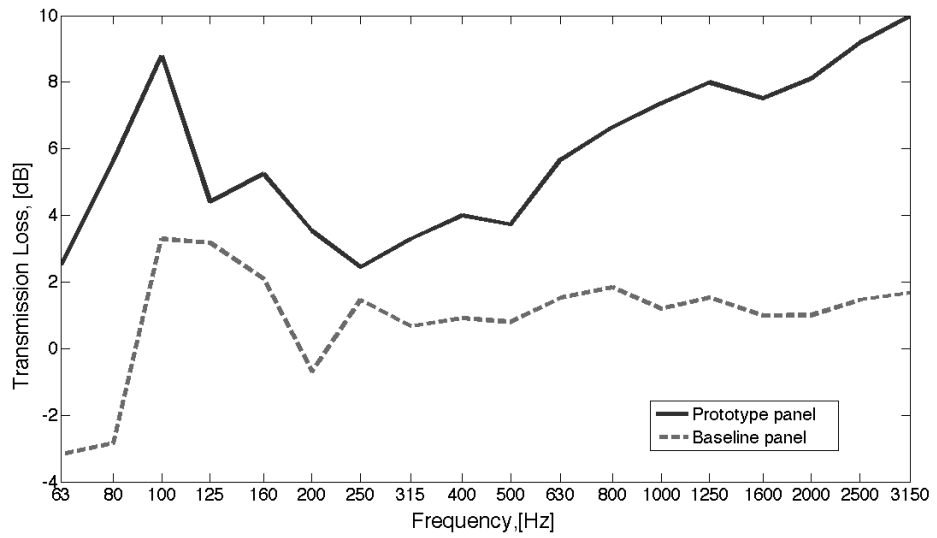


Figure 6.15.: The transmission loss comparison for the prototype and baseline baffled panels for the direct field load case.

Comparison of the transmission losses for the prototype baffled panel and the VA-one model of the prototype baffled panel is presented at Figure 6.16.

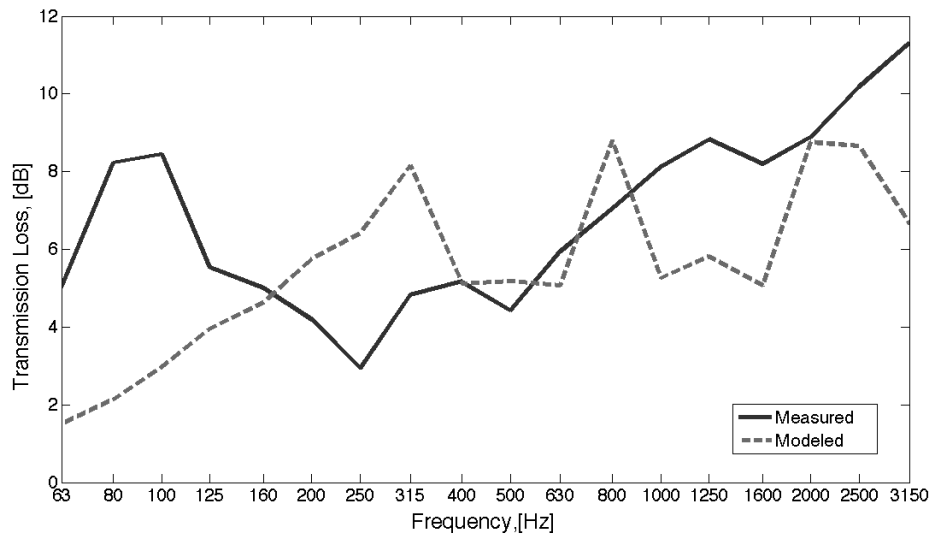


Figure 6.16.: Comparison of the transmission loss measured on the prototype baffled panel and modeled in VA-one.

### 6.3. Estimated emitted sound power

The transmission loss obtained during laboratory measurements of the prototype baffled panel was inserted into the front baffled panel plate in the SEA model of the power pack enclosure. The sound power level emitted from the power pack was estimated for the encapsulated power pack model with the enabled and disabled external sources. The results of the estimation and the comparison with the baseline model are presented at Figure 6.17 and 6.18.

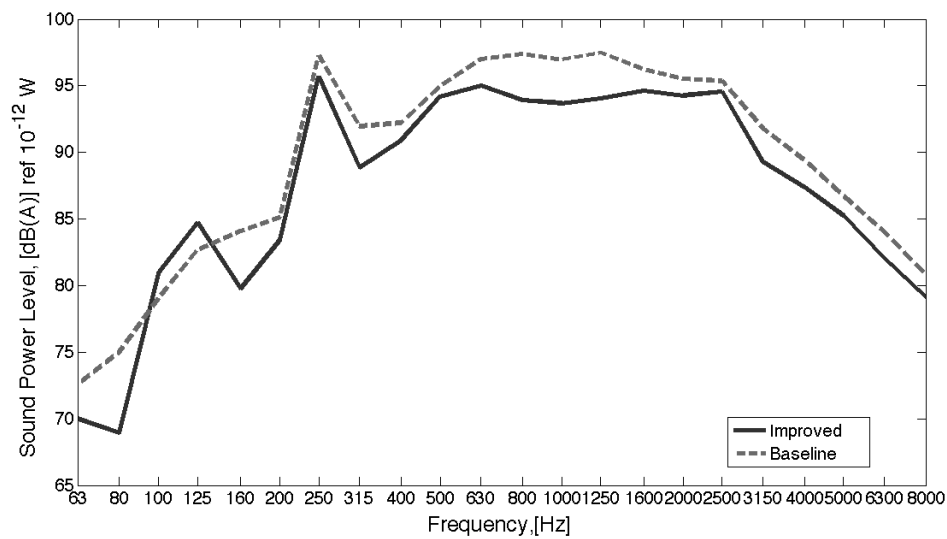


Figure 6.17.: Comparison of the sound power level emitted from the encapsulated power pack without the external sources for the baseline and improved front baffled panels.

## 6. Improved front baffled panel

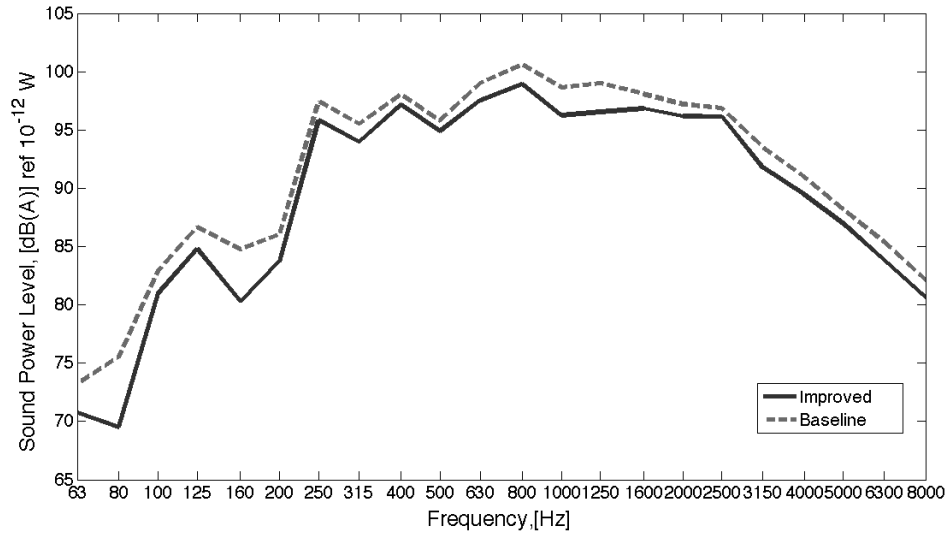


Figure 6.18.: Comparison of the sound power level emitted from the encapsulated power pack with the external sources for the baseline and improved front baffled panels.

Overall sound power level comparison of the emitted sound power from the baseline encapsulation and the encapsulation with the improved front baffled panel is presented in Table 6.1.

Table 6.1.: Overall sound power levels of predicted noise from the encapsulated power pack with the baseline and improved front baffled panels.

Cases	Emitted sound power of the baseline power pack, [dB(A)]	Emitted sound power of the improved power pack, [dB(A)]
Encapsulated power pack without external sources	106.8	104.8
Encapsulated power pack with external sources	108.8	107.3

## 6.4. Conclusion

As expected, the redesigned front baffled panel has better noise reduction properties if compared to the baseline model. The prototype panel was built and its transmission

loss was measured. Expectations of the improved baffled panel's properties were discussed in Subsection 6.1.3. The comparison of the transmission loss of the prototype and baseline baffled panels for the diffuse field load (see Figure 6.14) and direct field load (see Figure 6.15) cases shows that the transmission loss properties of the improved baffled panel are less affected by the incident direct field as compared to the baseline baffled panel. Improved performance is a result of the blades' inclination.

The comparison of the predicted transmission loss and the measured transmission loss of the prototype baffled panel is shown at Figure 6.16. The predicted transmission loss is overestimated for the frequency around 315 Hz due to the absorption model. The edge effect of the absorption was not taken into account in the VA-one model (see Figure 6.4). In the prototype panel edges were closed with tape but it didn't remove the edge effect completely. In the real improved baffled panel the absorption edges will be closed, hence the absorption effective area will be decreased.

The effect of the front baffled panel improvements is shown at Figures 6.17 and 6.18 and in Table 6.1. For the case of power pack operation without the external sources, the emitted sound power decreases by 2 dB(A). The improvements of the side baffled panels can increase the noise reduction effect even more. For the case of the power pack operation with the external sources, the emitted sound power decreases by 1 dB(A). The encapsulation improvements will not decrease emitted noise pollution in this case, because the external fan is one of the dominant noise sources (see Table 4.1) and it is placed outside of the encapsulation.

6. *Improved front baffled panel*

## 7. Summary

The computer model of the encapsulation for the power pack used in the surface core drilling rig CT20 was built, its noise reduction properties were investigated and improved. This work shows that it is possible to build the SEA model of the power pack and populate it with data from the simulations of different power pack components. The results of the simulations were compared and showed a good agreement with measured data. This approach allows to build a model during the pre-study stage of new product development. Besides, the statistical energy analysis is less sensitive to uncertainties in geometry than the finite element method.

The SEA model of the power pack can be used during the development of the next tier of the surface core drilling rig CT20 unit. In addition, current model can be used to set demands on new encapsulation properties and to investigate weak parts of the enclosure.

Possible improvements of the computer model and of the power pack unit are listed in the next subsection.

### 7.1. Future work

The model of the absorption can be improved by creating VA-one material with the same physical properties as the real absorption. This can be done by measuring foam samples with different thickness in the impedance tube and calculating Biot properties in the commercial software Foam-X.

An advanced model of used treatment can be implemented as a poro-elastic material subsystem. In the current version of VA-one it is impossible, therefore, absorption was modeled as a foam without a visco-elastic layer.

An analytical model for prediction of the transmission loss of big apertures with the treatment can be developed for random and normal angle incident sound. Such a model will reduce the "cost" on prediction of reduction properties of the whole encapsulation and will significantly decrease the calculation time.

A better prototype baffled panel has to be made to estimate the real improvements of the proposed design. The redesigned baffled panel described in this work shows the idea of how the panel can be improved. The prototype, which was built in this work is not sustainable and cannot be used in real application.

## *7. Summary*

Separation of the cooling system from the engine can decrease emitted noise from the entire power pack unit. The cooling fan can be temperature controlled and the RPM of the fan can be tune.

The external fan has to be carefully redesigned, because it is the second dominant noise source. Additional encapsulation can be installed to reduce noise emitted from the power pack. The external fan can be temperature controlled as well.

## References

- [Lyon 63] R. H. Lyon. *Journal of the Acoustical Society of America* (1963) 35 (11). Noise Reduction of Rectangular Enclosures with One Flexible Wall.
- [Jac 66] R. S. Jackson. *Journal of Sound and Vibration* (1966) 3 (I). Some Aspects of the Performance of Acoustic Hoods.
- [Old 91-1] D. J. Oldham, S.N. Hillarby. *Journal of Sound and Vibration* (1991) 150 (2). The Acoustical Performance of Small Close Fitting Enclosures, Part 1: Theoretical Models.
- [Old 91-2] D. J. Oldham, S.N. Hillarby. *Journal of Sound and Vibration* (1991) 150 (2). The Acoustical Performance of Small Close Fitting Enclosures, Part 2: Experimental Investigation.
- [Per 10] I. Pereira, M. Guettler, S. Merz. *Acoustics Australia* (2010) 38(3). Numerical Prediction of the Transmission Loss of Leaks in Trimmed Panels.
- [Sau 70] A. Sauter, W. Soroka. *Journal of the Acoustical Society of America* (1970) 44 (1). Sound Transmission through Rectangular Slots of Finite Depth between Reverberant Rooms.
- [Old 93] D. J. Oldham, X. Zhao. *Journal of Sound and Vibration* (1993) 161 (1). Measurement of the Sound Transmission Loss of Circular and Slit-Shaped Apertures in Rigid Walls of Finite Thickness by Intensimetry.
- [Mec 86] F. P. Mechel. *Journal of Sound and Vibration* (1986) 111(2). The Acoustic Sealing of Holes and Slits in Walls.
- [Gom 67] M. Gomperts, T. Kihlman. *Acustica* (1967) 18. The Sound Transmission Loss of Circular and Slit-Shaped Apertures in Walls.
- [Sga 07] F. Sgard, H. Nelisse, N. Atalla. *Journal of the Acoustical Society of America* (2007) 122 (1). On the modeling of the diffuse field sound transmission loss of finite thickness apertures.
- [Tro 09] N. Trompette, J. Barbty, F. Sgard, H. Nelisse. *Journal of the Acoustical Society of America* (2009) 125 (1). Sound transmission loss of rectangular and

## References

- slit-shaped apertures: Experimental results and correlation with a modal model.
- [And 12] P. Andersson, (2012), Division of Applied Acoustics, Chalmers, Sweden, private communication.
- [Mug 76] B. D. Mugridge. *Journal of Sound and Vibration* (1976) 44 (3). The Noise of Cooling Fans Used in Heavy Automotive Vehicles.
- [Tan 00] N. Tandon. *Sadhana* (2000) 25 (3). Noise-reducing designs of machines and structures.
- [Vig 08] T. E. Vigran. *Building Acoustics*. Taylor & Francis, 2008.
- [Nie 07] T. Nielsen. *Intensity Measurements in Building Acoustics*. Bruel & Kjaer application notes, 2007.
- [Lon 06] M. Long. *Architectural Acoustics*. Elsevier Academic Press, 2006.
- [Ver 06] I. Ver, L. Beranek. *Noise and Vibration Control Engineering*. Wiley, 2006.
- [ISO 354] ISO 354:2003 Acoustics - Measurement of sound absorption in a reverberation room.
- [ISO 9613] ISO 9613-1 Acoustics - Attenuation of sound during propagation outdoors - Part 1: Calculation of the absorption of sound by the atmosphere.
- [VA1g] VA One 2011. User's Guide.
- [VA1f] VA One 2011. Foam Module: user's guide, theory & QA.
- [VA1s] VA One SEA. High frequency training course.
- [ISO 9614] ISO 9614-2 Acoustics - Determination of sound power levels of noise sources using sound intensity - Part 2: Measurement by scanning.
- [BaK 93] *Sound Intensity*. Bruel & Kjaer, 1993.
- [Ste 91] D. Steinberg. *Cooling techniques for electronic equipment*. Wiley, 1991.
- [Cum 04] Application manual - Liquid Cooled Generator Sets by Cummins power (2004). [www.cumminspower.com/www/literature/applicationmanuals/t-030\\_p93-115.pdf](http://www.cumminspower.com/www/literature/applicationmanuals/t-030_p93-115.pdf) (last visited 5 jul 2012)
- [Abo 06] M. Abom. *An introduction to Flow Acoustics*. KTH, 2006.

- [Klo 02] J. Klos, S. Brown. The 2002 International Congress and Exposition on Noise Control Engineering (2002). Automated transmission loss measurement in the Structural Acoustic Loads and Transmission facility at NASA Langley Research Center.